



TATIELE DALFIOR FERREIRA

DEVELOPING A MATHEMATICAL MODEL FOR
PREDICTION OF FLAMMABLE GAS CLOUD SIZE BASED
ON CFD AND RESPONSE SURFACE METHODOLOGY

*DESENVOLVIMENTO DE UM MODELO MATEMÁTICO PARA
PREVER O TAMANHO DE NUVEM DE GÁS INFLAMÁVEL
BASEADO EM CFD E METODOLOGIA DE SUPERFÍCIE DE
RESPOSTA*

CAMPINAS

2014



UNIVERSIDADE ESTADUAL DE CAMPINAS
Faculdade de Engenharia Química

TATIELE DALFIOR FERREIRA

DEVELOPING A MATHEMATICAL MODEL FOR PREDICTION OF FLAMMABLE GAS
CLOUD SIZE BASED ON CFD AND RESPONSE SURFACE METHODOLOGY

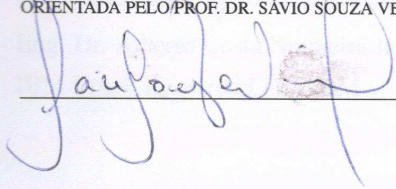
*DESENVOLVIMENTO DE UM MODELO MATEMÁTICO PARA PREVER O TAMANHO DE
NUVEM DE GÁS INFLAMÁVEL BASEADO EM CFD E METODOLOGIA DE SUPERFÍCIE DE
RESPOSTA*

Dissertation presented to the Faculty of Chemical Engineering of the University of Campinas in partial fulfillment of the requirements for the degree of Master in Chemical Engineering

Dissertação apresentada à Faculdade de Engenharia Química da Universidade Estadual de Campinas como parte dos requisitos exigidos para obtenção do título de Mestra em Engenharia Química

Supervisor/*Orientador*: SÁVIO SOUZA VENÂNCIO VIANNA

ESTE EXEMPLAR CORRESPONDE À VERSÃO FINAL DA DISSERTAÇÃO DEFENDIDA PELA ALUNA TATIELE DALFIOR FERREIRA, E ORIENTADA PELO PROF. DR. SÁVIO SOUZA VENÂNCIO VIANNA



CAMPINAS

2014

Ficha catalográfica
Universidade Estadual de Campinas
Biblioteca da Área de Engenharia e Arquitetura
Rose Meire da Silva - CRB 8/5974

F413d Ferreira, Tatiele Dalfior, 1988 -
Developing a mathematical model for prediction of flammable gas cloud size based on CFD and response surface methodology / Tatiele Dalfior Ferreira. - Campinas, SP: [s.n.], 2014.

Orientador: Sávio Souza Venâncio Vianna.
Dissertação (mestrado) – Universidade Estadual de Campinas, Faculdade de Engenharia Química.

1. Administração de risco. 2. Fluidodinâmica computacional (CFD).
I. Vianna, Sávio Souza Venâncio, 1975-. II. Universidade Estadual de Campinas. Faculdade de Engenharia Química. III. Título.

Título em Português: Desenvolvimento de um modelo matemático para prever o tamanho da nuvem de gás inflamável baseado em CFD e metodologia de superfície de resposta

Palavras-chave em Inglês: Risk management, (CFD)

Área de concentração: Sistemas de Processos Químicos e Informática

Titulação: Mestra em Engenharia Química

Banca examinadora:

Sávio Souza Venâncio Vianna [Orientador]

Roger Joseph Zemp

Alberto Costa Nogueira Jr

Data da defesa: 14-03-14

Programa de Pós-Graduação: Engenharia Química

UNIVERSIDADE ESTADUAL DE CAMPINAS
FACULDADE DE ENGENHARIA QUÍMICA
COMISSÃO DE PÓS-GRADUAÇÃO EM ENGENHARIA QUÍMICA
DEPARTAMENTO DE ENGENHARIA DE SISTEMAS QUÍMICOS

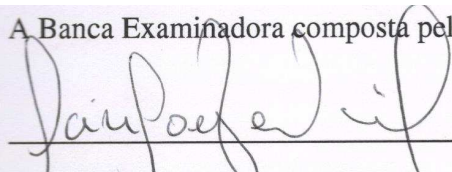
DISSERTAÇÃO DE MESTRADO

Developing a Mathematical Model for Prediction of Flammable Gas Cloud Size based on CFD and Response Surface Methodology

Autor: Tatiele Dalfior Ferreira

Orientador: Prof. Dr. Sávio Souza Venâncio Vianna

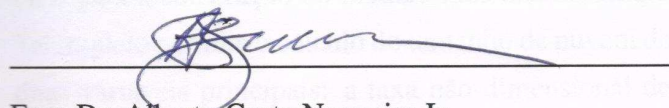
A Banca Examinadora composta pelos membros abaixo aprovou esta Dissertação:



Prof. Dr. Sávio Souza Venâncio Vianna
Faculdade de Engenharia Química - Unicamp



Prof. Dr. Roger Josef Zemp
Faculdade de Engenharia Química - Unicamp



Eng. Dr. Alberto Costa Nogueira Jr
IBM Brazil Research Lab - IBM

Campinas, 14 de Março de 2014.

ABSTRACT

This work proposes the development of a mathematical correlation for prediction of flammable gas cloud size in a typical offshore module. Real conditions regarding the ventilation and process plant operation were considered. A dispersion study of natural gas release in the module was conducted using Computational Fluid Dynamics (CFD) and the state of art as far as the gas dispersion modelling is concerned. A mathematical model was built based on the numerical results and Response Surface Methodology (RSM). The approach comprises into a single mathematical model the most relevant independent variables. The response surface curves calculate the flammable gas cloud volume as a function of the non-dimensional leak rate (that concerns the ventilation and the gas release rate) and the non-dimensional leak direction (which comprises the wind direction and the leak direction). The developed model had proved to be effective. It was able to predict flammable gas volume and good agreement with CFD results was observed.

RESUMO

Este trabalho tem como objetivo desenvolver um modelo matemático capaz de prever o tamanho de nuvem de gás inflamável formada em uma típica plataforma de petróleo considerando condições reais de ventilação e de operação de uma planta de processo. Para tanto, foi realizado um estudo de dispersão de gás inflamável (gás natural) na plataforma em questão utilizando Fluidodinâmica Computacional (CFD). Os resultados deste estudo de dispersão serviram como base para a construção do modelo matemático utilizando Metodologia de Superfície de Resposta. Tal modelo permite o cálculo do tamanho de nuvem de gás inflamável no ambiente estudado usando duas variáveis principais: a taxa não-dimensional de vazamento (que contabiliza a relação entre a taxa de vazamento de gás e a taxa de ventilação na plataforma) e a direção adimensional de vazamento (que computa a relação entre as direções de vazamento de gás e do vento). O modelo desenvolvido mostrou-se eficaz, pois foi capaz de prever com considerável grau de confiabilidade os tamanhos de nuvem de gás inflamável quando comparados aos valores fornecidos por simulações com CFD.

Contents

1	Introduction	1
1.1	General goal	3
1.2	Specific goals	4
1.3	This dissertation	4
2	The Flammable Gas Cloud	7
2.1	Gas dispersion phenomenon	7
2.2	Dispersion models	9
2.2.1	Jet model	9
2.2.1.1	High aspect ratio jet behaviour	11
2.2.1.2	Others forms to model jets	12
2.2.2	Plume and puff model	13
2.2.3	CFD models	15
2.3	Variables that influence the flammable gas cloud size	15
2.3.1	Ventilation rate	16
2.3.1.1	Wind speed and direction	16
2.3.1.2	Geometry of the module	16
2.3.2	The gas release	16

2.3.2.1	Gas density	17
2.3.2.2	Leak rate and direction	17
2.3.2.3	Leak location	17
2.4	Estimating the flammable gas cloud size	18
3	Mathematical Modelling and CFD	21
3.1	Mathematical modelling	21
3.1.1	The mass conservation	22
3.1.2	The momentum equation	22
3.1.3	The energy equation	23
3.2	Turbulence	24
3.2.1	Turbulence models	25
3.2.1.1	RANS models	26
3.2.1.2	The k - ε model	27
4	Response Surface Methodology	29
4.1	The basic ideas about Response Surface Methodology	29
4.1.1	Design of experiments	30
4.1.2	Statistical modelling	30
4.2	The RSM applications	31
5	Case Study	35
5.1	Geometry and mesh	35
5.2	Design of the dispersion simulations	36
5.2.1	Variables of interest	36
5.2.1.1	Ventilation and leak rate	37

5.2.1.2	Leak and wind direction	37
5.2.2	Simulations set up	39
5.3	Natural gas composition and release conditions	40
5.4	Boundary conditions and solver parameters	40
5.5	Estimating the flammable gas cloud size and development of the response surface model	43
6	CFD Results	45
6.1	Study of gas jet release	45
6.1.1	Axisymmetric jet simulation	46
6.1.2	High aspect ratio jet simulation	47
6.1.3	Study of the natural gas jet	51
6.2	Wind analysis	54
6.2.1	Wind speed profile tests	57
6.3	Computational domain size and mesh test	60
6.3.1	Computational domain size	60
6.3.2	Mesh tests	64
6.4	Evaluating the influence of accommodation module in ventilation rate	68
6.4.1	The variable R	70
7	Dispersion Simulations and Development of the Response Surface Model	71
7.1	Developing a response surface model considering releases in a horizontal plane	71
7.1.1	Comparing values predicted by response surface model with CFD dispersion simulations	78
7.1.2	Accounting the influence of the accommodation module	80
7.2	Developing a response surface model considering releases in "z" direction	84

8	Conclusions and Future Work	89
8.1	Conclusions	89
8.2	Future Work	91
	References	93
A	An Engineering Procedure for Gas Dispersion Analysis Using ANSYS CFX 12.0	99
A.1	Building the geometry and mesh	99
A.2	CFX - Pre Processor	100
A.3	CFX - Post Processor	100
B	Additional CFD Results	102

To my Parents.

Acknowledgment

I would like to thank God for the wisdom and perseverance that He has been bestowed upon me during this project and throughout my life.

My appreciation and thanks to my supervisor Professor Sávio S.V. Vianna. I would like to thank you for his encouragement and support and for allowing me to grow as a research scientist.

I would like to express my deep gratitude and respect to Professor Milton Mori for making this research possible. For providing the PQGE Lab for the development of this work and for his continuous help and support in all stages of this project.

I would also like to thank my friends in PQGE Lab for your friendship, support and cooperative in implementing this project.

I want to thank all of my friends who supported me and incited me to strive towards my goal.

I would like to thank my family (dad, mom and Gabi) for always believing in me, for their unconditional love and their support in my decisions. Your prayers for me was what sustained me thus far.

"The first requisite for success is to develop the ability to focus and apply your mental and physical energies to the problem at hand - without growing weary."

Thomas A. Edison

List of Figures

2.1	Schematic description of a turbulent jet (Pope (2000)).	10
2.2	Rectangular cross-sectional three-dimensional jet.	12
2.3	Schematic of the flow field of a rectangular jet showing the different decay zones (Wakes (2002)).	12
2.4	Jet flow with different zones (Benintendi (2010)).	13
2.5	Plume formed by a continuous release (AICHE (2000)).	14
2.6	Puff formed by an instantaneous release (AICHE (2000)).	14
3.1	Fluctuations in a turbulent flow.	26
5.1	A platform geometry based in an offshore module.	35
5.2	Simplified geometry with a single deck (Main Deck).	36
5.3	Wind directions in the platform.	37
5.4	Possible directions of the leakage and its representation into the platform.	38
5.5	Schematic representation of the angle φ for a leakage in the direction y^+	39
6.1	Geometry and mesh used in the Axisymmetric Jet study.	46
6.2	Simulation of a high pressure axisymmetric jet.	47
6.3	Schematic representation of the geometries of flange leaks (Wakes (2002)).	48
6.4	Comparing results from an axisymmetric jet simulation with a high aspect ratio jet behaviour.	49

6.5	Geometric representation of a gasket failure in a flange.	49
6.6	Simulation of a high aspect ratio jet behaviour using diferent parameters.	50
6.7	Computational domain and mesh used in the natural gas jet simulation.	51
6.8	Spreading angle of the natural gas jet.	52
6.9	Natural gas velocity profile in the centreline of the jet.	53
6.10	Natural gas superficial velocity profile at different heights.	53
6.11	Natural gas molar fraction profile in the centreline of the jet.	54
6.12	Vertical wind speed profile.	55
6.13	Vertical wind speed profile - Equation 6.1.	58
6.14	Vertical wind speed profile - Equation 6.3.	59
6.15	Vertical wind speed profile - Equation 6.4.	59
6.16	Wind velocity field in a plan at height 2.5 m over the main deck using the computational domains CD01 (a), CD02 (b) and CD03 (3).	61
6.17	Platform geometry with monitoring points. In this case, the computational domain CD01 has been used as an exemple.	62
6.18	Comparision between the values of average wind velocity in monitoring points located in the first level (at 2.5 m over main deck).	62
6.19	Comparision between the values of average wind velocity in monitoring points located in the second level (at 10 m over main deck).	63
6.20	Comparision between the values of average wind velocity in monitoring points located in the third level (at 20 m over main deck).	63
6.21	Comparision between the values of average wind velocity in monitoring points located in the first level (at 2.5 m over main deck).	66
6.22	Comparision between the values of average wind velocity in monitoring points located in the second level (at 10 m over main deck).	66

6.23	Comparison between the values of average wind velocity in monitoring points located in the third level (at 20 m over main deck).	67
6.24	Comparing the ventilation rate into the offshore module, for a wind speed of 2 m/s when considering or not the accommodation module in geometry.	68
6.25	Comparing the ventilation rate into the offshore module, for a wind speed of 4 m/s when considering or not the accommodation module in geometry.	69
6.26	Comparing the ventilation rate into the offshore module, for a wind speed of 6.5 m/s when considering or not the accommodation module in geometry.	69
7.1	Response surface models for the Quadrants 01 (a), 02 (b), 03 (c) and 04 (d).	75
7.2	Comparison between the values obtained through CFD simulations and the response surface models to the Quadrants 01 (a), 02 (b), 03 (c) and 04 (d). Vertical axis shows results predicted with the model proposed in this study. Horizontal axis shows cloud volumes obtained using CFD.	77
7.3	Comparing results from CFD simulations with response surface model for random dispersion scenarios. Vertical axis shows results predicted by the model proposed in this study. Horizontal axis shows cloud volumes obtained using CFD.	80
7.4	Comparison between the values obtained through CFD simulations considering the accommodation module in the geometry and the Response Surface Models to the Quadrants 01 (a), 02 (b), 03 (c) and 04 (d). Vertical axis shows results predicted with the model proposed in this study. Horizontal axis shows cloud volumes obtained using CFD.	83
7.5	Response surface model for leakages in z direction.	85
7.6	Comparison between the values obtained through CFD simulations and the response surface model for leakages in z direction. Vertical axis shows results predicted with the model proposed in this study. Horizontal axis shows cloud volumes obtained using CFD.	86
7.7	Comparing results from CFD simulations with response surface model for releases in z direction. Random dispersion scenarios including or not the accommodation module in the platform geometry were considered. Vertical axis shows results predicted by the response surface model. Horizontal axis shows cloud volumes obtained using CFD.	88

B.1	Result of the CFD simulation considering the dispersion scenario 08 (see Table 7.1). The flammable region in a plane at 15 metres over platform deck is verified.	102
B.2	Result of the CFD simulation considering the dispersion scenario 14 (see Table 7.1). The flammable region in a plane at 15 metres over platform deck is verified.	103
B.3	Result of the CFD simulation considering the dispersion scenario 15 (see Table 7.1). The flammable region in a plane at 15 metres over platform deck is verified.	103
B.4	Result of the CFD simulation considering the dispersion scenario 16 (see Table 7.1). The flammable region in a plane at 15 metres over platform deck is verified.	104
B.5	Result of the CFD simulation considering the dispersion scenario 17 (see Table 7.1). The flammable region in a plane at 15 metres over platform deck is verified.	104
B.6	Result of the CFD simulation considering the dispersion scenario 18 (see Table 7.1). The flammable region in a plane at 15 metres over platform deck is verified.	105
B.7	Result of the CFD simulation considering the dispersion scenario 22 (see Table 7.1). The flammable region in a plane at 15 metres over platform deck is verified.	105
B.8	Result of the CFD simulation considering the dispersion scenario 24 (see Table 7.1). The flammable region in a plane at 15 metres over platform deck is verified.	106
B.9	Result of the CFD simulation considering the dispersion scenario 25 (see Table 7.1). The flammable region in a plane at 15 metres over platform deck is verified.	106
B.10	Result of the CFD simulation considering the dispersion scenario 26 (see Table 7.1). The flammable region in a plane at 15 metres over platform deck is verified.	107
B.11	Result of the CFD simulation considering the dispersion scenario 32 (see Table 7.1). The flammable region in a plane at 15 metres over platform deck is verified.	107
B.12	Result of the CFD simulation considering the dispersion scenario 36 (see Table 7.1). The flammable region in a plane at 15 metres over platform deck is verified.	108

List of Tables

3.1	Constant values for the standard $k-\varepsilon$ turbulence model (ANSYS CFX (2011)). . . .	28
5.1	Natural Gas Composition.	40
5.2	Boundary conditions of the simulations.	41
5.3	Simulation Parameters.	41
6.1	Simulation Parameters for the Axisymmetric Jet study.	47
6.2	Parameters for the high aspect ratio jet study.	50
6.3	Values of L , z_0 and p for neutral atmospheric and sea surface.	57
6.4	Size of the computational domains under study.	60
6.5	Refinement on platform regions according to Mesh 01.	65
6.6	Refinement on platform regions according to Mesh 02.	65
6.7	Refinement on platform regions according to Mesh 03.	65
6.8	Mass flow rate of natural gas calculated to provide desirable values of R based on the average ventilation rate when the accommodation module is neglected in platform geometry.	70
6.9	Mass flow rate of natural gas calculated to provide desirable values of R based on the average ventilation rate when the accommodation module is included in platform geometry.	70
7.1	Dispersion Scenarios Based on an Experimental Design.	72

7.2	Random CFD Simulations.	78
7.3	Dispersion Simulations Considering the Accommodation Module in Platform Geometry.	81
7.4	Dispersion Scenarios Based on an Experimental Design for Leak Direction z. . . .	84
7.5	Random CFD Simulations.	86

Chapter 1

Introduction

Gas explosion safety is a concern in industrial plants, particularly in oil and gas industry. The onshore as well as offshore oil installations involve several zones with dense congestion areas and large quantities of flammable materials, which makes the activities of drilling, production and processing potentially hazardous. Large accidents involving gas explosions show the need for continuously address gas safety issues.

On December 2005, a vapour cloud explosion (VCE) occurred at Buncefield Oil Storage Depot, Hertfordshire, UK. Significant blast pressures were generated resulting in further loss of containment and subsequent fires in fuel storage tanks. As result of the accident, 43 people were injured and significant damage occurred to both commercial and residential properties in the vicinity. Total damages were of the order of \$1.5 billion (Johnson (2010)).

An accident involving vapour cloud explosion also occurred in the Amuay Refinery Complex, which contains the largest oil deposit on the planet, in Venezuela. In August 2012, there was a huge explosion caused by a gas cloud coming from an area of the plant that deals with natural gas, crude oil and naphtha. Two storage tanks and other base facilities were ignited. There has been 41 casualties and other 151 injured (CBC (2012)).

According to Kjellén (2007), offshore oil and gas production involves risk of accidents with a major loss-potential. In case of accidental explosion, large quantities of energy are released in a small and often confined space, causing considerable damage.

Offshore modules also involve traditional hazards with the potential for severe occupational accidents. Operators work hard and most times in confined spaces and with difficult access

to ransom or rescue. Das & Weinberg (2012) pointed out that the impairment of escape routes in the limited deck space of offshore modules further escalates the severity/risk of VCE events. The adverse weather conditions in offshore sites, may also increase the probability of serious accidents.

An example of offshore accident is the explosion occurred after a gas release on the Deepwater Horizon oil rig working on the Macondo exploration well for BP in the Gulf of Mexico, in April 2010. Eleven people died as a result of the accident and others were injured (BBC (2011)).

In Brazil, in March 2001, the Platform P-36 sank after two explosions. The number of deaths were also 11.

One of the major devastating explosions offshore has occurred in July 1988, on board the offshore platform Piper Alpha, located in the North Sea. The fire began with a little explosion in the compression module in the platform and shortly escalated to a massive accidental scenario that destroyed the whole module. The disaster caused the death of 167 people (out of 226) and cost billions of dollars in property damage. From this disaster, concerns about better assessment of the risks and the future risk management were intensified, in various industrial sectors (Paté-Cornell (1993)).

The risk analysis of vapour cloud explosion can significantly help risk decisions. Such analysis concerns quantifying the blast overpressure generated over distance and time, which depends on the filling degree of the platform and the concentration of flammable gas cloud, among other factors. The worst case scenario is the one in which the entire environment of the platform is filled with stoichiometric mixture of gas and air, although it is far too much conservative approach. A more realistic scenario requires a gas dispersion analysis to estimate the gas cloud size.

There are number of methods developed over recent years to provide estimatives of flammable gas build-up in accidental release and to quantify the risk from a gas explosion. Essentially they comprise mathematical correlations and three-dimensional analysis using Computational Fluid Dynamic (CFD).

The three-dimensional analysis using CFD is the best available approach. Several studies have been developed applying different ways to analyse the gas dispersion and evaluate the flammable gas cloud size through CFD codes. Some examples of them are shown by Cormier *et al.* (2009), Zhang *et al.* (2010) and Ivings *et al.* (2010).

The main drawbacks in CFD models are the computational effort, time and costs. In risk

analysis, several possible gas release scenarios must be conducted to analyse the overall risk and CFD can not be employed in every single scenario within a reasonable scale of time.

Especially during conceptual design when important decisions are made, the explosion estimates are often sought after without performing detailed CFD analysis. The analysis needs to be made quickly and on a series of concept designs until the "optimal" design is found. The use of detailed CFD methods in early stages, when structural design is being made, can take too much time and also be uncertain due to lack of information about the geometry, so it becomes impractical for the necessity to investigate many alternatives (Huser *et al.* (2009)). In these initial stages, mathematical correlations can be used and the CFD analysis is applied to assess only a few critical scenarios in detail at a later stage.

The application of mathematical models to estimate the flammable gas cloud size in offshore installations was introduced by Cleaver *et al.* (1999), who developed a set of correlations based on benchmarking data in an offshore module.

Based on the correlations developed by Cleaver *et al.* (1999), Huser & Kvernfold (2000) proposed the application of Response Surface Methodology (RSM) to predict the gas cloud size. This method allows to access the flammable volume through two response surfaces, providing breakthroughs in analysis of the flammable gas clouds.

However, there seems to be room for improvement as the utilisation of two equations places too much a burden on the engineer who is conducting the analysis. It is not always easy to set up the curves as it is not straightforward to adjust the independent parameters in the curve as well as to migrate from one expression to another mathematical expression. The development of a simpler mathematical model is necessary.

This work proposes a single correlation to predict the flammable gas cloud size in an offshore module. The approach couples into a single mathematical model the most relevant independent variables.

1.1 General goal

The current work is focused on the development of a mathematical model to estimate the flammable gas cloud size in an offshore module applying the response surface methodology. The

analysis of the gas dispersion were conducted based on CFD simulations of natural gas releases in an offshore platform. The numerical results from the dispersion simulations were used as input and benchmarking during the development of the model.

1.2 Specific goals

The specific goals of this work are:

- Create a geometry based on a real offshore module;
- Analyse the parameters that influence the gas dispersion and identify the most relevant for this study;
- Provide the correct modelling of the transport phenomena (momentum, mass and heat transfer) using the *ANSYS CFX 12.0* CFD software;
- Define a design of experiments for the dispersion simulations;
- Perform the dispersion simulations and develop the response surface;
- Compare the values of flammable volume predicted by the developed response surface model with the results provided by dispersion simulations in CFD.

1.3 This dissertation

For better understanding of this study, the dissertation structure is summarised below.

In Chapter 1 a brief introduction was presented concerning the gas explosion risks associated with the oil industry activities and the necessity of applying a combination of operational measures in design to prevent and mitigate accidents. It was also shown the motivations and the aim of this study.

Chapter 2 covers the first part of the literature review, which includes the main phenomena associated with gas dispersion and the factors that influence the flammable cloud size. The empirical models as well as the CFD models used for these studies are also discussed.

Chapter 3 presents the mathematical equations that must be solved to describe a fluid flow and the models that are used in the dispersion study. The steps applied in CFD analysis is also shown.

In Chapter 4 the Response Surface Methodology is introduced. The basic ideas about this methodology and the fields where it has been applied are shown here.

Chapter 5 presents the CFD modelling used to reach the objectives of this study. It is shown the geometry and mesh, the boundary conditions, the set up of the dispersion simulations and how the variables are defined, the softwares that are used at the simulations and for the post processing.

In Chapter 6 the CFD results are shown. It addresses the study of a jet release and the wind speed profile, that are used as boundary condition in the dispersion simulations. Others studies about the computational domain size, mesh tests and the platform geometry are also discussed.

Finally, Chapter 7 covers the results of dispersion simulations and the development of the response surface model. The comparison between the results provided by the model and the CFD simulations is shown. Conclusions and future work are presented in Chapter 8.

Chapter 2

The Flammable Gas Cloud

Analysis of possible accident scenarios or investigation of accidents usually begins calculating the mass of flammable material released. The next step is to calculate the air entrainment rates and how the material will be dispersed. With these information it is possible to find the fraction of the released mass that may be in the flammable region. Often this is a small fraction of the total amount released. Only the flammable mass within or near the flammable limits participates in a explosion or fire (AICHE (2000)).

The flammable gas cloud is defined by the volume occupied by the gaseous mixture of air and a flammable gas within the flammable limit.

The flammable limits, also called explosive limits, refer to the highest and lowest concentration of a flammable material in a mixture with air which is likely to ignite. These limits are determined experimentally and they are usually expressed by the volumetric concentration. The abbreviation LFL and UFL are used to refer the lower flammable limit and the upper flammable limit, respectively. Below the LFL, gaseous mixtures are "too lean" to burn, while concentrations higher than UFL are "too rich" to burn.

2.1 Gas dispersion phenomenon

The dispersion comprises the diffusion of a material into another in a certain region or volume. The studies of dispersion started with the dispersion of pollutants from industrial chimney

stacks and extended for hazardous releases from process plant (Lees (2005)).

Dispersion models are used to explain how the materials will be diffused. They are relevant to describe the release of flammable material, mixing of the material with air and the formation of a flammable gas cloud. Such models can identify the affected area and the material concentration in each region.

For gas dispersion, the models describe the transport of gaseous materials by air. In these cases the most important physical parameters that influence the material atmospheric dispersion and must be considered are (Lees (2005)):

- Meteorology;
- Topography;
- Elevation of the leak;
- Gas Density;
- Release Momentum.

The meteorological conditions that affect the dispersion are the wind features and the atmospheric stability condition. The atmosphere stability determines the degree of mixing. During the day the air temperature varies greatly with height (unstable condition) and the mixture air-gas by diffusion is intense. At night the temperature gradient is smaller (stable condition) and the dispersion is not as strong.

Wind characteristics influence not only the gas dispersion, but directly affect the flammable gas cloud size and will be analysed in next sections. The same will be done to the gas density, that is also an important parameter.

The topography affects the wind profile and the mixture near the surface. Each surface is assigned a roughness and a specific wind speed profile develops. The mixture of the material and air can be raised by the presence of obstacles in the surface.

The leak elevation influences the concentration of the dispersing material at ground level. Most hazardous releases are treated at this level and therefore, the concentration of the material is great near the ground.

In a gas leak, the dispersion of the material is determined by its momentum and buoyancy. If momentum forces predominate, the fluid forms a jet, while if buoyancy forces predominate, it forms a plume. Both types of emission are sometimes described as plumes, the jet being a forced plume (AIChE (2000)).

The flammable gas release normally occurs from facilities at high pressure and its behaviour is a jet. After the release, a gas cloud is carried by the wind in a form of plume.

2.2 Dispersion models

In section 2.1 it was shown how the gas dispersion occurs and the main factors that affect it. It was also mentioned the importance of using the dispersion models to represent correctly this phenomena. This section presents some of this models.

2.2.1 Jet model

As previously discussed, if the momentum of the material released from an orifice is high, the dispersion in the initial phase at least is due to the momentum, and the emission is described as a momentum jet.

Recirculation regions are formed near the jet creating wide air penetration. According to Wilkening *et al.* (2008), this is the main mechanism of mixing between air and gas released.

The behaviour of a circular (or conical) turbulent jet has been widely studied. It can be described by empirical features as following (Lees (2005)):

- The jet is conical and apparently diverges from a virtual point source upstream of the orifice;
- The dilution occurs by turbulent mixing;
- The time-mean velocity and concentration profiles are similar after 10 diameters and are approximately Gaussian;
- The concentration profile is wider than the velocity profile;

- The jet entrains air, but conserves its momentum, so that the momentum flux at any plane normal to the axis is constant.

Pope (2000) expressed some jet characteristics in a schematic way (Figure 2.1) and developed a relationship to represent the jet behaviour.

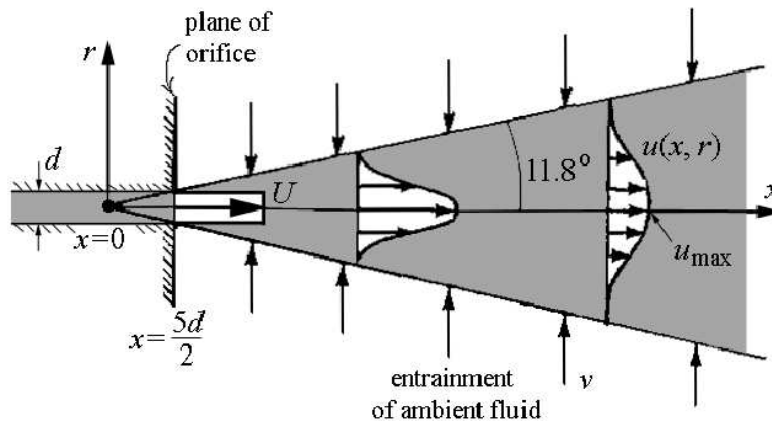


Figure 2.1: Schematic description of a turbulent jet (Pope (2000)).

Where:

x is the axial distance;

d is the diameter of orifice;

$u(x, r)$ is the velocity at distance x and in the radius r ;

u_{max} is the maximum velocity in the centreline of the jet.

Lees (2005) mentions different models to describe the dispersion by a turbulent jet including underexpanded, obstructed and sonic jets. The most applied models in engineering and others studies are based on axisymmetric jets.

The behaviour of an axisymmetric jet is well known and easy to be modelled, which makes it normally used as simplification in modelling situations. Some axisymmetric jet features are presented below (Mih (1989)):

- The potential core length is approximately equal to $6.9D$, from the jet exit (D is the diameter of orifice);

- The centreline velocity decay is well established and proportional to $1/\bar{x}$, where \bar{x} is the dimensionless distance from the orifice;
- The spreading angle from the centreline is 10 - 15°.

On the other hand, Wakes (2003), who had studied modelling aspects of the jet to describe the behaviour and its dispersion in offshore structure, observed that using axisymmetric jets to simulate leaks is not recommended for safety analysis. For the author, a real jet behaves as a high aspect ratio jet, that is very different of an axisymmetric one.

In her experimental work, Wakes (2002), found very different behaviours of the flow for jets starting from orifice with different gasket shapes, which indicate that the gasket shape is an important factor in the behaviour of the jet. It was also identified that the range of the jets spreading angles for the geometries studied, in many cases, do not correspond to that for an axisymmetric jet. The velocity profile of the axisymmetric jets was found only for certain geometries.

Furthermore, it was observed that using axisymmetric jets to simulate leaks may under predict the leaked gas concentration levels and the growth rate of the air-gas mixture and also to underestimate the gas cloud size.

Hence, Wakes (2003) argues that the utilisation of axisymmetric jets to simulate leaks should be addressed with care.

2.2.1.1 High aspect ratio jet behaviour

In process area the leaks are most likely to emanate from a fraying or flaws in pipeline structures, as a valve or flange. Such leaks are developed from a non-circular orifice shape and could get a high aspect ratio cross-sectional jet behaviour.

The term *high aspect ratio* was introduced first in aerodynamics to indicate the ratio of wing length and breadth. A high aspect ratio indicates long and narrow wings, whereas a low aspect ratio indicates short and stubby wings (Kermode (1972)).

In jet studies the term is used to indicate the jet shape and comprises the relation between the two cross-section dimensions in a three-dimensional jet (where the flow properties vary in all directions). Taking a example a rectangular cross-sectional jet (Figure 2.2), a high aspect ratio cross-sectional jet will have a large ratio between the length x and the width y .

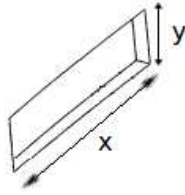


Figure 2.2: Rectangular cross-sectional three-dimensional jet.

The studies concerning high aspect ratio cross-sectional jets indicate that they behave in a different way to those with axisymmetric cross-sections.

Wakes (2002) has mentioned the main features a high aspect cross-sectional jet behaviour (Figure 2.3):

- in its early stages the jet is expected to have a potential core region that will be of a decreasing length as the aspect ratio increases. This behaviour is independent of the Reynolds number;
- The second region is a characteristic decay region;
- It exists an axisymmetric decay region in the far field.

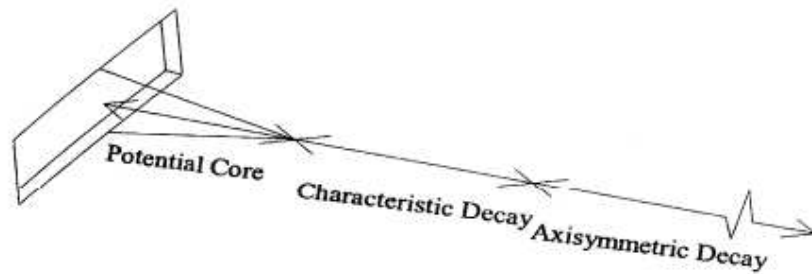


Figure 2.3: Schematic of the flow field of a rectangular jet showing the different decay zones (Wakes (2002)).

2.2.1.2 Others forms to model jets

Another forms to represent the jet behaviour has been developed by Benintendi (2010). The author developed analytical method to modelling a turbulent jet flow and sizing the gas volumes resulting from them, to be used in hazardous areas classification.

So, Benintendi (2010) has considered a typical jet with a circular orifice exit and identified the regions of it (Figure 2.4 shows a schematic division of the jet flow in regions). Each jet zone was analysed carefully considering the velocity profile, gas concentration and entrainment with air.

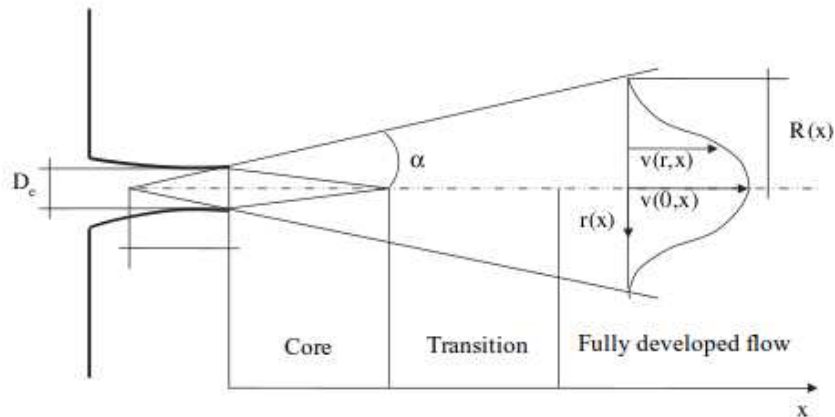


Figure 2.4: Jet flow with different zones (Benintendi (2010)).

Benintendi (2010) obtained a jet calculation procedure which enables a simple and reliable sizing of mixture air-gas volume. It can be adopted for hazardous area classification, improving the reliability of the results and at avoiding the oversizing of the classified zones.

A similar model were also developed by Benintendi (2011) considering the laminar regime and take into account the effect of density and viscosity differences between air and flammable gas.

2.2.2 Plume and puff model

The plume model describes a continuous release of material. In most cases, this model deals with an initial jet in which the momentum decays so that the emission undergoes transition to a buoyant plume (Wilkening *et al.* (2008)). Figure 2.5 shows a typical plume.

Lees (2005) mentioned some principal characteristics of a plume. Under turbulent conditions the plume is conical and apparently diverges from an equivalent point source, the position of the point source depending on the point of transition from laminar to turbulent flow. The time-mean velocity and time-concentration profiles are similar and are approximately Gaussian.

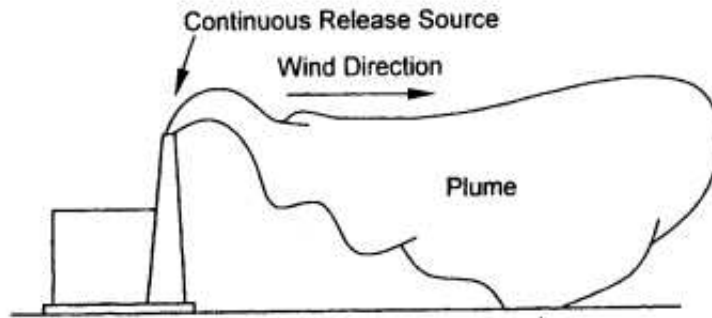


Figure 2.5: Plume formed by a continuous release (AICHE (2000)).

Puff model, or neutral and positively buoyant plume, describes the material concentration profile as time function from a single release with a fixed quantity of the material. An example would be a sudden leak due to rupture of a storage tank, giving a large vapour cloud that moves away from the breaking point. Figure 2.6 shows a puff formed by an instantaneous release.

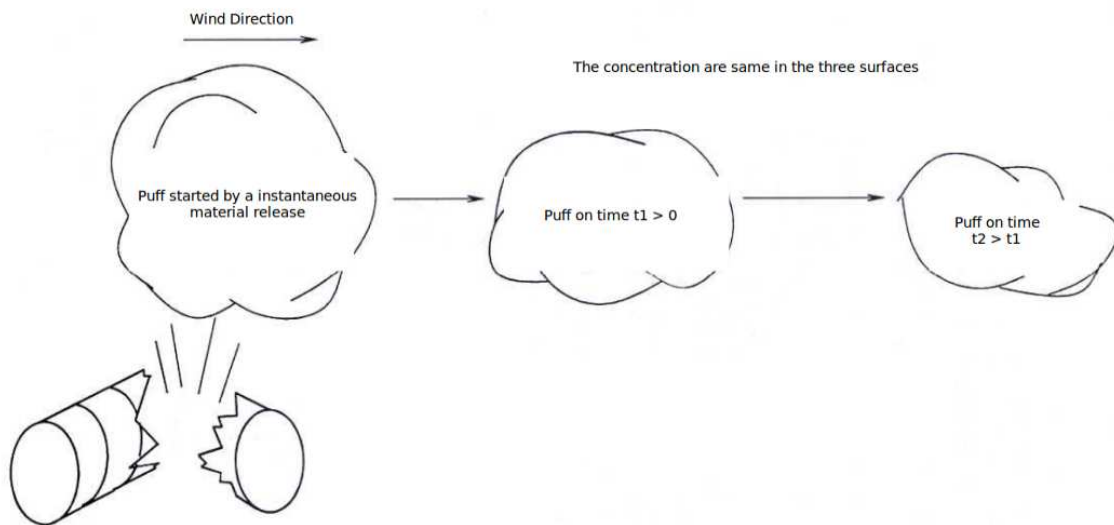


Figure 2.6: Puff formed by an instantaneous release (AICHE (2000)).

While the Plume refers to continuous emissions, puff considers emissions that are short in duration compared with the travel time (time for cloud to reach location of interest).

A plume can be described as a continuous leak puffs so the puff model can be used to describe it. For studies involving a dynamic plume, the puff model should be used. However, if the information of a plume in a state stationary is enough, the plume model is recommended because it is easier to apply.

2.2.3 CFD models

The fluid dynamic models are represented by differential equations. For each particular problem, these equations are subjected to specific boundary and initial conditions, which will characterize the fluid flow.

For problems with simple geometry, fluid flow and boundary conditions, the solution of these equations can be straightforward. However, almost all real problems have no analytical solution and a numerical approach is necessary. The numerical solution of the equations of continuity, momentum and energy can be obtained through Computational Fluid Dynamic (CFD).

CFD is defined as the set of methodologies that enable the computer to provide us with a numerical simulation of fluid flows (Hirsch (2007)). CFD has been widely applied in many fields and its utilisation is limited by the available models to describe all phenomena involved in every type of fluid flow and also by the computational resources.

The main strategy of CFD is to replace a continuous computational domain by a discrete domain, using a grid. In the discrete domain, each variable of flow is defined just in the grid points. The values of the variables in another locations are estimated by interpolation of the grid points.

The CFD solutions contain a great amount of information about the flow field (pressure, velocity, specific mass, etc...) which enables the comprehension of its behaviour. However, the results must be analysed with care. Some errors can be generated during the numerical solution and the model will have low representation compared with the real problem (Maliska (2004)).

2.3 Variables that influence the flammable gas cloud size

The phenomena that are involved on generation of flammable gas cloud has been studied by Cleaver *et al.* (1994). It was shown how each one of these phenomena can be modelled to predict accumulation of natural gas in a characteristic volume (an offshore module, for example).

Cleaver *et al.* (1994) investigated the dispersion of high pressure natural gas releases in a congested and partially confined volume. It was noted that the ventilation rate and the behaviour of gas release are the main factors that influence the generation of flammable gas cloud.

2.3.1 Ventilation rate

The ventilation rate corresponds to the total air flow within a region under study. It depends mainly on the wind features (speed and direction) and the geometry of the region.

Besides being used as input to find the cloud sizes the ventilation can also be used to decide which leak rate to simulate in order to find the largest flammable cloud (Qiao (2010)).

2.3.1.1 Wind speed and direction

The wind speed is important for the mixture between air and fuel, yielding a flammable cloud. As the wind speed increases, the gas is carried downwind faster, but the material is also diluted faster by a larger quantity of air, which can lead to a large flammable cloud.

The analysis of the influence of wind direction is related to the geometry of the module. The presence of a large structure in the module, depending on the wind direction, will cause great restriction to the air flow through the module. As consequence, if a gas cloud is formed, it will be impeded to disperse and will accumulate in a certain part of the module.

2.3.1.2 Geometry of the module

The air flow inside a module is often controlled by the presence of large structures into or near it. They will create large recirculation zones and set up the major patterns flow (Qiao (2010)). It is important to model such structure elements correctly.

2.3.2 The gas release

The release behaviour is one of the most important factor in dispersion analysis, being determined by interaction of the momentum and buoyancy driven motions (HSE (1992)). However, others factors about the release may also affect the gas dispersion and the generation of the flammable cloud and must be considered.

2.3.2.1 Gas density

The buoyancy represents the effective gravity force and depends on the relation between the gas and air density (Kundu (2002)). Thus the density can be considered the main property of the gas that influence the buoyancy forces and the mixture air-gas.

In practice, a gas lightweight will rise faster after leak and can be diluted by ventilation giving a great flammable gas cloud. On the other hand, a air-dense gas mixture will take place more slowly and the region of flammable gas could be smaller (Qiao (2010)).

The leak conditions, as pressure and temperature, that affect the gas density are also important.

2.3.2.2 Leak rate and direction

The leak rate directly influences the release momentum motion and, consequently, its behaviour. The interaction of the leak rate with the ventilation flow is also important to form the flammable gas cloud and must be analysed.

In general, a small release of gas can be easy diluted by ventilation and disperse while, a large release is harder to disperse. However the intensity of dispersion depends also on ventilation rate. For example, both configurations: small release with small ventilation rate and large release with high ventilation rate may originate a great flammable cloud. In contrast, a small release with a high ventilation rate and a large release with a small ventilation rate may yield a small region of flammable cloud (Cleaver *et al.* (1994)).

The relationship between leak and wind direction must be considered too. The mixture process of air-gas can be more effective when the leak is in the opposite direction to the wind, giving large flammable gas clouds.

2.3.2.3 Leak location

The analysis of the leak location is related with the gas density. For a module with different elevations, for example, the leak at low elevation with dense gas creates a gas cloud that is too rich to ignite at the lower part of the module. While, the higher the leak elevation, the easier the gas

gets diluted and, consequently, creates a large flammable cloud (Qiao (2010)).

2.4 Estimating the flammable gas cloud size

Lees (2005) presents analytical models developed by different authors to estimate the mass of gas within the flammable range in a cloud from a flammable gas release. They take into account the gas properties and the release behaviour. The wind behaviour is computed with the release behaviour and the effect of the geometry or process plant are neglected.

Epstein & Fauske (2007) have developed analytical expressions to predict the flammable fuel mass, the total flammable mass (fuel + entrained air) and the volume of the flammable region within a buoyant fuel-jet release. Such expressions are based on basic dimensionless parameters as Froude Number and include the effects of release momentum, buoyancy and orifice geometry. The analytical expressions could predict average fuel concentrations in the flammable regions of the clouds, which serve as indicators of the severity in case of vapour cloud explosions.

Like other analytical methods, the approaches discussed above consider mainly the release behaviour, but for risk analysis a more complete study is necessary.

Cleaver *et al.* (1999) have developed simple correlations to predict the flammable gas cloud size for a range of a gas releases scenarios. Experimental work was carried out using an offshore module with three different configurations of confinement. A high pressure natural gas releases was defined from three different release locations with five orientations at each one. The behaviour of both release and ventilation were analysed. Measurements were made of the gas release rate and exit conditions, the external wind speed and direction, the atmospheric conditions, the gas concentration and flow velocities within the module.

Based on the experimental results, Cleaver *et al.* (1999) mustered the parameters that affect the volume of gas-air mixture (within a flammable limits) on dimensionless groups, giving the following correlations:

$$L = V^{1/3} \tag{2.1}$$

$$R = \frac{m/\rho_s}{U_v L^2} \tag{2.2}$$

where:

L is the length scale for the module;

R is the dimensionless release parameter;

V is the volume of the module;

m is the mass flow rate of gas released;

ρ_s is the density of the gas at the release condition; and

U_v is the average ventilation velocity within the module.

It was observed that the release parameter (R) is related to the filling degree of the module by flammable mixture. Besides, for small releases the flammable volume is independent of the length scale of the module.

Starting from these conclusions, a simple correlation was developed to express the flammable gas cloud size dependence form:

$$\frac{V_f}{L^3} \propto R^{3/2} \quad (2.3)$$

Recently, Das & Weinberg (2012) have developed a methodology to improve the estimation of flammable mass for vapour cloud explosion modelling in offshore quantitative risk assessment. The method is based on a traditional ignition probability model known as *UKOOA* model.

According to the authors, the *UKOOA* model is based on a four-area approach using the area of each as a basis for assigning an ignition probability. A volume of flammable vapour is calculated in each of the four regions and is given as input of the probability model.

Das & Weinberg (2012) have modified the *UKOOA* model by accounting the effect of mitigation measures on release rate and adding a directional probability for wind. The platform geometry, congestion factors, offshore conditions, release direction and location and wind direction were also considered. Analytical correlations were developed for gas release and its dispersion. The results provided by these correlations were compared with CFD simulations giving good approximation. When it was compared with the conventional method, the new method provided better estimates of flammable mass.

The correlations developed by Das & Weinberg (2012) are more complex than that ones presented by Cleaver *et al.* (1999). They require more knowledge about the geometry of the module under study and the offshore conditions where it is installed. On the other hand, the Cleaver *et al.* (1999)'s correlations are easier to apply and can provide good estimations about the flammable cloud size, even when little is known about the geometry.

Chapter 3

Mathematical Modelling and CFD

In CFD, to solve any physical problem, the first step is to know well the phenomena and the system under study. It will permit to construct a mathematical model correctly and choose the best numerical tool. In the mathematical model it is important to include the identification of the system variables and their applications as well as the conditions of the study.

Once the problem is modelled, it is necessary to make use of some software with a CFD code. The CFD codes generally present four main elements: a geometry generator, a pre-processor (mesh and set up), a solver and a post-processor.

3.1 Mathematical modelling

In Fluid Mechanics the equations that govern the flow are obtained applying the principle of conservation to the following quantities:

- Mass;
- Momentum;
- Energy;

The application of each equation depends on the characteristic of problem. In some cases it is not necessary to solve all these equations while in other circumstances the utilisation of additional

model is required.

3.1.1 The mass conservation

The mass conservation in the differential form is shown below. The equation is also known as the *Continuity equation*:

$$\frac{\partial \rho}{\partial t} + \nabla \cdot (\rho \mathbf{u}) = 0 \quad (3.1)$$

The first term in left hand side represents the rate of change of fluid density with time. For flows in steady state this term is equal to zero.

The second term is the divergence term. It indicates the rate of change of the specific mass with respect to the spacial coordinates.

A fluid is usually called incompressible if its density does not change with pressure. In this case, and for steady state, the continuity equation becomes (equation 3.2):

$$\nabla \cdot \mathbf{u} = 0 \quad (3.2)$$

3.1.2 The momentum equation

The momentum equation, expressed in equation 3.3, originates from the application of Newton's second law of motion to an element of fluid. It includes the principle of angular moment and represents the variation of momentum as function of resultant forces acting on the fluid.

$$\frac{\partial}{\partial t}(\rho \mathbf{u}) + \mathbf{u} \cdot (\nabla \rho \mathbf{u}) = \rho g - \nabla P + [\nabla \tau] \quad (3.3)$$

The equation 3.3 can be applied to all directions of fluid flow. The group of equation is so called *Navier-Stokes Equations*.

The first term in the left represents the rate of increase of momentum while the second take into account the rate of momentum addition by convection and molecular transport.

The terms in the right represent the body force and pressure gradient, respectively. The last term in equation 3.3 is a second order tensor that computes the viscous effects.

Similarly to Continuity Equation, the equation of motion can be simplified according some flow features:

- The Navier-Stokes Equations to a Newtonian fluid and incompressible flow can be written as:

$$\frac{\partial}{\partial t}(\rho \mathbf{u}) + \mathbf{u} \cdot (\nabla \rho \mathbf{u}) = \rho g - \nabla P + \mu \nabla^2 \mathbf{u} \quad (3.4)$$

- For inviscid flow, the viscous effects could be negligible ($\mu = 0$):

$$\frac{\partial}{\partial t}(\rho \mathbf{u}) + \mathbf{u} \cdot (\nabla \rho \mathbf{u}) = \rho g - \nabla P \quad (3.5)$$

The equation 3.5 is the most common simplified form of Navier-Stokes Equations and it is known as *Euler Equation*.

3.1.3 The energy equation

The energy equation contains a large number of influences. For pure Newtonian fluids with ρ , \hat{C}_p , k and μ physical constants, the most general form is presented below (equation 3.6):

$$(\rho \hat{C}_p) \frac{D}{Dt} T = \nabla \cdot (k_T \nabla T) + \mu \phi_v + S_h \quad (3.6)$$

Here, \hat{C}_p is heat capacity at constant pressure (the circumflex over the symbol indicates a quantity per unity of mass), k_T is the thermal conductivity, ϕ_v is the dissipation function and the term S_h indicates the volumetric rate of heat generation. The dissipation function is usually negligible, except in systems with large velocity gradients (Bird (2002)).

The substantial derivative term can be written as $\frac{D}{Dt} = \frac{\partial}{\partial t} + \mathbf{u} \cdot \nabla$ so that the equation 3.6 becomes:

$$\frac{\partial}{\partial t}(\rho \hat{C}_p T) + \nabla \cdot (\rho \mathbf{u} \hat{C}_p T) = \nabla \cdot (k_T \nabla T) + \mu \phi_v + S_h \quad (3.7)$$

3.2 Turbulence

The great majority of fluid flows encountered in daily life and with practical engineering applications are turbulent.

Turbulence can be defined as an irregular motion of fluid flow in which the various quantities show a random variation with time and space coordinates, so that statistically distinct average values can be discerned (Wilcox (1994)).

Kundu (2002) mention some characteristics of turbulent flows:

- Irregularity - The flow is irregular, random and chaotic and consists a spectrum of different scales (eddy sizes). The largest eddies are the order of the flow geometry and the smallest eddies are given by viscous forces .
- Large Reynolds Number - Turbulence occurs at high values of Reynolds number, when inertial forces become more important than the viscous forces.
- Effective transport - In turbulent flows, the fluid particles are fast mixed while they are moving through the flow. As consequence, the transport and fluid mixture is much more effective compared with laminar flow.
- Three dimensional - Turbulent flow is always three-dimensional. The motion of fluid particles occurs due to fluctuations in position and time in a three dimensional velocity field.
- Dissipation - Turbulent flow is dissipative, which means that kinetic energy in smallest eddies are transformed in internal energy. The kinetic energy is transferred through different sizes of eddies from the largest to the smallest. The process of energy transfer is called energy cascade process.
- Continuum - The turbulent flow can be treat as continuum, even though the smallest turbulent scales in the flow are larger than the molecular scale.

At first, the Navier-Stokes equations describe both laminar and turbulent flows without the need of additional information. However, modelling turbulent flows span a large range of turbulent length and time scales and would generally involve length scales much smaller than the smallest

finite volume mesh used in numerical analysis (ANSYS CFX (2011)). The numerical solution of all scales is impractical when considering the current computational resources.

To compute turbulence and explore the greatest possible amount of its effects in the fluid flow some turbulence models have been developed.

3.2.1 Turbulence models

The available methods to solve the turbulence and calculate the quantities of interest are classified into two main groups.

In first group we can find the models capable to completely solve mathematically the transport equations and, consequently, the turbulence. The main method used in these models are the *Direct Numerical Simulation* (DNS).

In DNS, the equations are directly solved for all length and time scales of fluid flow. This method can capture all relevant phenomena without approximation or simplification, including the smallest scales. DNS can be considered the best way to solve the turbulence, but because all length-scales and time-scales are solved, DNS is computationally expensive. As the computational cost increases with Reynolds number ($\approx Re^3$), DNS is restricted to flows with low to moderate Re (Hirsch (2007)).

Other turbulence models as *Reynolds Averaged Navier-Stokes* (RANS) and *Large Eddy Simulation* (LES) are not able to capture all phenomena that involve the fluid flow. They are used to solve the transport equations for a mean velocity flow field and require less computational effort than DNS.

In RANS models all turbulent effects are modelled and the quantities are calculated based on their average values. Because RANS simulations do not directly solve the transport equations and turbulence scale, it is expected to be less accurate and reliable than LES and DNS. However, it has been presented good performance for many engineering studies with low computational costs. RANS methods are the most widely used approach in CFD simulations of industrial flows.

The *Large Eddy Simulation* is a method that partly solve the transport equations. Andrey Kolmogorov has defined the small length scale as the ones that could exist in a fluid flow without energy dissipation (*Kolmogorov scale*). In LES the equations are directly solved (as in DNS) for

large turbulent eddies, with length down to the Kolmogorov scale. The effects in smallest eddies are modelled using a *sub-grid* model. It is enough to capture most part of the turbulence effect with good accuracy.

Because it does not solve small scales, LES requires less computational effort than DNS but, when compared with RANS, LES is more computationally expensive. The LES models can be applied in situations where DNS is inapplicable, but its utilization is limited to moderate values of Reynolds number.

3.2.1.1 RANS models

In turbulent flows the properties exhibit aleatory fluctuations that must be considered. The Reynolds Stresses theory uses the concept of mean flow to solve turbulent problems (Pope (2000)). According to this theory the values of the properties are expressed as the sum of the average values and their respective fluctuations:

$$\Phi = \bar{\Phi} + \Phi' \tag{3.8}$$

where Φ is the value of the variable in a specific time, $\bar{\Phi}$ is its average time and Φ' is the turbulent fluctuation in a instant.

Figure 3.1 shows a example of an instantaneous velocity and its fluctuations around the mean velocity in a turbulent flow.

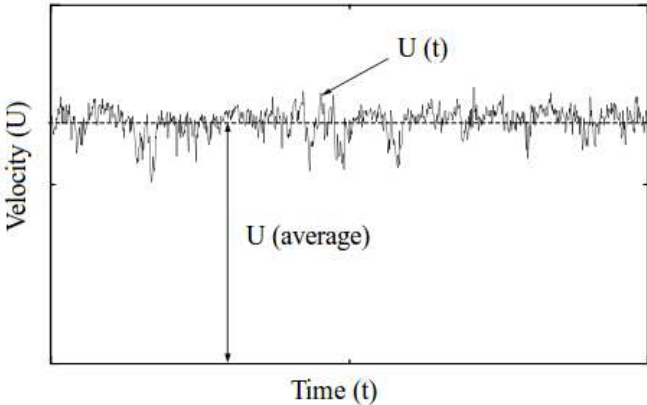


Figure 3.1: Fluctuations in a turbulent flow.

In RANS, the Navier-Stokes equations are modified by introducing average terms to represent the mean value of the variables in fluid flow. Such procedure introduces additional unknown terms, called "Turbulent" or "Reynolds" Stresses, that must be calculated in order to achieve the solution of the problem. The equations used to close the system define the turbulence model (ANSYS CFX (2011)).

The RANS models can be divided into two main classes: the eddy viscosity models and Reynolds stresses models.

Eddy viscosity models consider that turbulence consists a small eddies which are continuously forming and dissipating. They also assume that Reynolds stresses are proportional to mean velocity gradients. The main turbulence models in this category are:

- *Zero-Equation* or algebraic model;
- *One-Equation* model;
- *Two-Equation* models: $k-\varepsilon$, RNG $k-\varepsilon$ and $k-\omega$.

In Reynolds stresses turbulent models, all components of Reynolds stress tensor and the dissipation rate are presented in transport equations. Such equations are solved for the individual stress components. Here, the most common models are:

- Standard *Reynolds Stress* model: SSG and LLR;
- *Omega-Based Reynolds Stress* model.

The correct choice of the most appropriate turbulence model is crucial to a successful modelling and CFD simulation of a real problem as the dispersion of toxic and/or flammable substances.

3.2.1.2 The $k-\varepsilon$ model

The $k-\varepsilon$ model is considered the industry standard model and has proven to be stable and numerically robust. For general purpose simulations this model offers a good compromise in terms of accuracy and robustness (ANSYS CFX (2011)).

Cormier *et al.* (2009) have studied the key parameters that influence the application of computational fluid dynamics for LNG (liquefied natural gas) vapour dispersion modelling. Tests were performed to provide real data and three turbulence models were compared to modelling LNG release using CFD. They concluded, in concordance with other authors, that the SSG-RSM model provides the best fit, while the k - ε and RNG k - ε models were slightly less apt. However, the k - ε model requires lesser computational time, which makes it the most used model for gas dispersion simulation.

In k - ε model, k is the turbulent kinetic energy and ε is the turbulence dissipation rate. The values of k and ε can be directly obtained from differential transport equations as follows:

$$\frac{\partial}{\partial t}(\rho k) + \nabla \rho u k = \nabla \left(\left(\mu + \frac{\mu_t}{\sigma_k} \right) \nabla k \right) + (P^k - \rho \varepsilon) + P^{kb} \quad (3.9)$$

$$\frac{\partial}{\partial t}(\rho \varepsilon) + \nabla \rho u \varepsilon = \nabla \left(\left(\mu + \frac{\mu_t}{\sigma_\varepsilon} \right) \nabla \varepsilon \right) + \frac{\varepsilon}{k} (C_{1\varepsilon} P^k - C_{2\varepsilon} \rho \varepsilon + C_{1\varepsilon} P^{eb}) \quad (3.10)$$

where $C_{1\varepsilon}$, $C_{2\varepsilon}$, σ_k and σ_ε are constants (see Table 3.1). P^{kb} and P^{eb} represent the influence of buoyancy forces and P^k is the turbulence production due to viscous forces.

In equations 3.9 and 3.10 above, μ_t is the turbulent viscosity. The k - ε model assumes that this term is linked to the turbulent kinetic energy and dissipation by the following relation:

$$\mu_t = C_\mu \rho \frac{k^2}{\varepsilon} \quad (3.11)$$

Here, C_μ is a constant of the model also given in Table 3.1.

Table 3.1: Constant values for the standard k - ε turbulence model (ANSYS CFX (2011)).

Constant	Value
C_μ	0.09
$C_{1\varepsilon}$	1.44
$C_{2\varepsilon}$	1.92
σ_ε	1
σ_k	1.3

Chapter 4

Response Surface Methodology

The response surface methodology (RSM) comprises a collection of statistical and deterministic techniques that are used to model and to analyse problems wherein one or more response variables are affected by many independent (or controlled) variables and the relationship between both is unknown. The main idea of this method is to explore the influence of each independent variable on the response and find its optimal value over a certain region of interest (Hill & Hunter (2002)).

4.1 The basic ideas about Response Surface Methodology

According to RSM, a response variable, y , can be describe as a function of the most important control (or independent) variables (x_1, x_2, \dots, x_k) and the relationship between these variables can be approximated by a polynomial model:

$$y = f'(x)\beta + \epsilon \quad (4.1)$$

f' is a vector function of p elements that consists of powers and cross-products of powers of x_1, x_2, \dots, x_k up to a certain degree, β is a vector of p unknown constant coefficients refereed to as parameters and ϵ is a random experimental error assumed to have a zero mean.

The Response Surface Methodology consists of two main steps: design of experiments and the statistical modelling.

4.1.1 Design of experiments

In design of experiment, a reasonable number of tests are carried out in order to collect data to statistical analysis. Such tests consist of making changes on the input variables to identify the modifications in the output response. In each case, one specific response y is observed and it is correlated with a particular configuration of independent variables.

Mathematically, each experiment can be represented by a point with coordinates $x_j = (x_{1j}, x_{2j}, \dots, x_{nj})$ in a n -dimensional space and a value of y_j is observed.

In the design of experiments the independent variables involved in the process under study are called factors and the values that they can assumed are the levels. The experiments involve different combinations among the levels of two or more factors (Rodrigues & Iemma (2005)).

The factorial design is represented by the notation N^k , where k represents the number of factors and N the levels. Through this relation, it is possible to obtain the number of experiments that must be performed.

It is most common and easier to analyse the variables into two or three levels.

4.1.2 Statistical modelling

In this stage, the data obtained in experiments are interpolated giving a response surface. The polynomial model is also chosen in order to describe such surface and to predict the correlation between variables with good accuracy. The selection of the model depends on the aim of the study.

According to Box & Draper (1987), in most cases, a first-order (linear) or a second order (quadratic) polynomial model is used:

$$y = \beta_0 + \sum_{i=1}^k \beta_i x_i + \epsilon \quad (4.2)$$

$$y = \beta_0 + \sum_{i=1}^k \beta_i x_i + \sum_{i \neq j} \sum \beta_{ij} x_i x_j + \sum_{i=1}^k \beta_{ii} x_i^2 + \epsilon \quad (4.3)$$

The first-degree model is commonly used at the preliminary stage of the investigation or when the interest of the study is to approximate the response surface over a relatively small

region of independent variables. Such model can be described just in terms of the main variables or considering the interaction among these variables. In the first case, the response is a flat surface and when the interaction is considered, one curvature is introduced into the response function. However, in many cases the true response surface curvature is strong and the first-order model is inadequate (even with the interaction term included). In these situations, a second-order model is required.

The second-order model is the most common in response surface methodology. Many experimental studies use second-order models to solve real response surface problems with good approximation. The main reason for its great applicability is the flexibility of this model, which allows different functional forms.

An important consideration concerning the selection of the polynomial model is the computation costs. After to a certain degree, the increase rate in the polynomial accuracy reduces, while computational cost increases exponentially. Furthermore, higher order polynomials can exhibit misbehaviour in the sub-domains that are not covered by the experiments.

4.2 The RSM applications

The RSM was first used by Box and Wilson in 1951 (Box & Wilson (1951)). They identified this technique as a cheap and easy tool to predict response values for particular configuration of the control variables with good level of reliability, even though little is known about the process. Thereafter, the RSM has been applied in many fields, especially as an optimization tool.

Response surface methodology has been proposed, for example, as a tool for rapidly optimizing the activation parameters in order to obtain the highest possible CO_2 capture capacity of activated carbons. The optimum values of activation temperature and burn-off degree that maximize CO_2 uptake by the activated carbons (at 35 °C and atmospheric pressure) were obtained within the experimental region (Gil *et al.* (2013)).

Another application using the RSM is optimization of reaction conditions of cardanol-based epoxidised novolac resin (CNE) production proposed by Minakshi *et al.* (2011). It was possible to establish a relationship between the process variables and the extent of conversion

under a wide range of operating conditions which resulted in different extent of conversions. The predicted values obtained by the model were close to the experimental values indicating suitability of the model.

Mathematical models can also be developed using numerical data (experiments). Zhao *et al.* (2007) have performed numerical simulations of a demister vane with various geometries and operating conditions to study its separation efficiency. The prediction model was obtained based on RSM capable to estimate the effects of different geometries and operation conditions on the separation efficiency, and that could direct the optimum design of demisters. The predictive results were compared with some experimental and numerical data and it was found good agreement between them.

In process engineering, the response surface methodology has several applications improving and optimizing processes. Rastegar *et al.* (2012), for example, have used RSM to improve the performance of a bioreactor for treatment of petroleum refinery effluent. The bioreactor was used for waste-water treatment and simultaneous biogas production. It was possible to find models to reduce the effluent chemical oxygen demand and biogas production based on three critical factors giving better results than before optimization.

Jaliliannosrati *et al.* (2013) have used the response surface methodology to analyse the biodiesel production by two-step reactive extraction using a microwave system. It was investigated the influence of process variables (partCicles seed size, time of irradiation, agitation speed and catalyst loading) on conversion of triglyceride (TGs). The highest biodiesel yield (90.01 %) and conversion (97.29 %) were achieved at the optimum condition and the RSM could accurately predict the experimental results (regression coefficient ≈ 0.977).

The RSM has also been used in process control to ensure its safety and efficiency. Coetzer *et al.* (2008) have studied a fixed bed dry bottom gasification process. The response surface method was employed to construct a model for the pure gas yield and to calculate its propagating variance through the model due to the variability in the hard-to-control variables (coal particle size distribution and coal composition). It was presented an effective method for determining the optimum values for these variables which maximize the pure gas yield and simultaneously minimize its variance.

The examples above show that the response surface methodology has been widely applied to optimize process. On the other hand, few applications of RSM to process safety have been

considered.

Oyewole & Cant (2010) have used RSM to provide a safety model with the aim of minimizing incident rates. Safety intervention data were collected from the environmental health and safety department of an oil company. The model was developed to determine the safety intervention factors and interactions which minimize incident rates, with the aim of predicting a better resource allocation strategy.

Using numerical simulations (in CFD) and applying the RSM, Vianna (2012) has developed a predictive model to calculate the overpressure generated during an explosion. The mathematical model allowed to find the desired response using two main variables as input: the gas cloud size and the ignition point.

Huser & Kvernfold (2000) developed a work applying the response surface methodology to predict the generation of a flammable gas cloud. The authors have found a mathematical model to calculate the flammable gas cloud size on offshore platforms using the correlations described by Cleaver *et al.* (1999). A large number of CFD simulations, with different scenarios of gas releases, have been carried out to obtain response surfaces.

This methodology allowed to calculate the flammable gas cloud size using two response surfaces: one considering the influence of wind speed and the leak rate and the other dealing with the wind direction.

The effects of wind speed and leak rate were combined in a non-dimensional variable R , with the same physical meaning that one developed by Cleaver *et al.* (1999):

$$R = \frac{Q_g}{Q_a} = \frac{m/\rho_g}{(Q_{aref}/u_{ref})u} \quad (4.4)$$

where:

u is the wind speed;

Q_{aref}/u_{ref} is the reference ventilation rate;

Q_g is the gas volumetric flow rate;

Q_a is the air volumetric flow rate;

Using the value of R as input, it is possible to calculate the flammable gas cloud size by

the following equations:

$$\frac{V_f}{V} = \frac{C_3}{1 + \frac{1}{C_1 R^{P_1}} + C_2 R^{P_2}} \quad (4.5)$$

Here V is the volume of the module under study, V_f is the flammable gas cloud size and P_1 , P_2 , C_1 and C_3 are constants to be determined from CFD analysis in order to obtain the best fit. The parameter C_2 is derived from the second equation (Equation 4.6) as function of the maximum cloud size.

$$\frac{V_{fmax}}{V} = \begin{cases} A + B \cos(\alpha - \alpha_{max}) & \alpha \neq \alpha_W \\ \frac{V_{fmaxW}}{V} & \alpha = \alpha_W \end{cases} \quad (4.6)$$

The parameters in Equation 4.6 are:

A and B - constants dependant of the leak direction, determined from CFD simulations;

α - the wind direction;

α_W - the wind direction that opposes a large structure in the module causing large recirculation zones and, consequently large clouds;

α_{fmax} - the wind direction that gives the largest gas cloud, except α_W . It is related to the leak direction;

V_{fmax} - the largest flammable cloud.

The method developed by Huser & Kvernfold (2000) has brought advances in the analysis of flammable gas clouds, especially for making it independent of the installation. However, the use of two equations is not still desirable. It suggest that further studies must be conducted in order to improve the method and its reliability.

Chapter 5

Case Study

This chapter shows the considerations and tools that were adopted in the dispersion simulations and development of the response surface model.

5.1 Geometry and mesh

A typical offshore module was chosen to be used as geometry under study. As seen in Figure 5.1, the platform is considered having two deck levels, which comprise the process area. Its size is 110 m x 100 m and it lies at 55 metres above sea level.

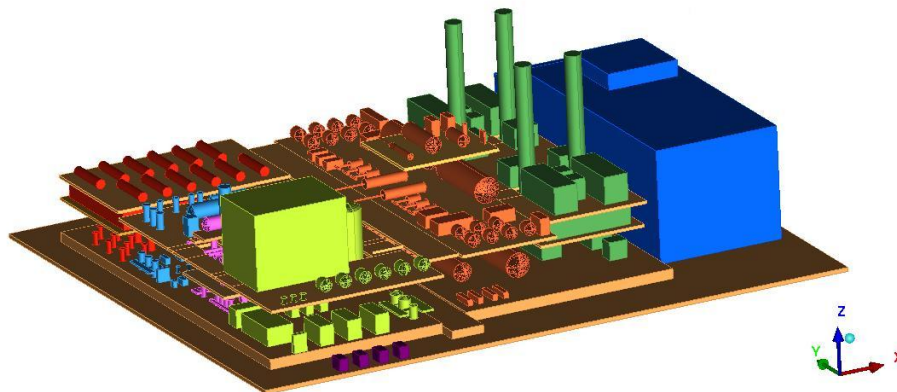


Figure 5.1: A platform geometry based in an offshore module.

In some preliminary analysis only a single deck (Figure 5.2) was considered. During the study of the wind speed profile and computational domain size a simplified geometry was used in order to spend less computational effort.

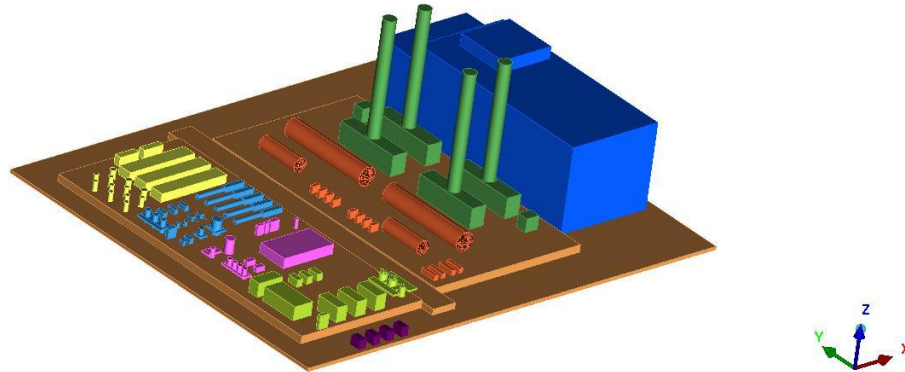


Figure 5.2: Simplified geometry with a single deck (Main Deck).

Due the complexity of the geometry a unstructured tetrahedral mesh was adopted. The software *ANSYS ICEM - 11.0* was used to construct the geometry and mesh.

5.2 Design of the dispersion simulations

Based on the findings from the design of experiments discussed in Section 4.1.1, the range of the variables relevant for the analysis were identified.

5.2.1 Variables of interest

The variables of interest in this study are those that influence the gas dispersion and also the flammable cloud size, discussed in Chapter 2. However, to develop the response surface, two main factors were considered: one that accounted for the effect of the ventilation and leak rate, and other that computed the relation between the wind and leak direction.

5.2.1.1 Ventilation and leak rate

Based on the works conducted by Cleaver *et al.* (1999) and Huser & Kvernfold (2000), the ventilation and leak rate were analysed through the non-dimensional factor " R " (Equation 4.4).

Huser & Kvernfold (2000) argue that the flammable cloud size increases as R increases, until it reaches the maximum value and then it reduces. Based on the historical measurements the maximum flammable cloud size is achieved for $R = 0.1$ and that for large values of R the cloud size is too little.

In risk analysis, when developing a response surface, we are interested in the worst case scenario. It corresponds to the maximum achievable overpressure that is fairly related to the largest flammable cloud. Therefore, a range from 0.03 to 0.3, for the parameter R was selected in order to account for various cloud sizes.

5.2.1.2 Leak and wind direction

The effect of leak direction and wind direction was combined in a variable named " ϕ " (φ). It was defined as the angle formed between the leak and wind direction.

Eight wind directions were considered as illustrated in Figure 5.3 below.

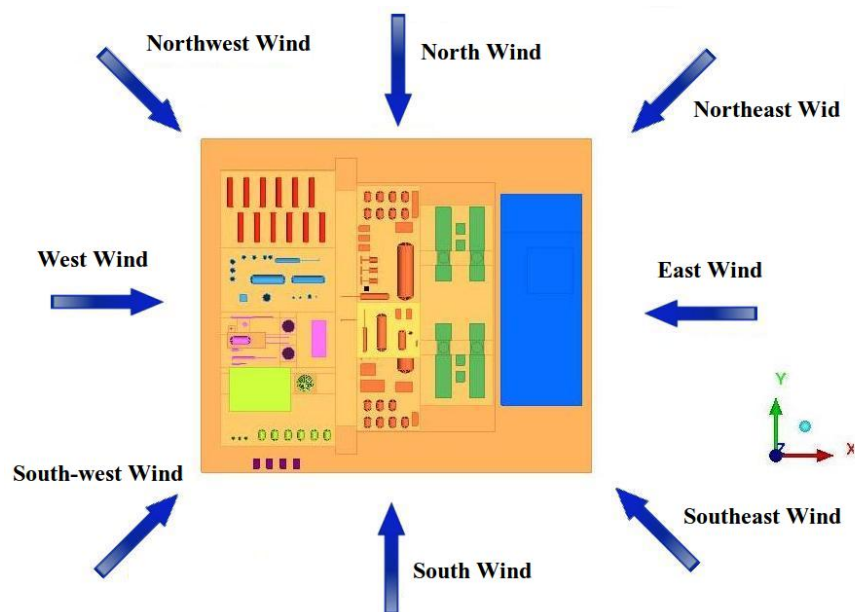


Figure 5.3: Wind directions in the platform.

It is important to note that, the wind direction coming from east interacts with the accommodation module (represented by the large blue block in the right side of the platform - Figures 5.1 and 5.3). Large recirculation zones are created into the module and the ventilation rate is considerably reduced. So the wind coming from east had to be carefully analysed.

The leakage was represented by a little box in the centre of the platform and can take six orthogonal directions: x^+ , x^- , y^+ , y^- , z^+ and z^- . The identification of these directions was assessed according to the platform orientation. Figure 5.4 shows the possible orientations and the leakage representation into the module.

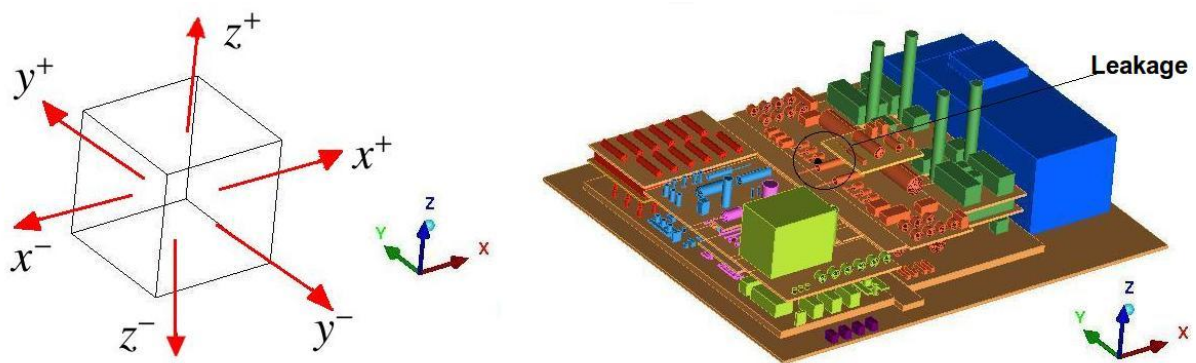


Figure 5.4: Possible directions of the leakage and its representation into the platform.

Considering the leak directions, for the orientations x and y , the angle φ is given as following:

- $\varphi = 0$: the leakage and the wind have the same direction;
- $\varphi = 180$: the leakage and the wind have the opposite direction;

For a specific leak direction " β ", taking as reference $\varphi = 0$, the others values of φ were found varying the wind direction in counter-clockwise. Figure 5.5 shows a example where $\beta = y^+$, the same approach was adopted to leak directions x^+ , x^- and y^- .



Figure 5.5: Schematic representation of the angle φ for a leakage in the direction y^+ .

The leak directions z^+ and z^- were analysed apart. Because the wind is perpendicular to the leakage the angle φ is the same for all wind directions.

The angle φ is a qualitative variable and can take values among 0° and 360° . Ranging from 45 degrees it gives 9 possible amounts, which is not desirable in design of experiments.

Considering φ in a trigonometric cycle, four quadrants were established, each one with three values of φ :

- Quadrant 01: $\varphi = 0^\circ, 45^\circ$ and 90° ;
- Quadrant 02: $\varphi = 90^\circ, 135^\circ$ and 180° ;
- Quadrant 03: $\varphi = 180^\circ, 225^\circ$ and 270° ;
- Quadrant 04: $\varphi = 270^\circ, 315^\circ$ and 360° .

5.2.2 Simulations set up

Based on the variables and their range, an experimental design 3^2 was conducted for each quadrant where the variables R and φ taken on three values. For the variable φ , the values of the quadrants described above were adopted, while for factor R , the values were 0.03, 0.15 and 0.3. Different scenarios of wind and leak direction and wind speed and leak rate were considered to represent the desirable values of R and φ .

5.3 Natural gas composition and release conditions

A typical composition of natural gas in a offshore module was adopted in the simulations (Table 5.1).

Table 5.1: Natural Gas Composition.

Component	Molar Fraction
C_1	0.861
C_2	0.071
C_3	0.030
C_4	0.013
C_5^+	0.010
CO_2	0.005
N_2	0.010

A pressurized gas pipeline was considered. The average pressure was taken as 200 kgf/cm².

In pipelines at high pressure, the fluid flow at the leakage is sonic, which involves high pressure and velocity gradients. For gas flow, great variations in pressure lead to changes in specific mass and temperature, and the compressibility becomes an important factor in the fluid flow. All these conditions increase the complexity of the numerical solution.

To solve this question, HSL (2003) suggests that the region near the leakage is not modelled. The leakage modelling starts a little further the release point where the flow can be considered subsonic. This simplification is possible by keeping the mass flow constant and taking an orifice area that gives a velocity lower than 360 m/s (sound speed).

5.4 Boundary conditions and solver parameters

The simulations were performed using the *ANSYS CFX 12.0* CFD software. This software uses an element-based finite volume method. The boundary conditions and parameters used at the simulations are presented in Tables 5.2 and 5.3, respectively.

Table 5.2: Boundary conditions of the simulations.

Region	Boundary Condition
Surfaces	no slip condition
Leakage	prescribed mass flow
Wind Source	prescribed velocity
Computational Domain Contour	Relative Pressure = 0

Table 5.3: Simulation Parameters.

Parameter	Value or type
Reference Pressure	1 atm
Flow Regime	Stationary and Incompressible (Subsonic)
Turbulence Model	$k - \varepsilon$
Advection Scheme	<i>Upwind</i>
Time scale	Auto timescale (1.0)
Convergence Criterion	RSM
Maximum Residual	1×10^{-5}
Minimum and Maximum Number of Iterations	100 - 1000

In Table 5.2, the no slip condition indicates that the velocity on the surfaces is zero. It means that a boundary layer is developed in the fluid flow and the velocity increases from the surfaces until the flow is fully developed.

At the regions "*leakage*" and "*wind source*" the boundary conditions assumed prescribed values. The vector that represents the mass flow and the velocity is directed into the computational domain enabling the entrance of fluid flow.

In fourth boundary condition, the relative pressure was set to zero which ensures no pressure difference between the computational domain and the outer region. Thus the domain contour represents just a limit for the calculations and the outer region of the computational domain can be understood as a continuation of the internal region.

In Table 5.3, the first parameter indicates that the value of 1 atm was used as the reference pressure for the calculations.

The simulations were conducted considering the stationary and incompressible flow regime. The flammable cloud size is calculated when it reaches the stationary condition: the cloud

stops to grow and presents a constant volume.

In numerical solution of the transport equations a Reynolds-Averaged Navier Stokes (RANS) approach was used. The $k - \varepsilon$ turbulence model was chosen because it provides good results for dispersion simulations and is easy to apply (as discussed in Section 3.2.1.2).

In CFX solver different discretization methods are applied to solve the differential equations. First and second order advection schemes can be selected to calculate the advection terms in the discrete finite volume equations. Based on the finite-element method, shape functions are used to evaluate the diffusion terms.

The *Upwind* scheme was chosen to solve the advection terms in the discretized equations. It is a first order numerical scheme and gives a robust performance for typically convective problems (as gas dispersion for example).

In the upwind scheme, interpolation functions are used to estimate the magnitude of the variables and its derivatives on the faces of the control volume from their respective values at the nodal point (ANSYS CFX (2011)). The value of the property ϕ at an interface is equal to the value of ϕ at the grid point on the *upwind* side of the face.

For steady-state problems, the CFX solver applies a false time-step as a means of under-relaxing the equations as they iterate towards the final solution. The *Auto timescale* is a fluid time-scale control option that uses an internally calculated physical time-scale based on the boundary conditions, flow conditions and domain geometry. This is usually robust and conservative (ANSYS CFX (2011)). The factor 1.0 was used as multiplier the auto time-scale value calculated by the solver.

The RSM (Root Mean Square) residual was used as the convergence criterion. It represents a measure of how well the solution is converged and can be obtained by plotting the residuals for each equation at the end of each time-step. A reasonably converged solution requires a maximum residual level no higher than 10^{-4} (ANSYS CFX (2011)). The value usually adopted for the maximum RSM residual is 10^{-5} .

A minimum and maximum number of iterations were defined. The first value ensures that a minimum number of iterations is done even if the maximum residual was achieved. For stationary flow conditions it is verified that the convergence criterion must be reached with less than 500 iterations (ANSYS CFX (2011)).

5.5 Estimating the flammable gas cloud size and development of the response surface model

After the dispersion simulations, the flammable gas cloud sizes were calculated using *ANSYS CFX - Post Processor*. Two isosurfaces were defined based on the upper and lower flammable limits of natural gas (UFL = 15% and LFL = 5%, in volumetric fraction). A first isosurface covered the volume where the natural gas concentration was higher than LFL while the second isosurface comprised the volume where the natural gas concentration was smaller than UFL. The flammable region was defined by the difference between these two volumes and the function *volumeInt* was used to calculate the flammable volumes.

The analysis of the data was conducted in the software *Statistica 7.0* that provided the mathematical tools to the development of the response surface model.

Chapter 6

CFD Results

Prior to starting the simulations used in the development of the mathematical model, it was necessary to analyse the parameters that influence the phenomenon in order to obtain a reliable result. This chapter discusses results regarding the release and wind behaviours. It also presents a study of the computational domain size, mesh tests and the effect of accommodation module in the ventilation rate into the platform geometry.

6.1 Study of gas jet release

In accidental release from pressurized pipelines, the momentum of gas is large and it behaves as a jet. An analysis concerning the jet behaviour and how it influences the gas dispersion is necessary once the gas cloud is preceded of it.

CFD studies require experimental data to compare with the model and validate it. In cases of flammable gas dispersion in a process area it is infeasible to collect experimental data. However, it is possible to find several data for jet releases that can be used to validate the simulations of the leakage. Modelling correctly the gas behaviour near the leakage is a way to ensure that all dispersion cases are properly modelled.

Following the validation near the leak release, the jet behaviour was investigated taking into account the gas composition.

6.1.1 Axisymmetric jet simulation

In order to investigate how to model and simulate an axisymmetric jet behaviour, a typical high pressure jet was chosen. It consists a jet of air, originated from an orifice with 2.7 mm of diameter. The exit conditions were Mach number 1 and air density 2.25 kg/m^3 (Birch (1987)).

Figure 6.1 shows the computational domain and mesh that was used in the simulation. A computational domain was defined as a box with size of 0.3 m in its basis and 3 metres of height. An unstructured tetrahedral mesh with a special refinement in the exit and along the central axis of the jet was used, which gave a mesh with 1,700,000 elements.

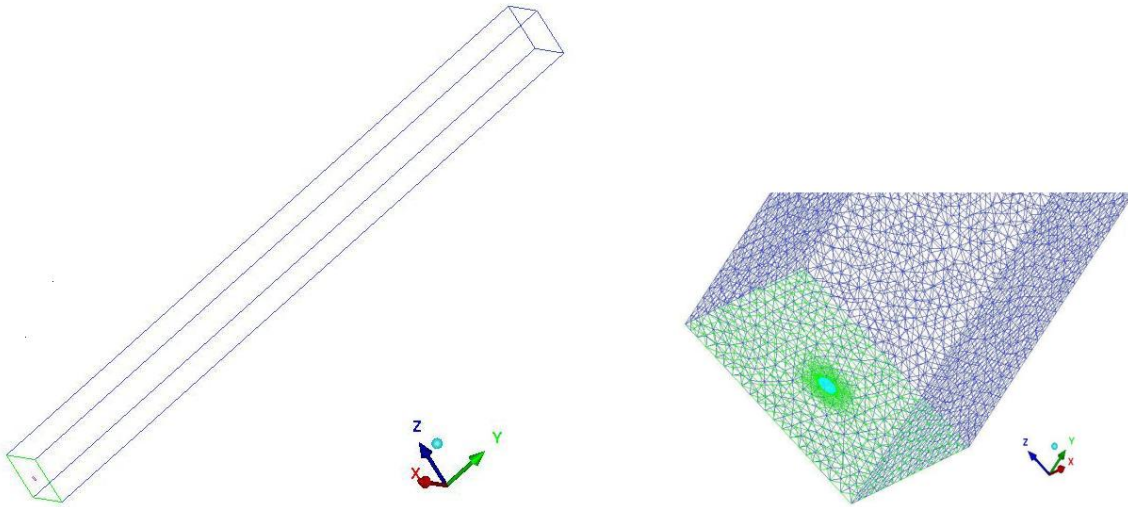


Figure 6.1: Geometry and mesh used in the Axisymmetric Jet study.

The boundary conditions used in this simulation are shown in Table 6.1.

Figure 6.2 shows the result of the simulation. The vertical axis represents a non-dimensional velocity that is defined by ratio between the centreline jet velocity and the velocity at the exit of the jet. The horizontal axis represents the ratio between the axial distance (x) and the orifice diameter (d). It is possible to observe that the simulation result is very close to the experimental data, which indicate that the model used to simulate an axisymmetric jet is appropriated.

Table 6.1: Simulation Parameters for the Axisymmetric Jet study.

Parameter	Value or type
Reference Pressure	1 atm
Flow Regime	Isothermal, Stationary, Subsonic and Incompressible
Turbulence Model	$k - \varepsilon$
Advection Scheme	<i>Upwind</i>
Time scale	auto timescale (1.0)
Convergence Criterion	RSM
Maximum Residue	1×10^{-5}
Maximum Number of Interactions	1000

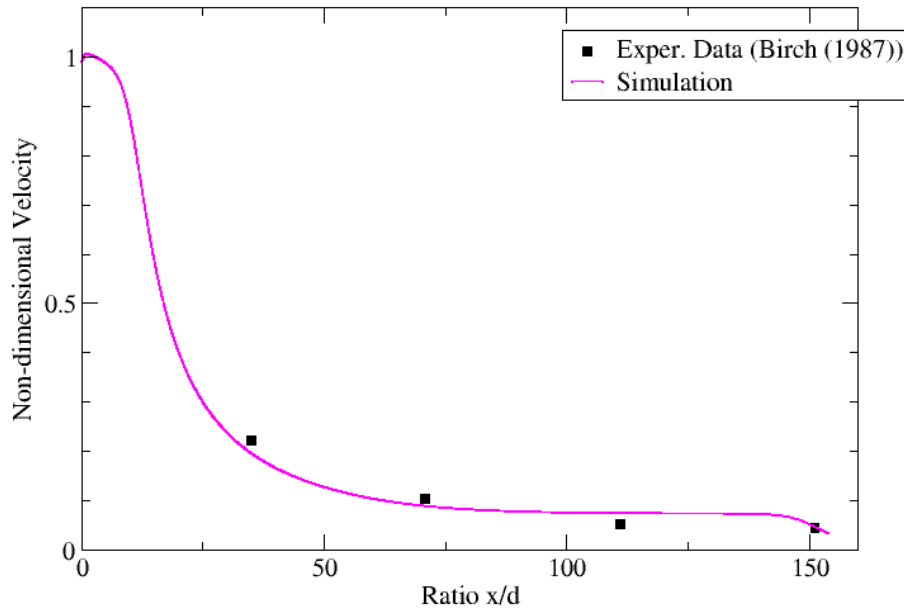


Figure 6.2: Simulation of a high pressure axisymmetric jet.

6.1.2 High aspect ratio jet simulation

The high aspect ratio jet study was performed based on the work of Wakes (2002), who conducted an experimental investigation about the principles that affect the high aspect ratio cross-sectional jet behaviour. An experimental apparatus was built using a pressurized air pipeline with a flange failure in gasket. Several flange failures with different aspect ratio was tested and using different values of pressure at the pipeline.

Figure 6.3(a) shows the geometry of flange leaks used in the work of Wakes (2002). The delta (δ) indicates the gasket thickness (that was 2 mm for all geometries), while α and β indicate the angle of the inner and outer pipe, respectively. Nine different geometries were developed using this configuration and one of them was chosen to be reproduced and model a high aspect ratio jet: $\alpha = 75$ and $\beta = 45$ (6.3(b)).

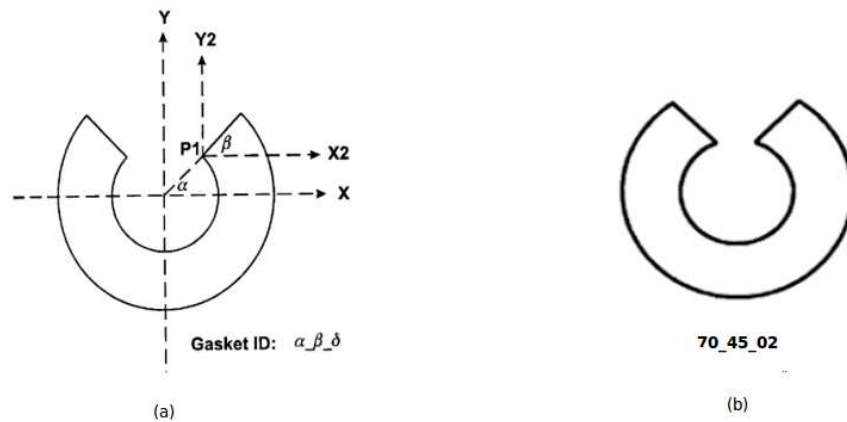


Figure 6.3: Schematic representation of the geometries of flange leaks (Wakes (2002)).

The aspect ratios of the selected geometry are 85.7:1 for the outer pipe and 26.6:1 for the inner pipe. The leak conditions were the pressure of 137.9 kPa and the mass flow rate of 0.15 kg/s.

First, a axisymmetric jet with the conditions described on the Wakes (2002) work was simulated. A circular orifice with 25.5 mm of diameter was defined to represent the leakage and a box with size of 1 m in its basis and 10 m of height was set out as computational domain. A tetrahedral mesh was used and the number of mesh elements were about 2,100,000.

The simulation parameters were the same ones employed in section 6.1.1 (Table 6.1). Figure 6.4 presents the result of this simulation. It is observed that a high aspect ratio behaves in a different way to an axisymmetric jet.

The potential core of the axisymmetric jet is preserved for a larger space compared with a high aspect one, which means that the effective mix gas-air will start later in this jet. So, near the leakage, the generation of the flammable mixture will differ depending on the kind of the jet that will be used. However, in the far field their behaviours seem be alike and maybe the kind of the jet do not interferes in the flammable gas cloud size. So, some analysis will also be conducted to investigate this question.

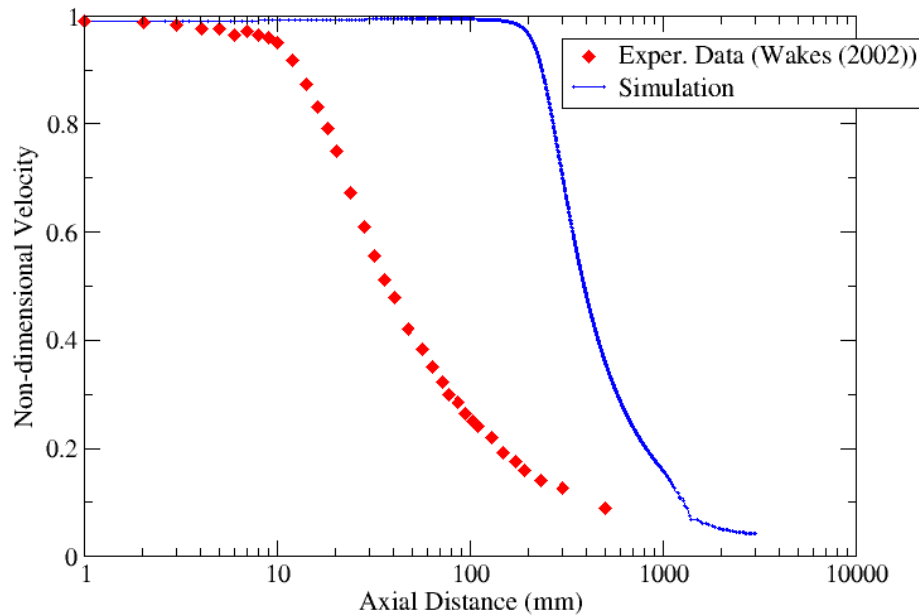


Figure 6.4: Comparing results from an axisymmetric jet simulation with a high aspect ratio jet behaviour.

In order to simulate a high aspect jet behaviour, a flange failure region was reproduced, as shown in Figure 6.3. The computational domain was defined like a box with a rectangular basis ($x = 0.3$ m and $z = 2$ m) and 2 metres of height. Due to the small gasket thickness it was necessary to use a refined mesh at the leak zone that gave a great number of mesh elements (4,260,000). Figure 6.5 shows the geometry that has been used in this case.

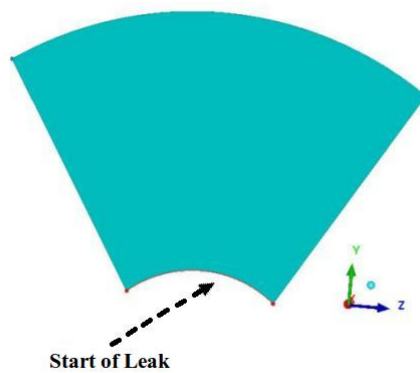


Figure 6.5: Geometric representation of a gasket failure in a flange.

The simulation of a high aspect jet behaviour had many problems. The parameters used for axisymmetric jet simulation could not be applied for this case and several tests was conducted

to find out the best way to model this kind of jet behaviour. Table 6.2 presents some changes that has been done in the model and mesh for this attempts.

Table 6.2: Parameters for the high aspect ratio jet study.

Case	Parameter Modified	Mesh Features
Simulation01	Hybrid advection scheme	No changes on mesh
Simulation02	Hybrid advection scheme and time scale of 0.01	No changes on mesh
Simulation03	Hybrid advection scheme	Refinement on mesh

Figure 6.6 shows the simulation results for the cases described in Table 6.2. It is possible to observe that the results do not agree faithfully with the experimental data.

The best result was achieved using a hybrid advection scheme and a extra-refined mesh (case *Simulation03*). However the refinement gave a too large mesh with 9,280,000 elements that, combined with the advection scheme, greatly increase the computational effort.

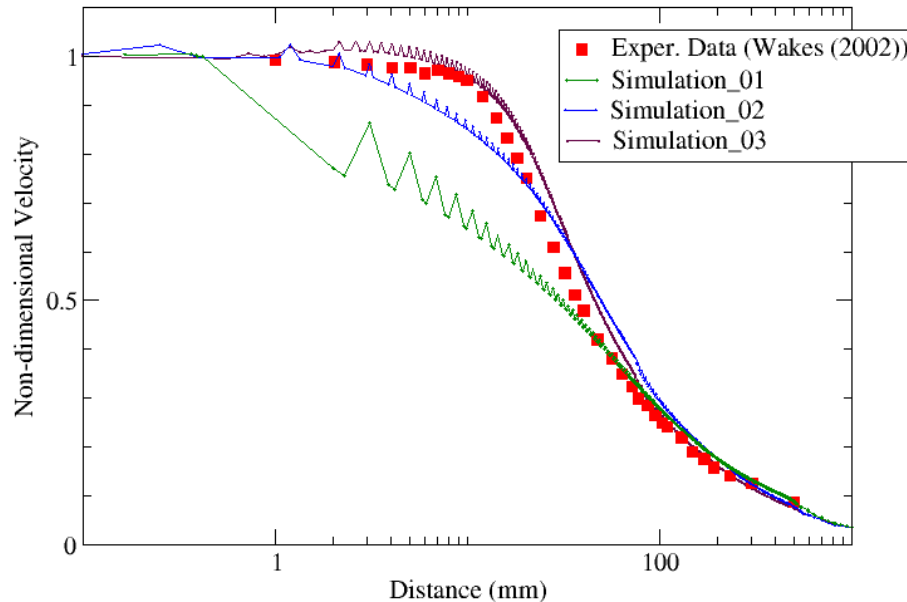


Figure 6.6: Simulation of a high aspect ratio jet behaviour using diferent parameters.

The difficulties in simulating a high aspect ratio jet behaviour suggest the need further investigation in order to improve the modelling. Thus, a traditional circular orifice shape was chosen to represent the leakage in the dispersion simulations.

6.1.3 Study of the natural gas jet

The flammable gas clouds are formed from releases with great mass flow rate. A release of 80 kg/s of natural gas was chosen. Taking the upstream release pressure as 200 kgf/cm² and considering the specific heat ratio of methane (the major component in natural gas) as 1.29, the gas density and temperature at the leakage are 1.44 kg/m³ and -115 °C, respectively. At these release conditions, a sonic flow is developed.

As discussed in section 5.3, when the fluid flow is supersonic the numerical solution becomes complex and a strategy used in dispersion studies is consider just the leakage region where the fluid flow is subsonic. Thus, an average velocity of 340 m/s (lower than sound speed) was adopted so that the area of the leakage was 0.1634 m² and the diameter of the orifice was 0.456 metres.

It is important to note that the diameter described above is not the real leak diameter but just an "apparent diameter", that was used to solve the subsonic part of the fluid flow. The real leak diameter can be found applying a discharge model as described in Lees (2005).

As in previous jet studies, a rectangular box was defined as the computational domain with 10 m in its base and 100 m of height. A tetrahedral mesh was used and the number of mesh elements were about 2,200,000. Figure 6.7 shows the computational domain and mesh that was used in this simulation.

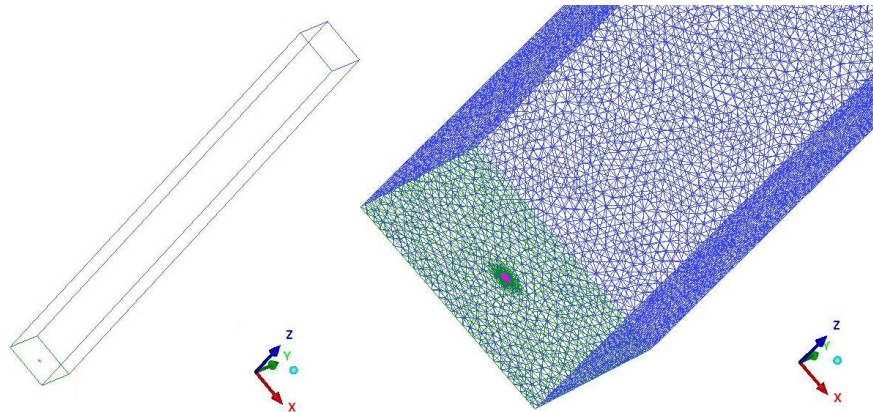


Figure 6.7: Computational domain and mesh used in the natural gas jet simulation.

The boundary conditions were the same ones that will be used in the dispersion simulations (Tables 5.2 and 5.3). The results are presented below.

The spreading angle of the jet relates directly with the flammable gas cloud size that will be formed. The flammable cloud size increases as the spreading angle increases. The explosive mixture is also reached quicker. Figure 6.8 shows the spreading angle for the natural gas simulation.

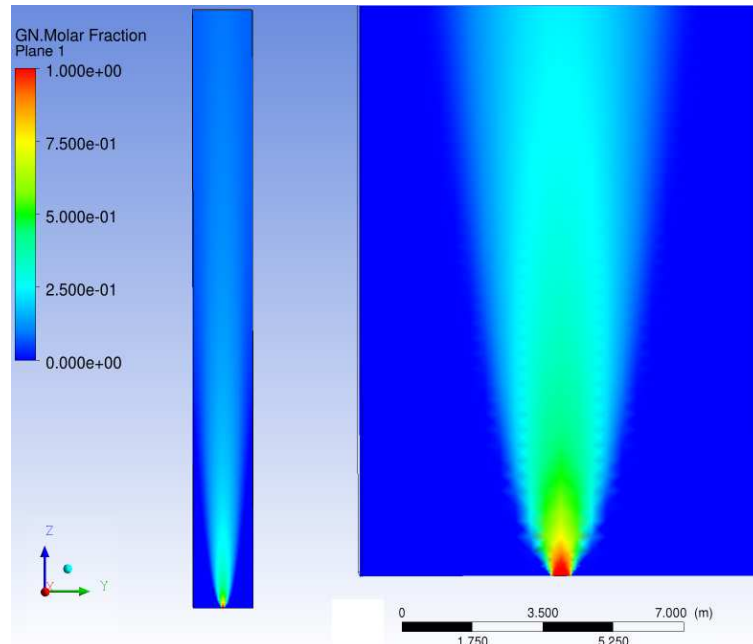


Figure 6.8: Spreading angle of the natural gas jet.

It was possible to evaluate the spreading angle of the jet as been 15.8° . This value is a little different that one described by Lees (2005), who suggests a theoretic spreading angle of 18° , but, it is close to the experimental values found by Wakes (2002): 12° . Even when using a circular orifice, the spreading angle of the jet is near to the high aspect ratio one, which means a good representation of the real release.

Another important variable to describe the jet behaviour is the velocity profile. The centreline velocity profile shows how the velocity of the jet decreases with the distance from the release point, which implies where and when the mixture of the gas and air will reach a concentration within the flammable limits.

The centreline velocity profile of the jet is shown in Figure 6.9. Figure 6.10 shows the velocity profile of the jet at different heights, ranging from 0.05 metres to 100 metres away from the leak release.

The behaviour of the jet depends on the velocity profile at the gas entrance in the

computational domain. Wakes (2003) suggests to set up a velocity profile in the entrance, for release simulations. In this study the mass flow rate was specified at the leakage and the velocity profile was developed from it.

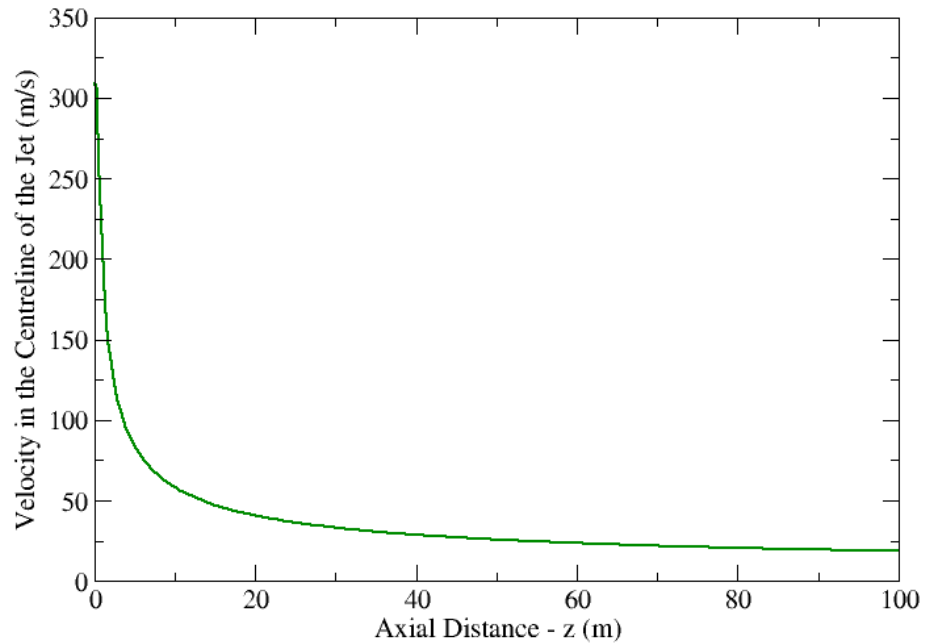


Figure 6.9: Natural gas velocity profile in the centreline of the jet.

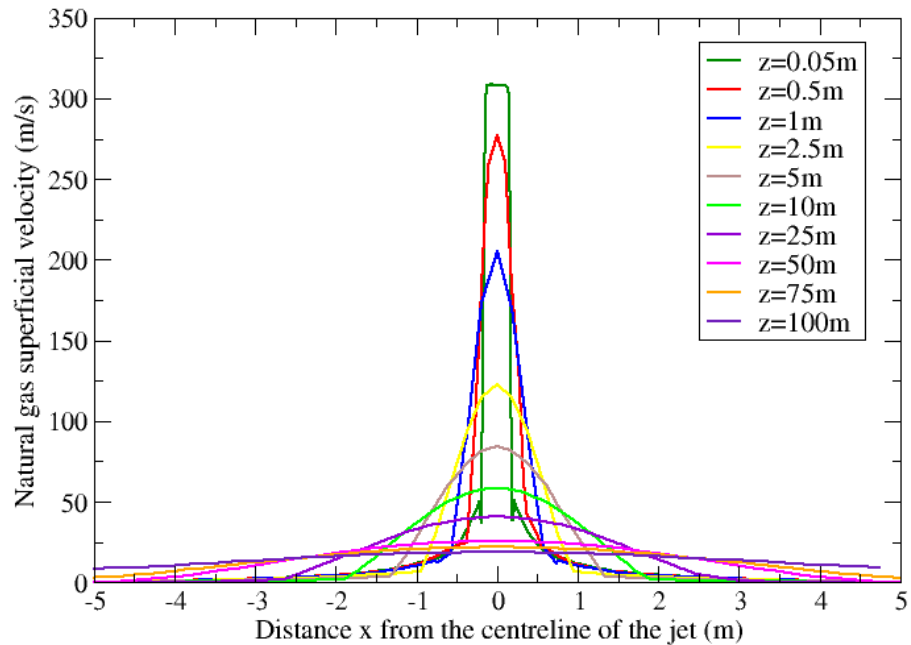


Figure 6.10: Natural gas superficial velocity profile at different heights.

The concentration levels are also an important variable to be studied in the jet. They are used to determine whether an area is within the upper and lower flammability limits and therefore whether it is at risk of explosion (Wakes (2002)). The natural gas molar fraction along the jet was analysed. The flammable limits are given in volumetric fraction.

Figure 6.11 shows the natural gas molar fraction in the centreline of the jet. It is possible to observe that the gas concentration in the centreline of the jet reaches the flammability region 40 metres distant from the origin of the release.

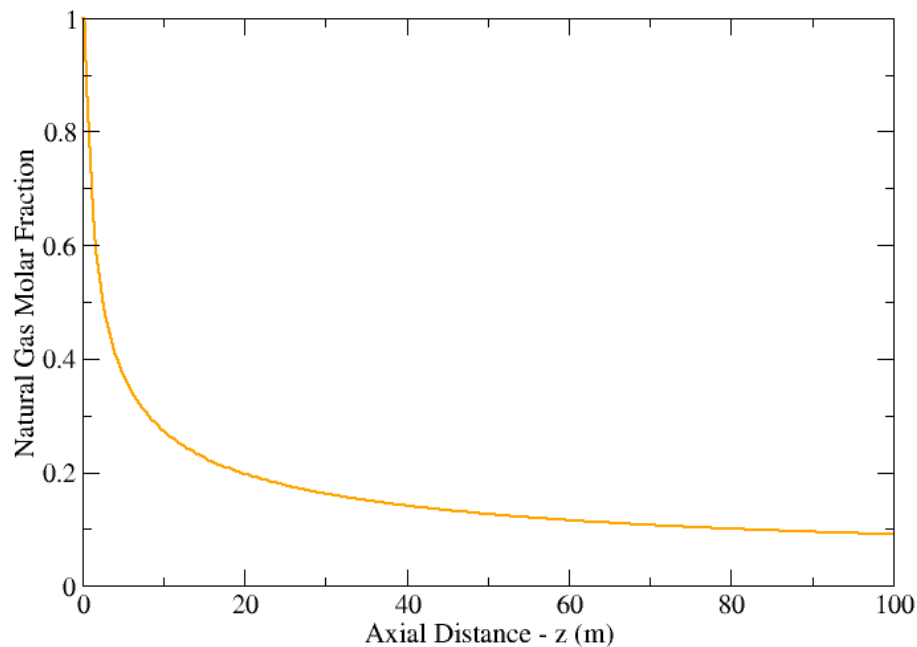


Figure 6.11: Natural gas molar fraction profile in the centreline of the jet.

6.2 Wind analysis

In Chapter 2 (Section 2.3) it was discussed the importance of wind speed and direction when dealing with flammable clouds. In this section it will be shown how to model the wind profile.

In atmospheric studies a superficial atmospheric boundary layer (SABL) is defined between the surface and the air. It presents a turbulent behaviour with large variations in temperature, humidity and wind speed with height.

A vertical wind speed profile is observed in SABL. Due to the wind shear, the velocity is zero near the surface and increases exponentially with the height until becomes almost constant at high values of z . Figure 6.12 illustrates a typical wind speed profile.

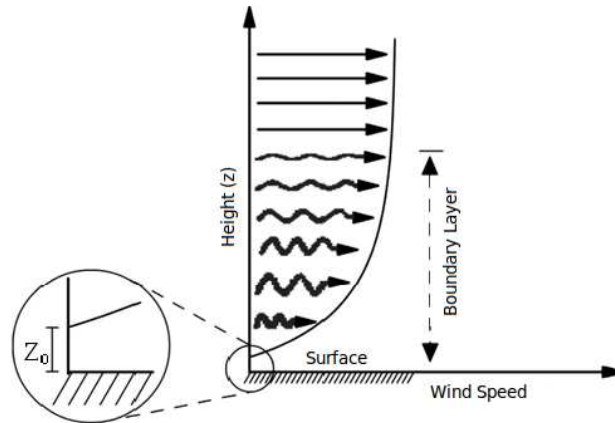


Figure 6.12: Vertical wind speed profile.

In figure 6.12 above, z_0 is the roughness length and it represents the height where the velocity is zero.

The wind speed profile in atmospheric boundary layer can not be easily assessed due to many parameters influencing the phenomenon. The most common model used to describe this profile is the Monin-Obukhov theory.

The Monin-Obukhov theory, in homogeneous and stationary flow conditions, predicts a log-linear profile:

$$u(z) = \frac{u_*}{\kappa} \left[\ln \left(\frac{z}{z_0} \right) - \psi \left(\frac{z}{L} \right) \right] \quad (6.1)$$

Here:

$u(z)$ is the wind speed at height z (m/s);

u_* is the friction velocity (m/s);

κ is the *Von Kármán* constant (taken as 0.41);

z_0 is the surface roughness length (m);

ψ is a universal stability function;

L is the *Monin-Obukhov* length (m).

According to equation 6.1, knowing the wind speed at one height, it is possible to determine a wind speed profile through two parameters: the surface roughness and the *Monin-Obukhov* length.

The surface roughness can be estimated by vertical wind profile data. It varies depending on the surface, in water, for example, the value of z_0 is very low compared to the land. Additionally, the surface roughness may not be constant. In sea, it depends on the wave field, which in turn is determined by wind speed, distance to coast, etc (Lange *et al.* (2004)).

The *Monin-Obukhov* length, L , expresses the relationship between the convective and the turbulent flow. It is used to take account the atmospheric stability, being positive during stable conditions (night-time), negative during unstable conditions (daytime) and approaches infinity for neutral conditions (Hanna (1982)). It is defined as:

$$L = \frac{u_*^3}{\kappa(g/T)(-\overline{w'T'})} \quad (6.2)$$

where g is the acceleration due to gravity (m/s^2), T is the absolute temperature (K), and $(-\overline{w'T'})$ is the surface heat flux (J/m^2).

Different methods are available to derivate the *Monin-Obukhov* length. Some examples are sonic, gradient and bulk method. Values for L can also be found on tables as function of wind speed and meteorological conditions (AICHE (2000)).

For neutral conditions, the equation 6.1 can be simplified. In this case: $L \simeq \infty$, and the second term in its equation is set to zero:

$$u(z) = \frac{u_*}{\kappa} \ln\left(\frac{z}{z_0}\right) \quad (6.3)$$

The equation 6.3 can become a power law relation if the velocity is compared to a velocity at a fixed height (Hanna (1982)):

$$u(z) = u_{10} \left(\frac{z}{10}\right)^p \quad (6.4)$$

Here, u_{10} is the wind speed at height 10 metres and p is the power coefficient. The power coefficient is a function of atmospheric stability and surface roughness.

6.2.1 Wind speed profile tests

The area under study comprises an offshore module that lies at approximately 55 metres above sea level. At this height it is expected that the wind boundary layer is fully developed and the wind speed is almost constant. To examine if it was possible to consider the velocity as constant or if it was necessary to set a velocity profile for this dispersion study, tests were performed using equations 6.1, 6.3 and 6.4 for wind speed profile.

For this wind speed analysis, an average wind velocity of 6.5 m/s at 10 m over sea level was adopted. A neutral atmospheric was chosen and it was necessary to estimate the *Monin-Obukhov* length (L), surface roughness (z_0), friction velocity (u_*) and power coefficient (p) for this stability condition.

Typical values of L , z_0 and p can be found in AICHE (2000). For neutral stability atmospheric class and sea surface they are given in Table 6.3.

Table 6.3: Values of L , z_0 and p for neutral atmospheric and sea surface.

<i>Monin-Obukhov</i> length (L) (m)	> 100
surface roughness (z_0) (m)	1×10^{-4}
power coefficient (p)	0.15

z_0 can also be obtained through models for sea surface. The most common model takes into account the wave field by its dependence on friction velocity u_* and is known as the *Charnock* relation (Charnock (1955)):

$$z_0 = z_{ch} \frac{u_*^2}{g} \quad (6.5)$$

Here, z_{ch} is the empirical Charnock parameter and its standard value of $z_{ch} = 0.0185$ has been used.

Since it is a preliminary analysis, in order to reduce the computational costs, the tests were conducted on a simple geometry, just with a single deck (as showed in Figure 5.2). A computational

domain starting on level of the sea ($z = 0$) was also used.

Figures 6.13, 6.14 and 6.15 show the results of the simulations. It is possible to recognize the wind exponential profile, as seen in Figure 6.12, for all simulated equations.

For equations 6.3 and 6.4, the profiles are very similar (Figures 6.14 and 6.15). In these cases the wind speed at heights over 30 m practically does not change. For equation 6.1 (Figure 6.13), it is presented a slight variation on wind speed even with the developed profile (approximately 1 m/s at heights between 40 and 90 metres).

The difference between the results is due to considerations that have been done during the development of equations. Equation 6.1 is the most complete, but it requires many parameters that should be estimated, while equations 6.3 and 6.4 are simpler.

It can be observed in all Figures (6.13, 6.14 and 6.15) that at heights over 55m (offshore module level considered) the wind speed profile is almost constant. So that a constant value of wind speed can be used on next simulations.

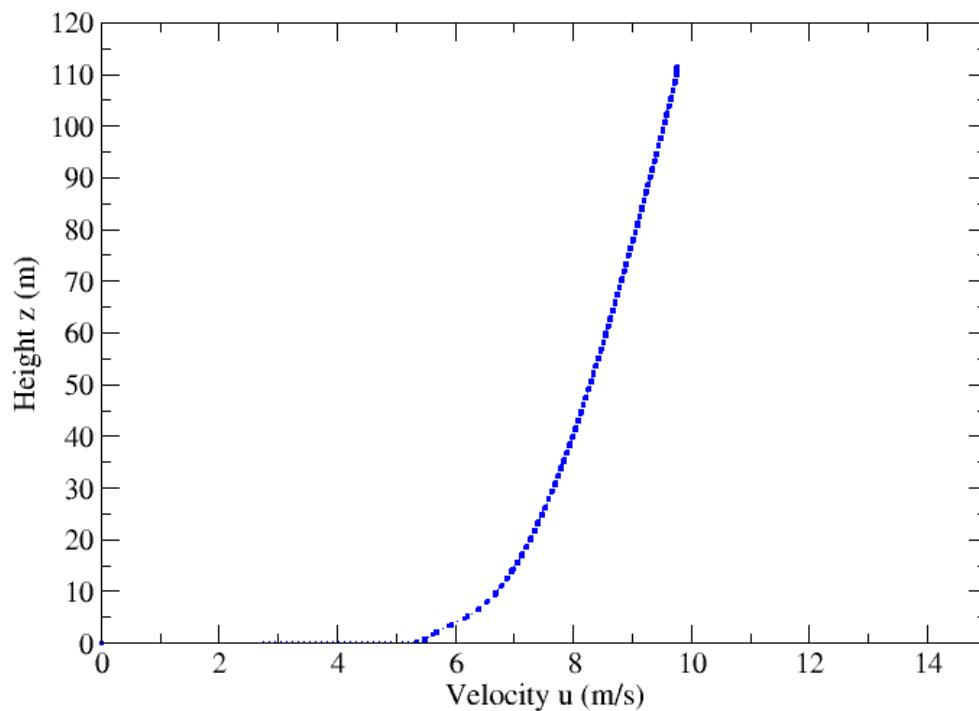


Figure 6.13: Vertical wind speed profile - Equation 6.1.

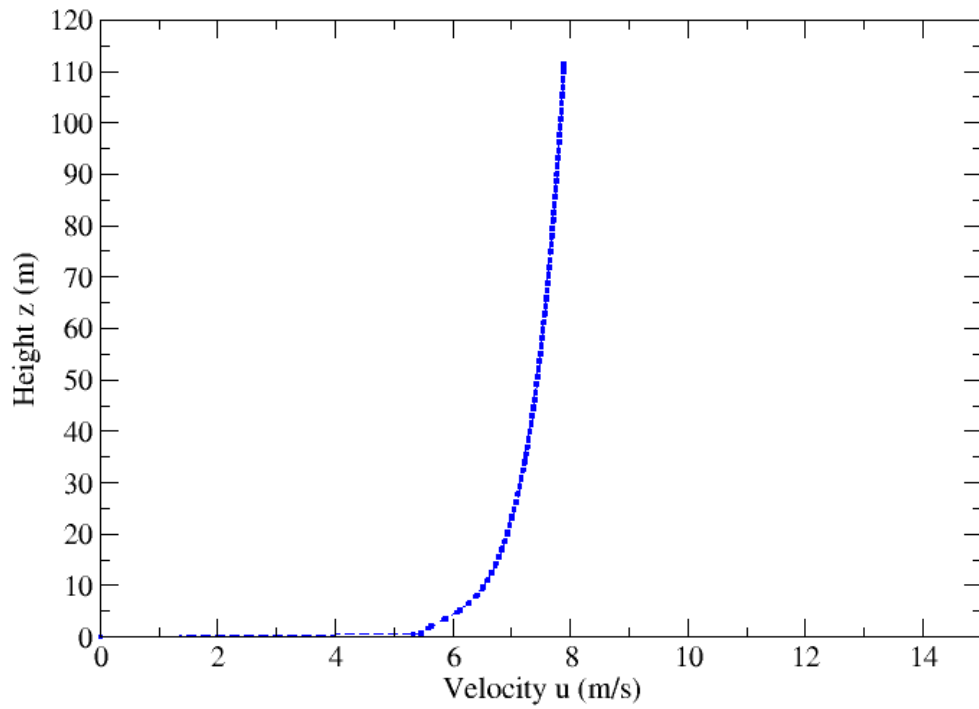


Figure 6.14: Vertical wind speed profile - Equation 6.3.

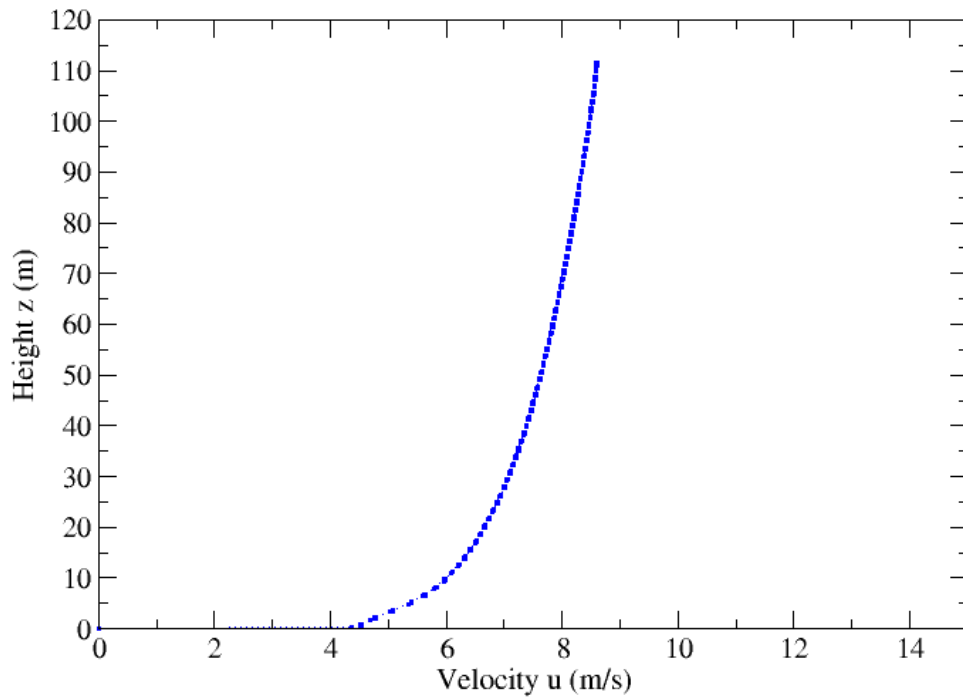


Figure 6.15: Vertical wind speed profile - Equation 6.4.

6.3 Computational domain size and mesh test

6.3.1 Computational domain size

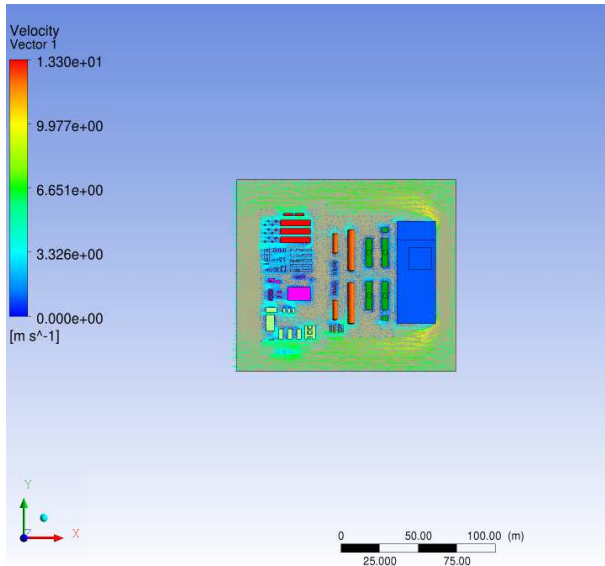
A study was performed in order to check which computational domain size can be used on the simulations. Here, a simple geometry (as showed in Figure 5.2) was also adopted and three computational domains with different size were chosen (Table 6.4). A wind speed of 6 m/s blowing from east was considered in the simulation and the ventilation into the module was analysed.

Table 6.4: Size of the computational domains under study.

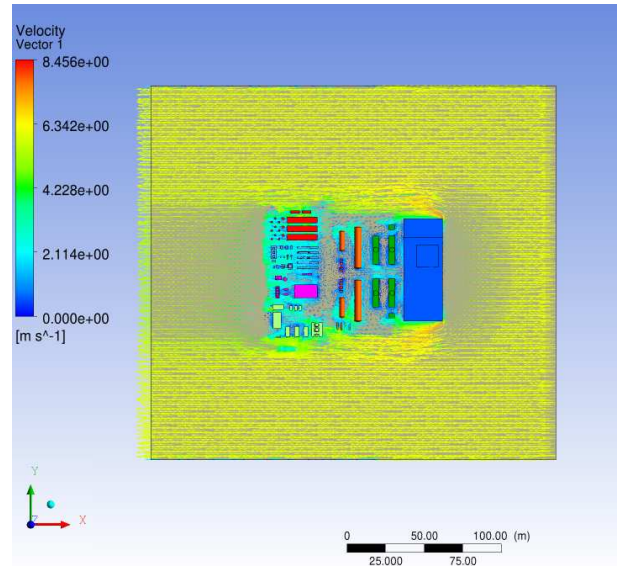
Domain	x(m)	y(m)	z(m)	Mesh elements
Computational Domain 01 (CD01)	142	124	72	2,354,843
Computational Domain 02 (CD02)	262	242	72	3,848,189
Computational Domain 03 (CD03)	348	328	72	5,314,616

Figure 6.16 shows the wind velocity field in a plane at height 2.5 m over the main deck using the three computational domains. It is possible to observe that large recirculation zones are formed into the module and they are better defined when the computational domain contour is further away (as in Figure 6.16 (b) and (c)). In a qualitative analysis, there seems to be not much difference in recirculation zones when using the computational domains CD02 and CD03, which suggests that both CD02 and CD03 could be used in the proposed study.

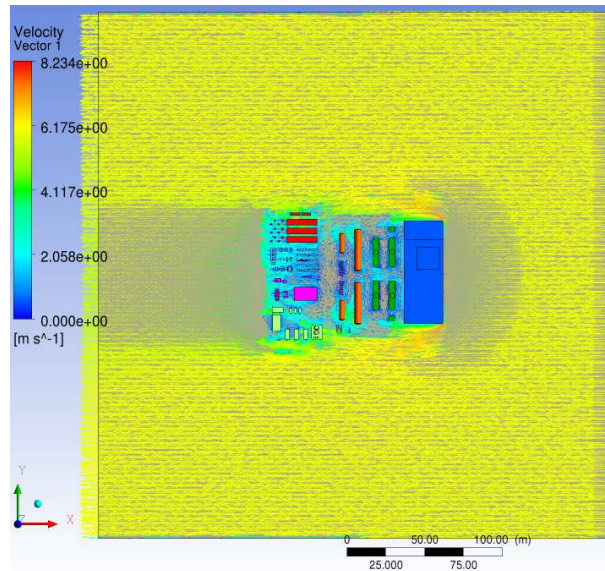
A quantitative analysis was also performed. Thirty nine monitoring points were distributed into the module considering three different levels: at height 2.5, 10 and 20 metres over the main deck (thirteen points for each plane) and the average wind velocity was calculated in each one of them. Figure 6.17 shows the monitoring points in the platform region. Figures 6.18, 6.19 and 6.20 shows the scattering among the values of average wind velocity calculated in monitoring points when different computational domain sizes are used.



(a) Computational Domain CD01



(b) Computational Domain CD02



(c) Computational Domain CD03

Figure 6.16: Wind velocity field in a plan at height 2.5 m over the main deck using the computational domains CD01 (a), CD02 (b) and CD03 (3).

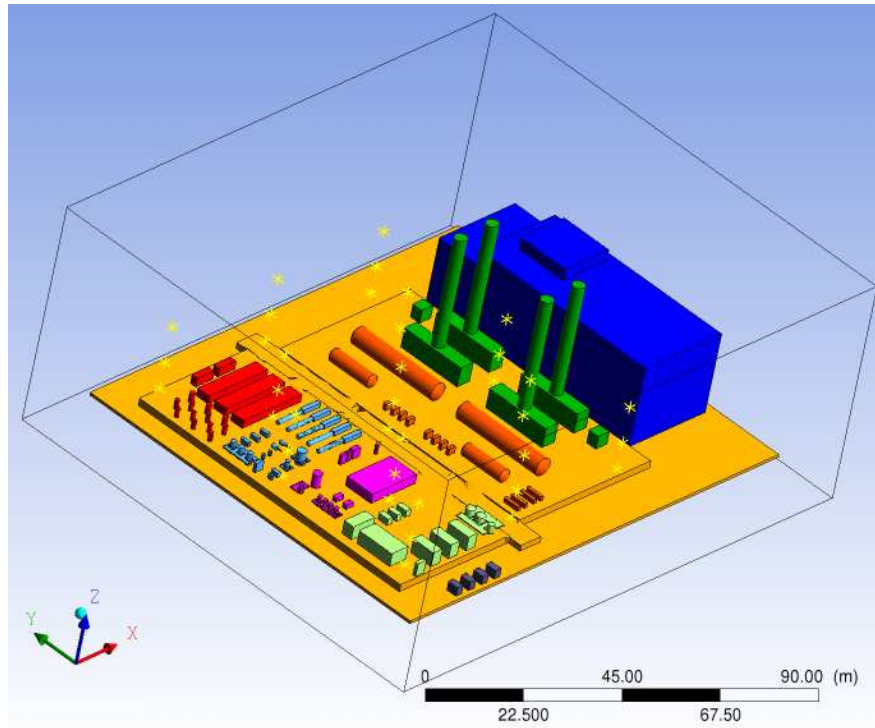


Figure 6.17: Platform geometry with monitoring points. In this case, the computational domain CD01 has been used as an example.

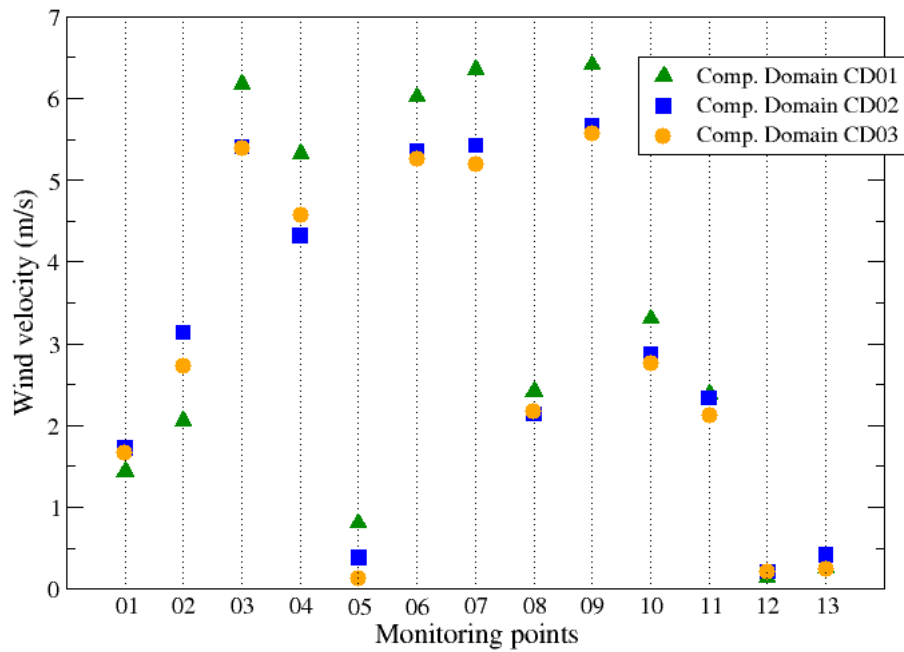


Figure 6.18: Comparison between the values of average wind velocity in monitoring points located in the first level (at 2.5 m over main deck).

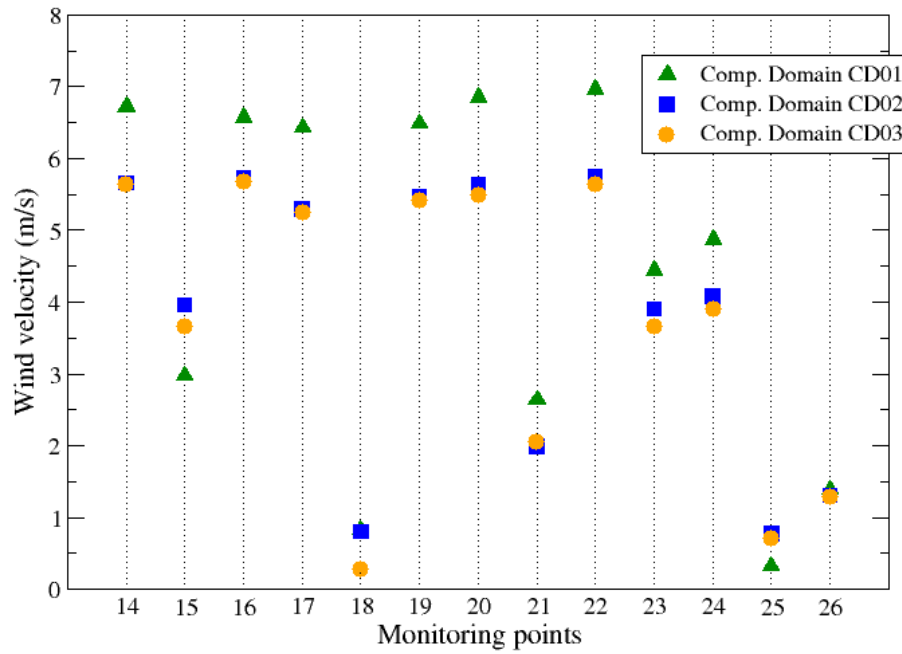


Figure 6.19: Comparison between the values of average wind velocity in monitoring points located in the second level (at 10 m over main deck).

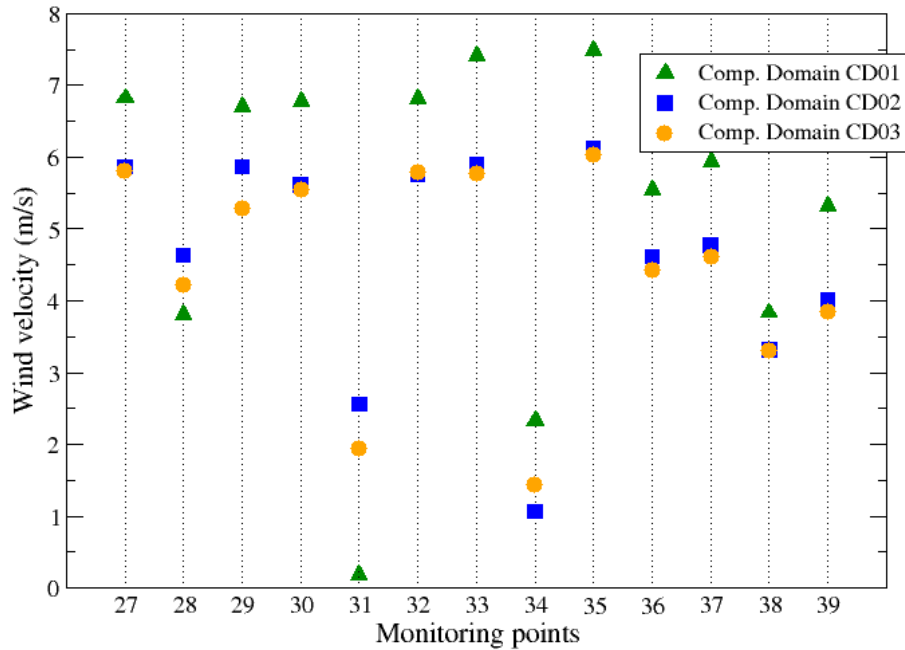


Figure 6.20: Comparison between the values of average wind velocity in monitoring points located in the third level (at 20 m over main deck).

Comparing the results of the simulations using the computational domains CD01 and CD02, it is possible to verify that the differences in the calculated wind velocity are about 12% for the monitoring points in the level at height of 2.5 m, 15-17% in the level at height of 10 m and 17-20% for the monitoring points in the level at height of 20 m.

The differences between the wind velocity in monitoring points considering the computational domain CD01 and CD03 is also great (almost 14% for the monitoring points in the first level, 16-20% in the second level and 20% for the monitoring points at height of 20 m).

When comparing the computational domains CD02 and CD03, the differences in the calculated wind velocities are between 2 and 6% for most monitoring points, including those ones in different planes.

The quantitative analysis also shows a little difference in numerical solution when using the computational domains CD02 and CD03 in the simulations. However, according to Table 6.4, as the computational domain increases, mesh increases too. The computational domain CD02 gives an intermediate mesh and provides similar results to the computational domain CD03 that is ≈ 1.4 times bigger.

6.3.2 Mesh tests

As well as the computational domain size, the correct choice about mesh size is also important in CFD analysis. The control volumes should be dimensioned so that their size does not interfere in numerical solution.

A dispersion scenario with a wind speed of 4 m/s coming from east and a natural gas release of 150 kg/s in direction y^+ was chosen. The entire platform geometry were used and the computational domain CD02 was selected (as discussed in previous section).

Three meshes with different refinement on the platform regions were analysed. They are presented in Tables 6.5, 6.6 and 6.7.

In all three meshes, a growth rate of 20% was selected. It means that starting from the smallest control volume, the next element will be 20% bigger than the preceding element until it achieve the largest element size that can exist into the computational domain (defined as "global size").

A notation was defined for the leakage region based on the number of elements that it will contain. Looking to tables below, in Mesh 01 the leakage was load with 5 control volumes while in Mesh 02 it will contain 12 elements and in Mesh 03, 20 elements.

Table 6.5: Refinement on platform regions according to Mesh 01.

Region	Max. element size (m)
Leakage	$r/5$
Facilities	1
Decks	5
Global size	10
Total of elements: 1,459,149	

Table 6.6: Refinement on platform regions according to Mesh 02.

Region	Max. element size (m)
Leakage	$r/12$
Facilities	0.5
Decks	3
Global size	7
Total of elements: 3,095,377	

Table 6.7: Refinement on platform regions according to Mesh 03.

Region	Max. element size (m)
Leakage	$r/20$
Facilities	0.3
Decks	2
Global size	6
Total of elements: 5,799,324	

The numerical solutions provided by each mesh were analysed based on both ventilation rate into the module and flammable gas cloud size.

Similarly to the computational domain size study, here, the average wind velocity into the platform was calculated in 39 monitoring points (the same ones previously described in Section 6.3.1). Figures 6.21, 6.22 and 6.23 show the comparison between the values of average wind velocity calculated in monitoring points when different mesh sizes are used.

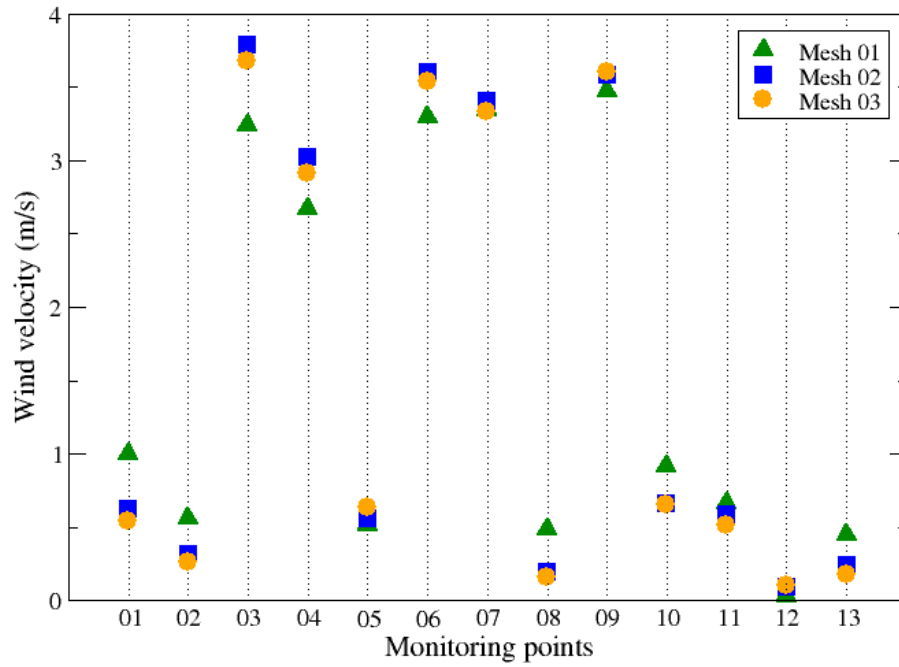


Figure 6.21: Comparison between the values of average wind velocity in monitoring points located in the first level (at 2.5 m over main deck).

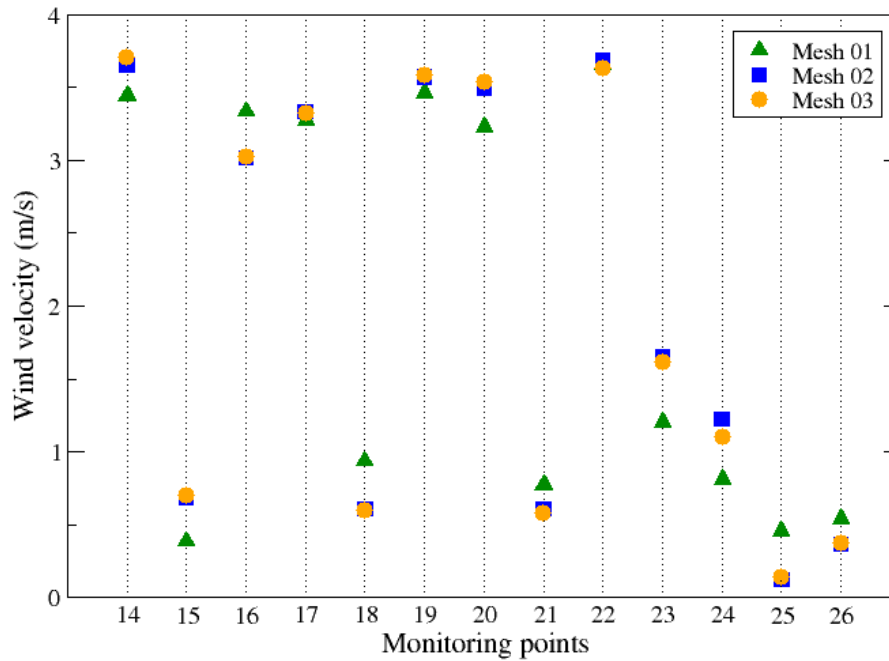


Figure 6.22: Comparison between the values of average wind velocity in monitoring points located in the second level (at 10 m over main deck).

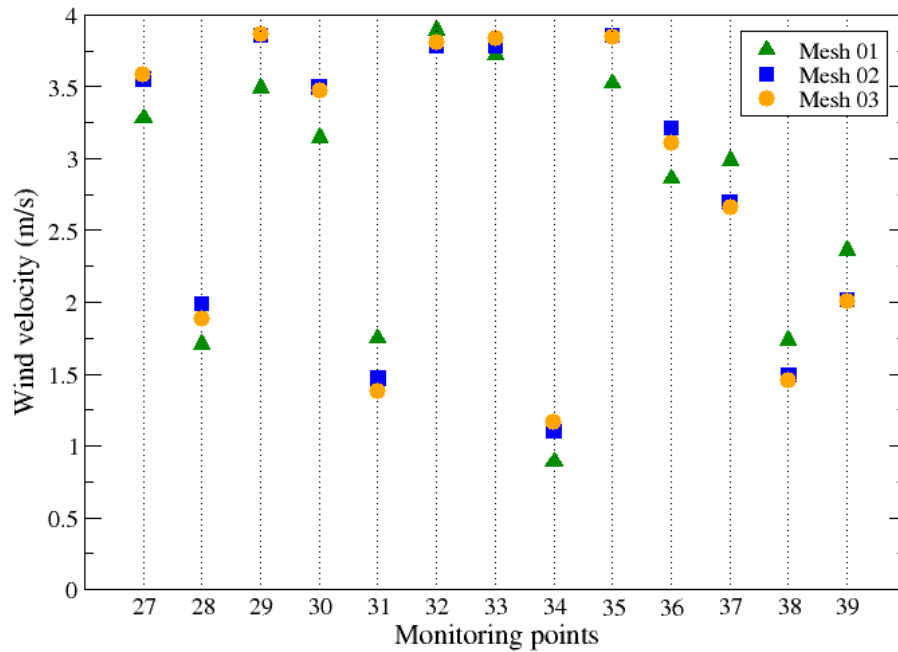


Figure 6.23: Comparison between the values of average wind velocity in monitoring points located in the third level (at 20 m over main deck).

The analysis of the plots shows that when using Mesh 02 the calculated values are near those provided by Mesh 03 (differences in the calculated wind velocities were between 4 and 9% for almost all monitoring points). However, when comparing both Meshes 02 and 03 with Mesh 01 the differences in the calculated wind speed is higher ($\approx 15\%$).

The flammable gas cloud sizes were also calculated. The flammable volumes obtained when using meshes 01, 02 and 03 were $7,308\text{ m}^3$, $8,943\text{ m}^3$ and $9,325\text{ m}^3$, respectively. It is possible to verify that difference in the flammable volume provided by meshes 02 and 03 is small ($\approx 4\%$). However, comparing mesh 01 and 02 the difference is almost 22% and this value increases to 27.6% when considering mesh 01 and 03.

Both analysis of wind velocity and the calculated flammable volumes show a little difference in numerical solution when considering meshes 02 and 03 in the simulations, so both can be used. However, it is observed that mesh 03 is more refined than mesh 02 which gives more elements into the calculation domain and, consequently, increases the computational time. Thus a mesh like mesh 02 will be adopted on next simulations.

6.4 Evaluating the influence of accommodation module in ventilation rate

In order to check how the presence of the accommodation module can influence the ventilation rate in the platform some tests were performed considering the eight possible wind directions described in Section 5.2.1.2.

Three different values of wind velocity were analysed: 2, 4 and 6.5 m/s. Figures 6.24, 6.25 and 6.26 show the differences in ventilation rate into the module when considering or not the accommodation module. It is possible to observe for all wind speed that the ventilation rate into the module is similar for all wind directions (the differences are lower than 10%), when the accommodation module is neglected in platform geometry.

When considering the accommodation module in platform geometry, the presence of the such structure reduces 36% the ventilation rate into the module for wind coming from east and \approx 11% for west wind . For other wind directions, the presence of the accommodation module hardly affects the ventilation rate in the platform (approximately 5%).

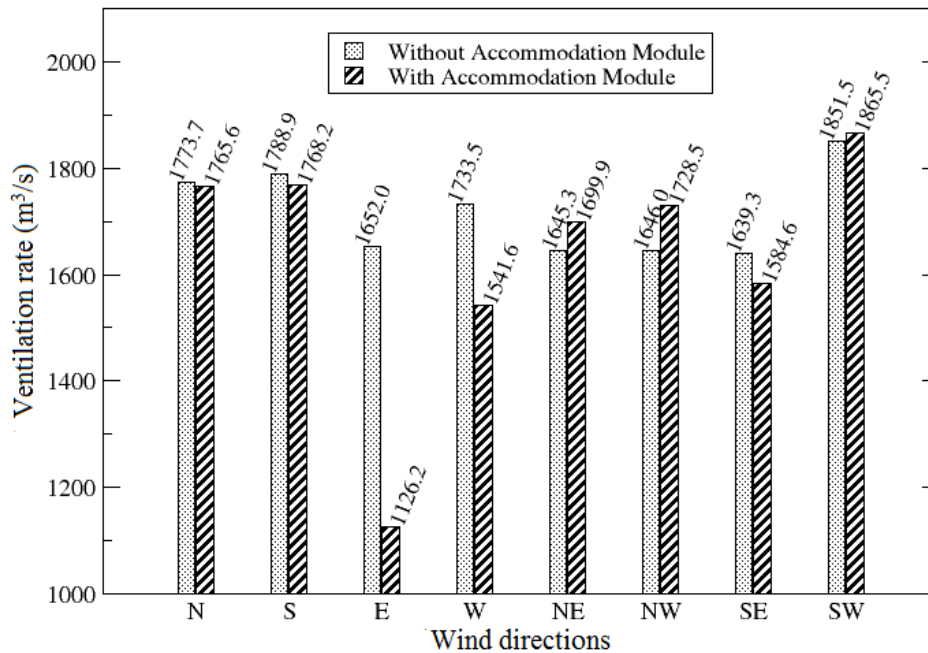


Figure 6.24: Comparing the ventilation rate into the offshore module, for a wind speed of 2 m/s when considering or not the accommodation module in geometry.

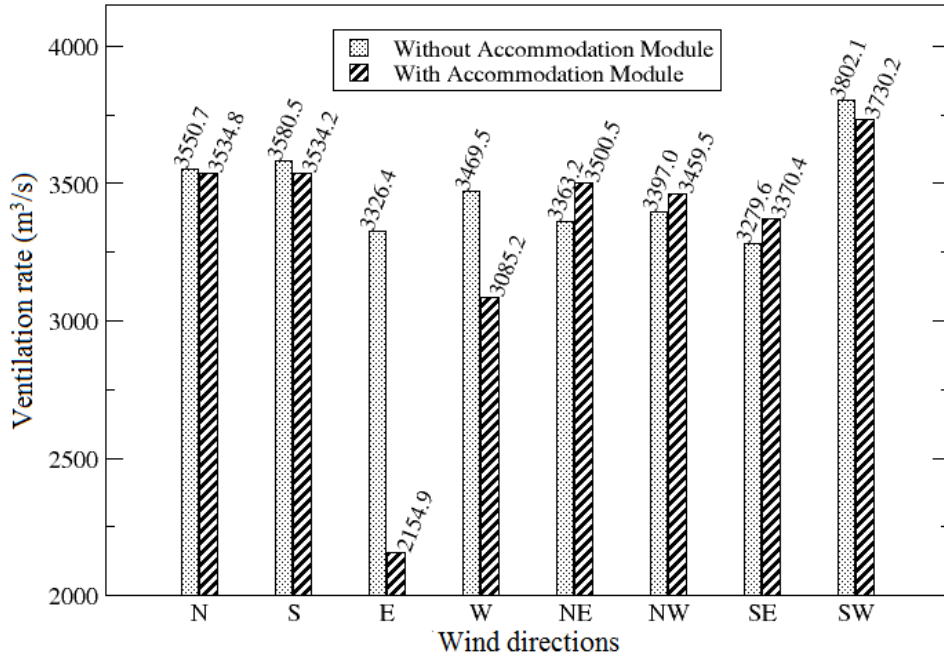


Figure 6.25: Comparing the ventilation rate into the offshore module, for a wind speed of 4 m/s when considering or not the accommodation module in geometry.

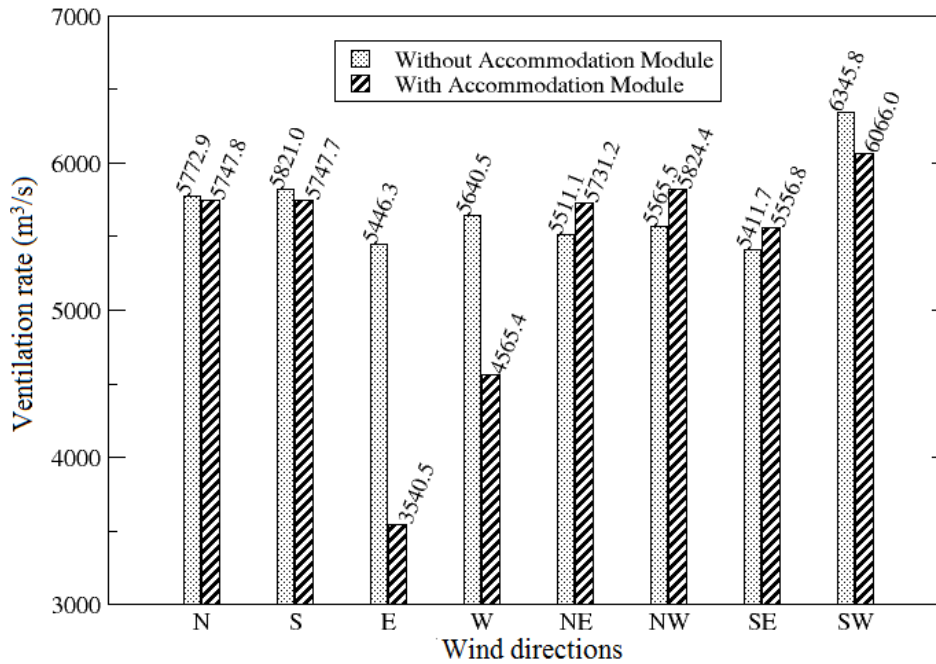


Figure 6.26: Comparing the ventilation rate into the offshore module, for a wind speed of 6.5 m/s when considering or not the accommodation module in geometry.

6.4.1 The variable R

According to equation 4.4 if the ventilation rate varies the variable R also changes, so R is affected by the presence of the accommodation module in the geometry.

In order to find the desirable values of R (0.03, 0.15 and 0.3) values of mass flow rate of natural gas were calculate through equation 4.4. The ventilation rate provided by the east wind velocities of 2, 4 and 6.5 m/s when the accommodation module is included or not in the geometry and the release conditions given in section 5.3 were considered.

The values of mass flow rate combined with the wind speed to obtain R equal to 0.03, 0.15 and 0.3 when the accommodation module is included or not are shown in Tables 6.8 and 6.9. It is possible to verify that to achieve same values of R different mass flow rate must be used for platform geometry with and without the accommodation module.

Another observation is that as R increase, mass flow rate increases too and depending on the wind velocity it reaches impractical values. It explains why a range of 0.03 - 0.3 was chosen for the variable R .

Table 6.8: Mass flow rate of natural gas calculated to provide desirable values of R based on the average ventilation rate when the accommodation module is neglected in platform geometry.

R	M. Flow (kg/s)		
	Velocity u = 2 m/s	Velocity u = 4 m/s	Velocity u = 6.5 m/s
0.03	24.47	48.94	79.52
0.15	122.35	244.70	398.00
0.3	244.70	489.39	796.00

Table 6.9: Mass flow rate of natural gas calculated to provide desirable values of R based on the average ventilation rate when the accommodation module is included in platform geometry.

R	M. Flow (kg/s)		
	Velocity u = 2 m/s	Velocity u = 4 m/s	Velocity u = 6.5 m/s
0.03	14.98	30.00	48.77
0.15	74.91	149.80	243.86
0.3	149.80	300.00	487.71

Chapter 7

Dispersion Simulations and Development of the Response Surface Model

This chapter shows the results of dispersion simulations and how the response surface model was obtained. It also covers the comparison between the values of flammable gas cloud size obtained in CFD simulations with those predicted by the response surface model.

7.1 Developing a response surface model considering releases in a horizontal plane

Based on the analysis discussed in Section 5.2.1, the variable φ was defined as the angle formed between the leak and wind direction considering the leak in the orientations x and y (in a horizontal plane).

Initially, the accommodation module was not considered in platform geometry. The process area was assumed symmetric so that the wind direction has little influence on ventilation rate. Such strategy was adopted to verify the effect of the variable φ on flammable cloud size and also make sure if it was possible to develop a response surface based on the two proposed variables. Dispersion scenarios including the accommodation module in the geometry were analysed later.

As seen in Section 5.2.2 an experimental design with 9 tests were developed for each

quadrant. The CFD cases listed in Table 7.1 presents the variables R and φ and the configuration of leak and wind direction used in each dispersion scenario. The calculated flammable volumes are also shown. Some dispersion scenario plots can be found in Appendix B.

The progress of the simulations in *ANSYS CFX - 12.0* was monitored by the convergence criterion: RSM (Root Mean Square) residual $\leq 1.0 \times 10^{-5}$. For all simulated cases, a number between 200 and 300 iterations were required to reach such criterion.

A monitoring point was placed into the platform region and the development of the flammable cloud was also verified. When the final solution was close to be achieved the calculated flammable volume in this point became constant.

Table 7.1: Dispersion Scenarios Based on an Experimental Design.

Scenario	Quadrant	R	φ	Leak Dir.	Wind Dir.	Flammable cloud size (m³)
01	01	0.03	0	x^+	W	1095.24
02	01	0.03	45	x^-	NE	1933.70
03	01	0.03	90	y^+	E	1635.73
04	01	0.15	0	y^-	N	7891.46
05	01	0.15	45	x^+	SW	5313.24
06	01	0.15	90	x^-	N	5769.19
07	01	0.3	0	y^+	S	5875.72
08	01	0.3	45	y^-	NW	15389.3
09	01	0.3	90	x^+	S	7629.71
10	02	0.03	90	x^-	N	2942.72
11	02	0.03	135	y^+	NE	1622.01
12	02	0.03	180	y^-	S	2942.43
13	02	0.15	90	x^+	S	7959.67
14	02	0.15	135	x^-	NW	9884.08
15	02	0.15	180	y^+	N	19040.90
16	02	0.3	90	y^-	W	13756.50
17	02	0.3	135	x^+	SE	9446.75
18	02	0.3	180	x^-	W	12027.80
19	03	0.03	180	y^+	N	3759.36

20	03	0.03	225	y^-	SE	2223.15
21	03	0.03	270	x^+	N	1852.17
22	03	0.15	180	x^-	W	17168.60
23	03	0.15	225	y^+	NW	8610.10
24	03	0.15	270	y^-	E	12630.40
25	03	0.3	180	x^+	E	11739.10
26	03	0.3	225	x^-	SW	10413.70
27	03	0.3	270	y^+	W	8765.37
28	04	0.03	270	y^-	E	5486.90
29	04	0.03	315	x^+	NW	1102.42
30	04	0.03	360	x^-	E	1594.47
31	04	0.15	270	y^+	W	5386.44
32	04	0.15	315	y^-	NE	9866.87
33	04	0.15	360	x^+	W	4201.90
34	04	0.3	270	x^-	S	7786.19
35	04	0.3	315	y^+	SW	7233.69
36	04	0.3	270	y^-	N	14263.1

A response surface model was built to represent the numerical experiments and the correlation between the independent variables R and φ and the flammable gas cloud size. A second order model (as given in Equation 4.3, Section 4.1.2) was chosen to describe the response surface.

Even as the methodology adopted to represent all ranges of the variable φ , the response surfaces were separately developed for each quadrant giving a amount of four different expressions:

- **Quadrant 01:**

$$y = -385.92 + 14,659.25 \cdot x_1 + 37,794.39 \cdot x_2 + 6,443.20 \cdot x_1 \cdot x_2 - 51,900 \cdot x_1^2 - 164,004.60 \cdot x_2^2 \quad (7.1)$$

- **Quadrant 02:**

$$y = 14,927.24 + 45,874.62 \cdot x_1 - 115,476.00 \cdot x_2 - 11,566.97 \cdot x_1 \cdot x_2 - 28,426.26 \cdot x_1^2 + 178,819.63 \cdot x_2^2 \quad (7.2)$$

- **Quadrant 03:**

$$y = 57,011.28 + 47,897.71 \cdot x_1 - 181,355.90 \cdot x_2 - 4,032.97 \cdot x_1 \cdot x_2 - 33,580.71 \cdot x_1^2 + 136,758.40 \cdot x_2^2 \quad (7.3)$$

- **Quadrant 04:**

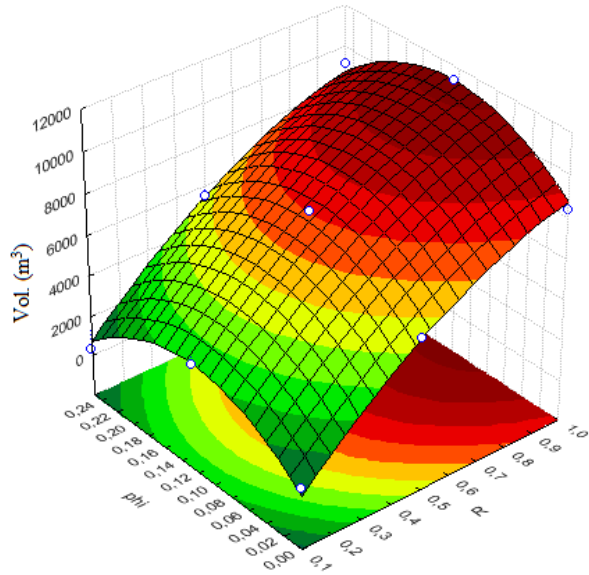
$$y = 40,427.97 - 29,583.64 \cdot x_1 - 66,221.70 \cdot x_2 + 46,709.14 \cdot x_1 \cdot x_2 - 3,156.67 \cdot x_1^2 - 24,672.43 \cdot x_2^2 \quad (7.4)$$

In Equations 7.1, 7.2, 7.3 and 7.4 above x_1 represents the variable R and x_2 represents φ . The values of both variables are normalized. y is the response (flammable gas cloud size (m³)).

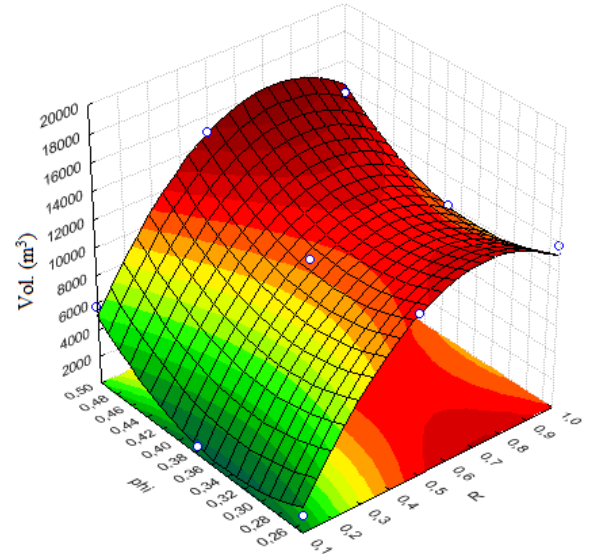
The graphical representation of the response surfaces is shown in Figure 7.1. The analysis of the plots indicate that the gas cloud behaviour is not same for all quadrants. On the other hand, there seems to be similarities for pairs of quadrants that represent the same relationship between the leak and wind direction.

The quadrants 02 and 03 (Figure 7.1 (b) and (c)) represent the series of angles φ where the leakage and the wind tend to have opposite directions. It is verified the maximum cloud volume is achieved when wind is entirely opposite to leakage and $\varphi = 180^\circ$ (in normalised form $\varphi = 0.5$). However, for both quadrants, the variable φ does not have as much influence as R in the flammable cloud size.

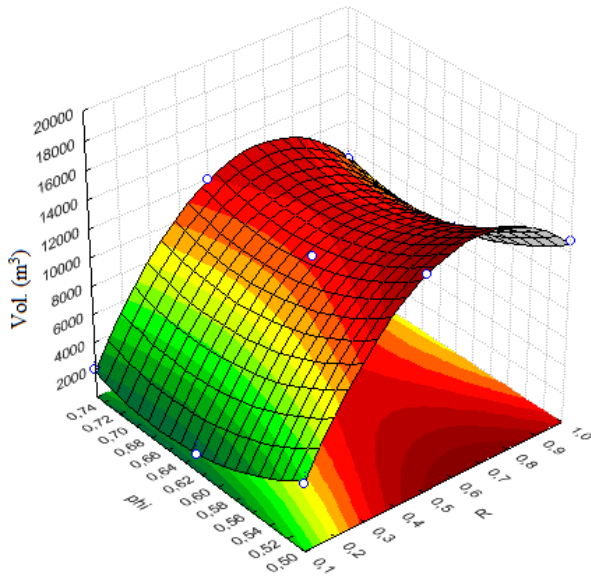
Regarding the variable R, these quadrants (02 and 03) exhibit a saddle profile. For small values of R (low ratio between leak rate and wind speed) the gas will be fast diluted by the air which leads to small flammable clouds. As R increases the concentration of the gas released increases too, giving larger flammable clouds. However, for large values of R, the gas concentrations exceed the Upper Flammable Limit (UFL) and the flammable cloud size reduces. A similar result is found in



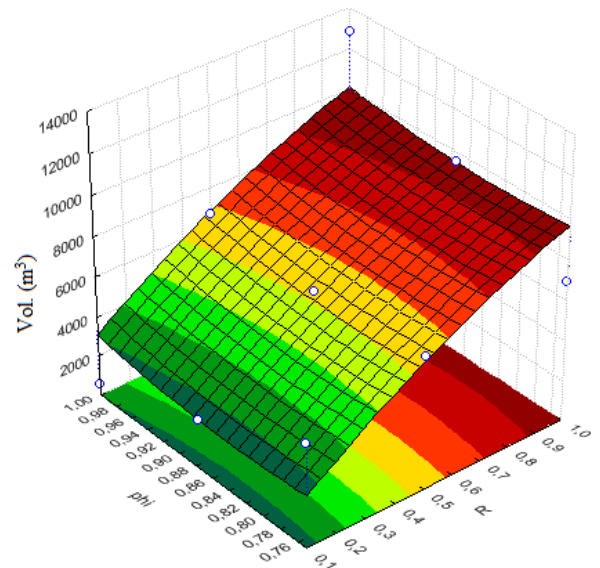
(a) Quadrant 01



(b) Quadrant 02



(c) Quadrant 03



(d) Quadrant 04

Figure 7.1: Response surface models for the Quadrants 01 (a), 02 (b), 03 (c) and 04 (d).

other study about gas dispersion (Huser & Kvernfold (2000)). It is also observed that values of $R \approx 0.18$ (in normalised form $R \approx 0.6$) yield the largest flammable clouds.

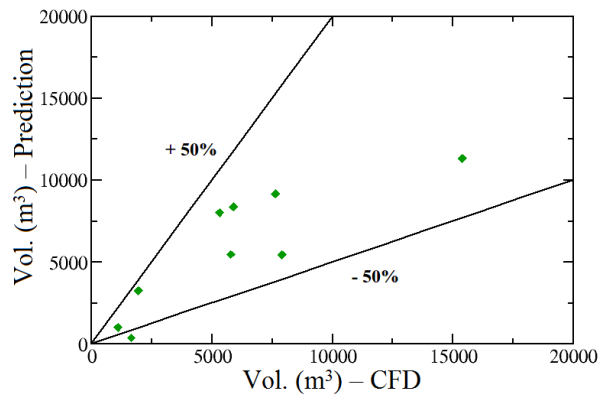
The flammable cloud behaviour for quadrants 02 and 03 explained above may be related to the fact that when wind and leakage take opposite directions an effective mixture between air and the released gas will occur. However when wind and leakage take the same direction ($0^\circ < \varphi < 90^\circ$ and $270^\circ < \varphi < 360^\circ$) a different phenomenon is observed, as shown in Figure 7.1 (a) and (d) that represents the quadrants 01 and 04, respectively.

For quadrants 01 and 04 the flammable cloud size increases as R increases, so the largest flammable clouds are found for highest values of R . It means if we take a constant ventilation rate the higher the leak rate the greater will be the flammable volume.

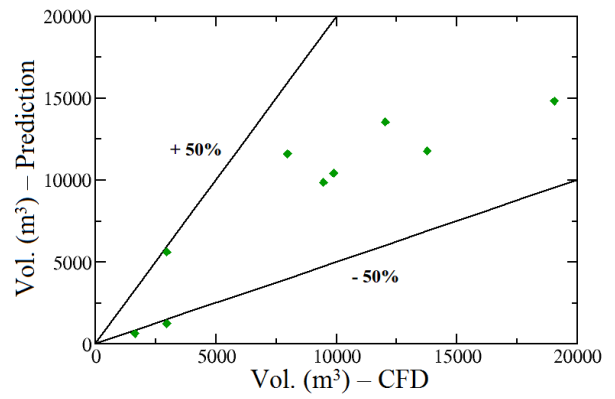
As verified for the pair of quadrants 02-03, in quadrants 01 and 04 the influence of the variable R in the flammable cloud size is greater than φ . It is also important to note that the flammable volumes observed in quadrants 01-04 are smaller compared with the volumes found for quadrants 02 and 03.

The comparison between the flammable volumes obtained in CFD simulations with the values predicted by the response surface model is shown in Figure 7.2. It is possible to observe that almost all cases fall within 50% tolerance interval.

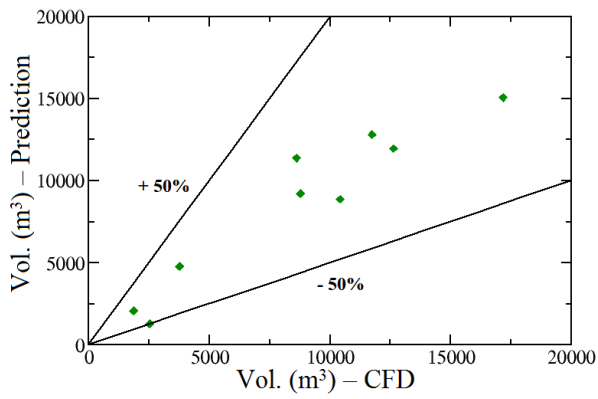
Based on the simplifications and limitations, in dispersion analysis, a factor of two is considered to be acceptable to predict flammable cloud size (Hanna et al. (2004)). In this study, the differences among the simulated cases and the values predicted by the response surfaces are smaller (four times) than the adopted tolerance. Thus, the developed response surface model can provides a satisfactory performance when gas dispersion in an offshore module is considered.



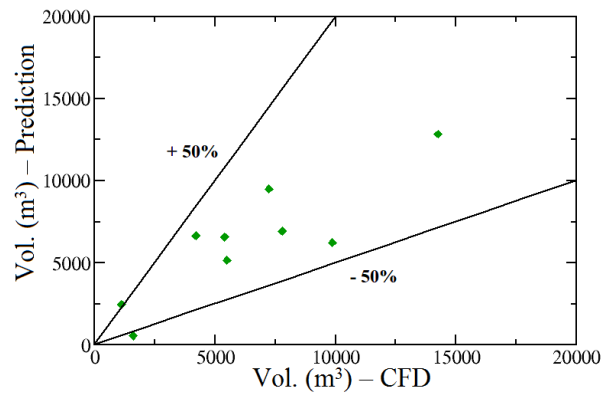
(a) Quadrant 01



(b) Quadrant 02



(c) Quadrant 03



(d) Quadrant 04

Figure 7.2: Comparison between the values obtained through CFD simulations and the response surface models to the Quadrants 01 (a), 02 (b), 03 (c) and 04 (d). Vertical axis shows results predicted with the model proposed in this study. Horizontal axis shows cloud volumes obtained using CFD.

7.1.1 Comparing values predicted by response surface model with CFD dispersion simulations

To evaluate the reliability of the developed response surface model, random cases were simulated in CFD and their results compared with values predicted by the model. In these cases, the dispersion scenarios were different from those used in building the response surfaces (adopted in design of experiments). Table 7.2 below shows the random CFD simulations used in this analysis.

Table 7.2: Random CFD Simulations.

Scenario	Quadrant	R	φ	Leak Dir.	Wind Dir.	Flammable cloud size (m ³)
Rand 01	01	0.03	0	x^+	W	1095.17
Rand 02	01	0.03	90	x^-	N	2942.72
Rand 03	01	0.09	0	y^+	S	2120.93
Rand 04	01	0.09	90	y^-	E	10329.80
Rand 05	01	0.15	0	y^-	N	7891.46
Rand 06	01	0.15	90	x^+	S	7959.67
Rand 07	01	0.21	45	x^+	SW	4023.91
Rand 08	01	0.24	0	x^-	E	4906.44
Rand 09	01	0.24	90	y^+	W	6129.14
Rand 10	01	0.27	45	y^+	SE	5869.46
Rand 11	01	0.3	0	x^+	W	6362.44
Rand 12	01	0.3	90	x^-	N	7292.76
Rand 13	02	0.03	90	x^-	N	2942.72
Rand 14	02	0.03	180	y^+	N	3759.36
Rand 15	02	0.06	90	x^+	S	5634.96
Rand 16	02	0.06	135	x^-	NW	3970.83
Rand 17	02	0.09	90	y^-	E	10329.80
Rand 18	02	0.09	180	x^+	E	12054.10
Rand 19	02	0.12	135	x^+	SE	8886.75
Rand 20	02	0.15	90	x^+	S	7959.67
Rand 21	02	0.15	180	x^-	W	17168.60

Rand 22	02	0.24	90	y^+	W	6129.14
Rand 23	02	0.24	180	y^-	S	12297.90
Rand 24	02	0.3	90	x^-	N	7292.76
Rand 25	02	0.3	180	y^+	N	16046.60
Rand 26	03	0.03	180	y^+	N	3759.36
Rand 27	03	0.03	270	y^-	E	5486.90
Rand 28	03	0.03	225	x^-	SW	2815.35
Rand 29	03	0.09	180	x^+	E	12054.10
Rand 30	03	0.09	270	x^-	S	5258.88
Rand 31	03	0.15	180	x^-	W	17168.60
Rand 32	03	0.15	270	y^+	W	5386.44
Rand 33	03	0.24	180	y^-	S	12297.90
Rand 34	03	0.24	270	x^+	N	4459.64
Rand 35	03	0.3	180	y^+	N	16064.60
Rand 36	03	0.3	270	y^-	E	15137.10
Rand 37	04	0.03	270	y^-	E	5486.90
Rand 38	04	0.03	360	x^+	W	1195.17
Rand 39	04	0.09	270	x^-	S	5258.88
Rand 40	04	0.09	360	y^+	S	2120.93
Rand 41	04	0.06	315	x^+	SW	3240.58
Rand 42	04	0.15	270	y^+	W	5386.44
Rand 43	04	0.15	360	y^-	N	7891.46
Rand 44	04	0.24	270	x^+	N	4459.64
Rand 45	04	0.24	360	x^-	E	4906.44
Rand 46	04	0.24	315	x^-	SE	5251.79
Rand 47	04	0.3	270	y^-	E	15137.10
Rand 48	04	0.3	360	x^+	W	6362.44

Figure 7.3 shows the comparison between the values predicted by the response surface model and the CFD results when considering the random dispersion scenarios given above.

As previously analysed, it is also observed here that the great majority of the results are within $\pm 50\%$. Furthermore it seems in most cases the values predicted by the model are larger than those ones obtained in CFD simulations, when accounting the same dispersion scenario, which means the developed response surface model can take a conservative approach.

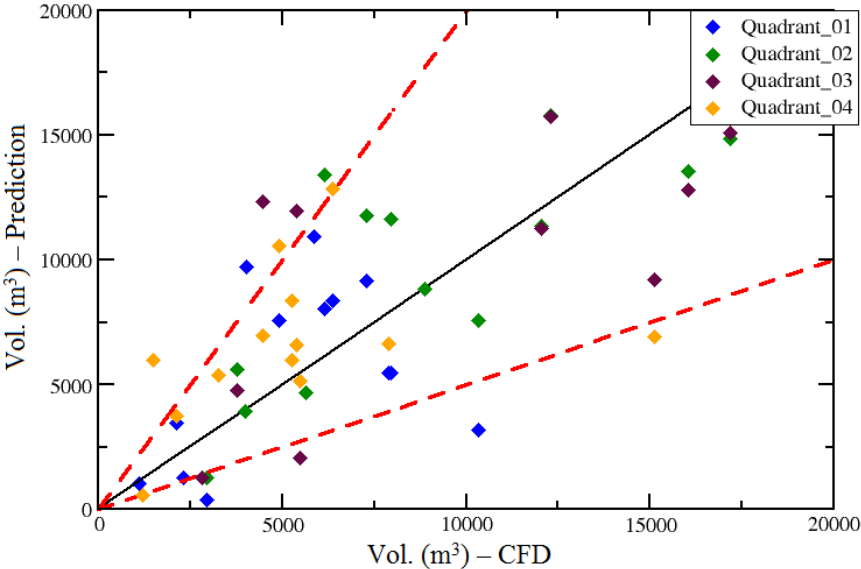


Figure 7.3: Comparing results from CFD simulations with response surface model for random dispersion scenarios. Vertical axis shows results predicted by the model proposed in this study. Horizontal axis shows cloud volumes obtained using CFD.

The response surfaces analysed until now were developed based on dispersion simulations disregarding the ventilation effects caused by the accommodation module in the platform geometry, but to obtain a complete model, they need to be taken into account.

7.1.2 Accounting the influence of the accommodation module

The influence of the accommodation module in the variable φ is unknown. Maybe the recirculation zones created by the interaction between this geometric structure and the east wind affect the adopted configuration of angles φ . In this case, new response surfaces must be developed. In an optimistic view, the variable φ will not be influenced by the recirculation zones and the first obtained response surfaces can also be applied for the geometry with the accommodation module.

In order to verify how the accommodation module influences the variable φ , some dispersion simulations were performed considering this structure in platform geometry.

As verified in Section 6.4, when the accommodation module is included in the platform, the ventilation rate is affected by the east and west wind direction (specially east wind). So such wind directions were analysed. Table 7.3 shows the dispersion scenarios adopted here.

It is important to keep in mind that, according to analysis given in section 6.4.1, to achieve the same values of variable R used before ($R = 0.03, 0.15$ and 0.3), different values mass flow rate were adopted in these cases when including the accommodation module in the geometry.

Table 7.3: Dispersion Simulations Considering the Accommodation Module in Platform Geometry.

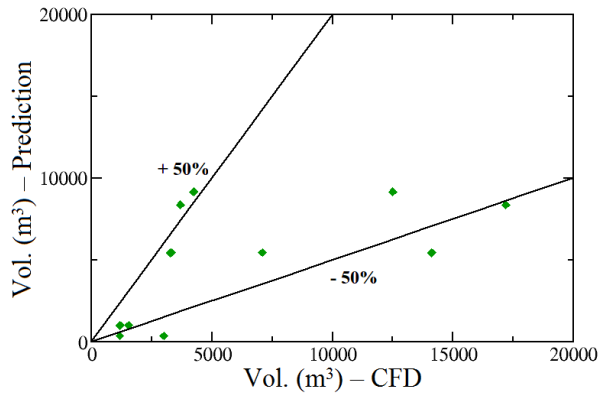
Scenario	R	Wind Dir.	Leak Dir.	φ	Quadrant	Flammable cloud size (m³)
EW 01	0.03	E	x^+	180	2 and 3	4114.85
EW 02	0.15	E	x^+	180	2 and 3	18976.10
EW 03	0.3	E	x^+	180	2 and 3	14224.20
EW 04	0.03	E	x^-	0	1 and 4	1175.31
EW 05	0.15	E	x^-	0	1 and 4	3264.17
EW 06	0.3	E	x^-	0	1 and 4	3674.70
EW 07	0.03	E	y^+	90	1 and 2	1161.19
EW 08	0.15	E	y^+	90	1 and 2	3303.64
EW 09	0.3	E	y^+	90	1 and 2	4227.87
EW 10	0.03	E	y^-	270	3 and 4	2403.24
EW 11	0.15	E	y^-	270	3 and 4	7908.05
EW 12	0.3	E	y^-	270	3 and 4	8624.95
WW 01	0.03	W	x^+	0	1 and 4	1538.87
WW 02	0.15	W	x^+	0	1 and 4	14109.70
WW 03	0.3	W	x^+	0	1 and 4	17199.30
WW 04	0.03	W	x^-	180	2 and 3	3195.52
WW 05	0.15	W	x^-	180	2 and 3	14674.50
WW 06	0.3	W	x^-	180	2 and 3	10511.80
WW 07	0.03	W	y^+	270	3 and 4	1267.88
WW 08	0.15	W	y^+	270	3 and 4	4412.83

WW 09	0.3	W	y^+	270	3 and 4	7458.11
WW 10	0.03	W	y^-	90	1 and 2	2988.45
WW 11	0.15	W	y^-	90	1 and 2	7084.63
WW 12	0.3	W	y^-	90	1 and 2	12493.60

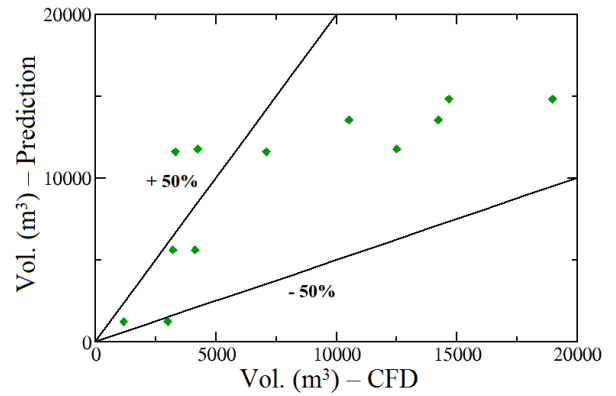
The first goal was not to develop a new response surface, but just to compare the results of the simulations accounting the accommodation module with the values predicted by the developed model by taking on the original configuration of angles φ . Figure 7.4 shows such comparison.

The analysis of the plots in Figure 7.4 shows that the differences between the values predicted by the model and the results of the simulations are within a range of $\pm 50\%$. This result is similar to that ones found before and allow us to conclude that the first obtained response surfaces can also be applied for the geometry with the accommodation module.

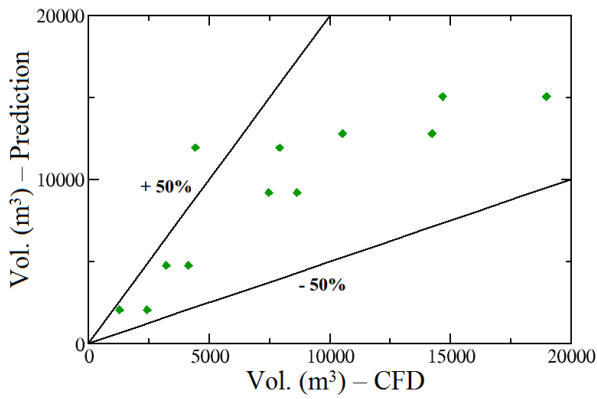
So, the developed model can describe all ventilation effects, including the wake wind effects caused by the accommodation module. Little adjustments are necessary just in the variable R when the dispersion scenario includes the wake wind side (in this case, east wind).



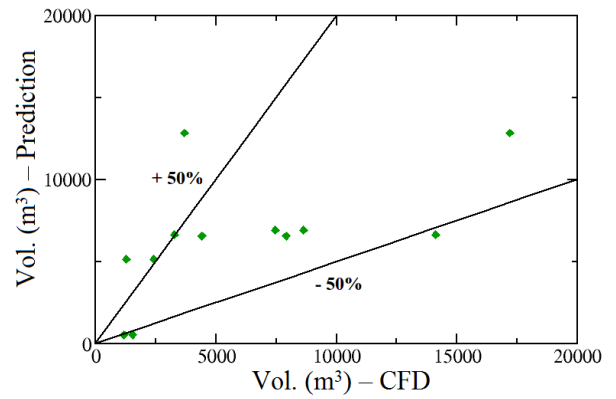
(a) Quadrant 01



(b) Quadrant 02



(c) Quadrant 03



(d) Quadrant 04

Figure 7.4: Comparison between the values obtained through CFD simulations considering the accommodation module in the geometry and the Response Surface Models to the Quadrants 01 (a), 02 (b), 03 (c) and 04 (d). Vertical axis shows results predicted with the model proposed in this study. Horizontal axis shows cloud volumes obtained using CFD.

7.2 Developing a response surface model considering releases in "z" direction

As discussed in Section 5.2.1, the concept of φ could not be applied for the leak directions z^+ and z^- . Thus, a new design of experiments was developed to account for the effect of these leak directions in flammable gas cloud size.

A qualitative variable named "z" was used to describe the leak direction and could take two values: 0 for the leak direction z^+ and 1 for the leak direction z^- . The variable R was used to account the interaction between the leak and ventilation rate and the values of 0.03 and 0.3 were adopted. As each variable has taken only two values, a experimental design 2^2 was developed giving a amount of four experiments. The CFD cases are listed in Table 7.4.

The same strategy used before in the development of the response surfaces for the leak directions x^+ , x^- , y^+ and y^- were also adopted in this analysis. Thus in the dispersion cases described in design of experiments the accommodation module was not included in platform geometry.

Table 7.4: Dispersion Scenarios Based on an Experimental Design for Leak Direction z.

Scenario	R	z	Wind Dir.	Flammable cloud size (m ³)
01	0.03	z^+	W	938.97
02	0.3	z^+	E	7902.75
03	0.03	z^-	S	5303.08
04	0.3	z^-	N	37097.9

Because the variables have assumed only two values and few numerical experiments were conducted, a first order model (as given in Equation 4.2, Section 4.1.2) was used in the development of the response surface. The expression that describes the obtained reponse surface model is presented below:

$$y = 165.2 + 7737.53 \cdot x_1 + 1605.11 \cdot x_2 + 27590.04 \cdot x_1 \cdot x_2 \quad (7.5)$$

Here, x_1 represents the variable R and x_2 represents z . The values of both variables are normalized and y is the response (flammable gas cloud size (m³)).

The graphical representation of the response surface model for leaks in z direction is shown in Figure 7.5. It is possible to verify that large flammable clouds are formed when the leak direction is z^- (in the plot $z = 1$). In this case, the gas jet release interacts with the deck floor and its momentum greatly reduces so the gas dispersion is more effective giving a large flammable cloud. Regarding the variable R , it is observed that the flammable cloud size increases as R increases. Such behaviour is similar that one found for the quadrants 1 and 4 where leak and wind taken same direction.

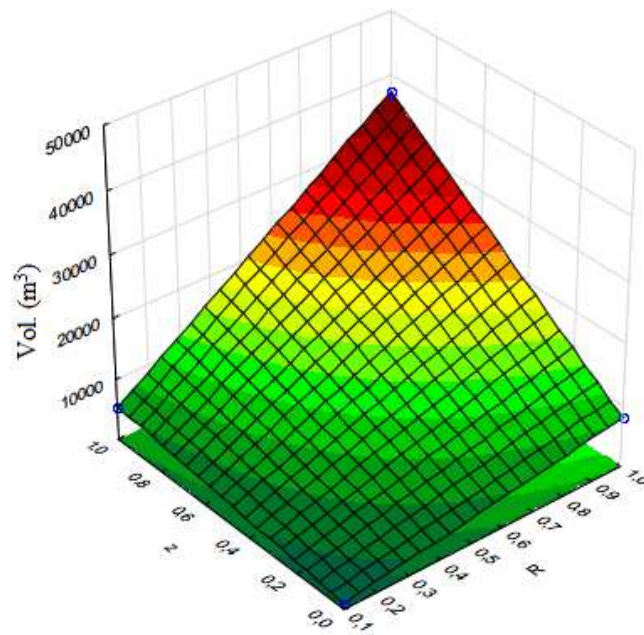


Figure 7.5: Response surface model for leakages in z direction.

Figure 7.6 shows the comparison between the flammable volumes predicted by the developed model and the results obtained in CFD simulations. It is observed that the response surface model provides a very good agreement with CFD results.

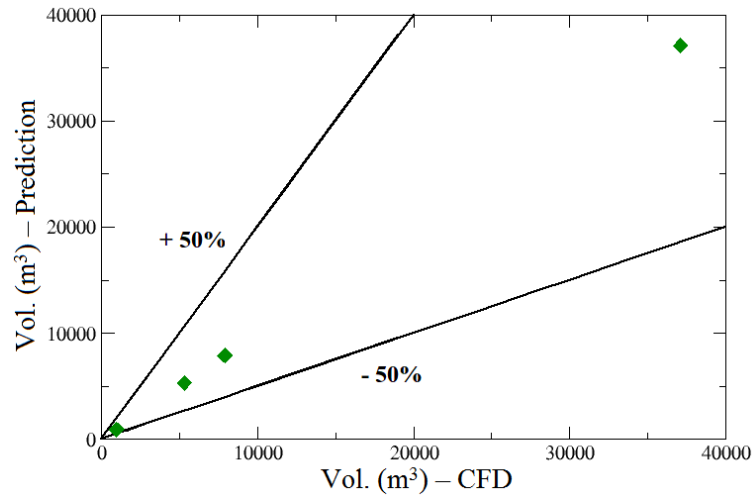


Figure 7.6: Comparison between the values obtained through CFD simulations and the response surface model for leakages in z direction. Vertical axis shows results predicted with the model proposed in this study. Horizontal axis shows cloud volumes obtained using CFD.

Random cases were also simulated in CFD in order to assess if the developed response surface model for releases in z direction was reliable. It was considered dispersion scenarios where the accommodation module was included or not in the platform geometry. Table 7.5 shows these random CFD simulations. It is important to observe that in the first twelve dispersion cases the accommodation module was not included in the geometry, while the last cases have accounted the effect of such structure in the platform geometry.

Table 7.5: Random CFD Simulations.

Case	R	z	Wind Dir.	Flammable cloud size (m ³)
Without A.M. 01	0.03	z ⁺	S	383.11
Without A.M. 02	0.09	z ⁺	W	4725.86
Without A.M. 03	0.15	z ⁺	NE	5745.46
Without A.M. 04	0.21	z ⁺	NW	4074.76
Without A.M. 05	0.27	z ⁺	SE	6983.43
Without A.M. 06	0.3	z ⁺	SW	8446.28
Without A.M. 07	0.03	z ⁻	N	4057.14
Without A.M. 08	0.09	z ⁻	E	22418.90

Without A.M. 09	0.15	z^-	NE	25519.43
Without A.M. 10	0.21	z^-	NW	25367.11
Without A.M. 11	0.27	z^-	SE	44151.34
Without A.M. 12	0.3	z^-	SW	39378.92
With A.M. 13	0.03	z^+	E	363.31
With A.M. 14	0.09	z^+	W	787.90
With A.M. 15	0.15	z^+	E	2550.31
With A.M. 16	0.21	z^+	W	3309.65
With A.M. 17	0.27	z^+	E	2857.06
With A.M. 18	0.3	z^+	W	6611.56
With A.M. 19	0.03	z^-	E	4902.26
With A.M. 20	0.09	z^-	W	10532.20
With A.M. 21	0.15	z^-	E	22521.73
With A.M. 22	0.21	z^-	W	23987.22
With A.M. 23	0.27	z^-	E	24209.20
With A.M. 24	0.3	z^-	W	39912.54

The comparison between the values predicted by the response surface model and the results of the CFD random dispersion simulations given above is shown in Figure 7.7. It is observed that almost all results fall within 50% tolerance interval, even when including or not the accommodation module in the platform geometry. So, as well as the response surface model developed for the leak directions x and y , the response surface obtained for the leak direction z also provided good fit with CFD results.

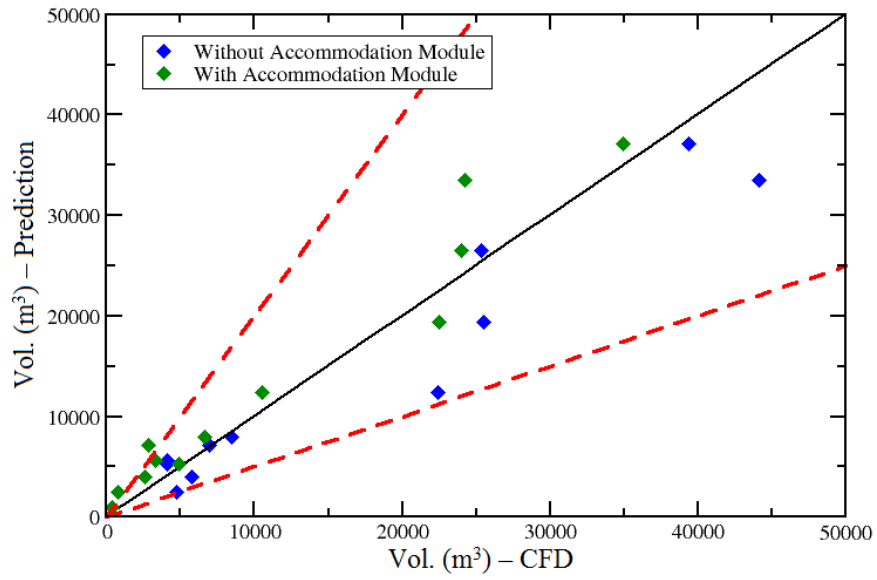


Figure 7.7: Comparing results from CFD simulations with response surface model for releases in z direction. Random dispersion scenarios including or not the accommodation module in the platform geometry were considered. Vertical axis shows results predicted by the response surface model. Horizontal axis shows cloud volumes obtained using CFD.

Chapter 8

Conclusions and Future Work

8.1 Conclusions

A response surface model was developed for prediction of flammable gas cloud sizes in an offshore module.

First a study concerning gas dispersion in an offshore module was developed. The variables that influence the phenomenon were identified and grouped in two factors: R that accounted the effect of the ventilation and leak rate, and φ that computes the relation between the wind and leak direction.

The next step consisted in CFD modelling. Different analysis regarding the ventilation and leak rate were performed. Some tests were also conducted in order to find the mesh refinement and computational domain size that were used in dispersion simulations.

Two experimental cases of gas jet release were successfully reproduced in *ANSYS CFX - 12.0*: an axisymmetric and a high aspect ratio jet. The simulation of an axisymmetric jet was easier performed and spent less computational effort. This type of jet was chosen to represent the gas release in dispersion simulations.

Modelling features used at an axisymmetric jet simulation were applied in the study of a natural gas jet release. In such study the spreading angle of the jet and the velocity and concentration profiles were analysed. The findings were similar to those found in the literature for gas jet behaviour.

The results obtained in jet analysis have indicated that the gas behaviour near the leakage was correctly modelled. Such analysis have ensured that the preceded gas dispersion was also properly modelled and the results of the dispersion simulations in CFD were reliable.

Regarding the ventilation rate into the module, the analysis of wind speed profile shown that at the level of the platform the wind velocity is stable so that a constant value was set for the wind speed in the dispersion simulations.

The influence of the wind direction in ventilation rate was also investigated. It was possible to verify that recirculation zones are formed in the deck region due the interaction between the wind and the platform structures influencing the ventilation rate into the module.

It was also observed that the wind direction had a little influence on ventilation rate when considering the platform geometry without the accommodation module. However, when such structure was included in platform geometry a large dead zone is formed in the deck and the ventilation rate greatly reduces (- 36%) for east wind direction. Such effect was less intense for west wind direction (10%) and almost insignificant for the other wind directions ($\approx 5\%$).

In CFD dispersion simulations different configurations of wind and leak direction and ventilation and leak rate were considered. For each dispersion scenario a flammable gas cloud was obtained. It was observed that the largest flammable clouds were found when leak and wind had taken opposite directions. Because the wind was directed toward the leak, an effective mixture between the air and the gas released occurred giving large flammable volumes.

For the development of the response surface model in a first time only the leak directions x and y were considered. In these cases a second order mathematical model was used. It was possible to verify that the behaviour of the gas cloud was not the same for all angle formed between the leak and wind direction. Different response surfaces had to be used when calculating cloud sizes.

The division of the possible angles in quadrants seemed to be a good form to identify the different behaviours of the flammable cloud size when leak and wind take the opposite or same directions.

The saddle profile presented in the quadrants 2 and 3 was expected when leak and wind are in opposite direction. The behaviour found in quadrants 1 and 4 shown that the flammable cloud size increases as R increases when leak and wind take the same direction.

A response surface was also developed to account the leak direction z and a first order

model was used. It was verified that when considering the leak directions z^+ and z^- the differences in gas dispersion and also in flammable volume are due the type of the jet that is formed: when the leak direction is z^+ a upward free jet is formed, while when the leak direction is z^- the leakage is directed toward the ground and an impinging jet is formed. So the largest flammable clouds were found when the leak was directed toward to the deck floor (z^-). Regarding the variable R, large flammable volumes were obtained for large values of R.

So, the fully complete model includes five response surfaces: four considering the leak directions x and y and one that accounts the leak direction z .

The results provided by the all response surfaces were well fitted with CFD data within a tolerance of 50%. This is considered very good agreement as far as validation of gas dispersion data was considered.

Another important consideration is that even the accommodation module was included in the geometry under study, the developed model was able to predict the flammable volumes with good accuracy compared with CFD simulations. Thus it can be considered a complete model for the type of geometry under study (an offshore platform).

The presented response surface model is a simplified prediction form and can be applied in early stages of the design when little is known about the geometry or when the geometrical model is not available. Additionally, the approach has proofed to be very robust when combined with CFD data. Through the model every possible release scenario can be assessed in a risk analysis, which is infeasible using CFD simulations.

8.2 Future Work

The flammable gas cloud size is a function of the leak rate, which in turns depends on the leak size that originates the release. The size of the leak is a stochastic variable since there is no way to predict it beforehand. However, probabilities values are available for hole sizes. The proposed response surface model can be very useful when combining with Monte Carlo techniques. The approach will calculate probabilistic cloud sizes.

The response surfaces were developed based on a second order mathematical model. However, high-order models may provide a better fit with CFD results. In order to improve the

proposed response surface model, the utilisation of other mathematical models is suggested.

Some attempts were made to model a high aspect ratio jet behaviour, but an advanced investigation has become infeasible in this work. Thus, other studies have been developed in order to evaluate the influence of the jet orifice shape in flammable gas cloud size. By taking the same platform geometry and dispersion scenario, releases from a high aspect ratio and axisymmetric jets have been outlined and the flammable volumes have been compared. This study can provide a new method of jet modelling for gas dispersion that makes the risk analysis more realistic.

Bibliography

AMERICAN INSTITUTE OF CHEMICAL ENGINEERS (AIChE). *Guidelines for Chemical Process Quantitative risk Analysis*, 2nd edition, Wiley Interscience, New York, USA, 2000.

ANSYS CFX, INC. *CFX - 12.0 User's Guide*, 2011.

BBC news. US oil spill: 'Bad management' led to BP disaster. Available from: <www.bbc.co.uk/news/world-us-canada-12124830>, accessed in 09.02.2013.

Benintendi, R. Turbulent jet modelling for hazardous area classification. *Journal of Loss Prevention in the Process Industries*, 23, p. 373-378, 2010.

Benintendi, R. Laminar jet modelling for hazardous area classification. *Journal of Loss Prevention in the Process Industries*, 24, p. 123-130, 2011.

Birch, A. D., Huges, D. J. and Swaffield, F. Velocity decay of high pressure jets. *Combustion Science and Technology*, v. 52, p.161-171, 1987.

Bird, R.B.; Stewart, W.E.; Lightfoot, E.N. *Transport Phenomena*. 2nd edition, John Wiley & Sons, Inc., New York, USA, 2002.

Box, G.E.P and Wilson, K.B. On the experimental attainment of optimum conditions. *Journal of the Royal Statistical Society Series B*, A89, p. 1-45, 1951.

Box, G.E. and Draper, N.R. *Empirical model building and response surfaces*. John Wiley & Sons, Inc., Wiley series in probability & mathematical statistics, Morgantown, USA, 1987.

CBC news. 39 killed in Venezuela oil refinery explosion. Available from: <www.cbc.ca/news/world/story/2012/08/25/venezuela-refinery-explosion.html>, accessed in 08.20.2013.

Celik, I.B. *Introductory Turbulence Modeling*. John Wiley & Sons, Inc., Morgantown, USA, 1999.

- Charnock, H. Wind stress over a water surface. *Quarterly Journal of the Royal Meteorological Society*, 81, p.639-640, 1955.
- Cleaver, R. P.; Humphreys, C. E. and Robinson, C. G. Accidental generation of gas clouds on offshore process installations. *Journal of Loss Prevention in the Process Industries*, Vol. 7, No.4, p. 273-280, 1994.
- Cleaver, R.P., Burggs, S., Buss, G.Y., Savvides, C., Connoly, S. and Britter, R.E. Analysis of gas build-up from high pressure natural gas releases in naturally ventilated offshore modules. *8th Annual conference on offshore installations: Fire and explosion engineering*, London, UK, 1999.
- Coetzer, R.L.J., Rossouw, R.F. and Lin, D.K.J. Dual response surface optimization with hard-to-control variables for sustainable gasifier performance. *Journal of the Royal Statistic Society*, 57, Part 5, p. 567–587, 2011.
- Cormier, B.R., Qi, R., Yun, G., Zhang, Y. and Mannan, M.S. Application of computational fluid dynamics for LNG vapor dispersion modeling: A study of key parameters. *Journal of Loss Prevention in the Process Industries*, 22, p.332-352, 2009.
- Das, B. and Weinberg, M. Improving a flammable mass estimation for vapour cloud explosion modeling in a offshore QRA. *Safety Science*, 50, p.1218-1227, 2012.
- Epstein, M. and Fauske, H.K. Total flammable mass and volume within a vapor cloud produced by a continuous fuel-gas or volatile liquid-fuel release. *Journal of Hazardous Materials*, 147, p. 1037–1050, 2007.
- Gil, M.V., Martínez, M., García, S., Rubiera, F., Pis, J.J. and Pevida, C. Response surface methodology as an efficient tool for optimizing carbon adsorbents for CO_2 capture. *Fuel Processing Technology*, 106, p.56-61, 2013.
- Hanna, S.R., Briggs, G.A. and Hosker, R.P.Jr. *Handbook on Atmospheric Diffusion*, Technical Information Center U.S Department of Energy, Springfield, USA, 1982.
- Hanna, S.R., Hansen, O.R., Dharmavaram, S. FLACS CFD air quality model performance evaluation with Kit Fox, MUST, Prairie Grass, and EMU observations. *Atmospheric Environment*, 38, p.4675-4687, 2004.
- Hill, W.J. and Hunter, W. A review of response surface methodology: A literature survey. *Technometrics*, Vol. 8, No.4, p. 571-590, 2002.
- Hirsch, C. *Numerical Computation of Internal and External Flows - Fundamentals of Computational Fluid Dynamics*, Vol.1, 2nd edition, John Wiley & Sons, Oxford, UK, 2007.

- Health & Safety Executive. Representative Range of Blast and Fire Scenarios. *The Steel Construction Institute for HSE*, Offshore Tecnology Information (OTI), n. 92.586, London, UK, 1992.
- Health & Safety Laboratory. Outstanding safety questions concerning analisys of ventilation and gas dispersion in gas turbine enclosures: Best Practice Guidelines. *Fire and Explosion Group*, Buxton, UK, 2003.
- Huser, A. and Kvernfold, O. Explosion risk analysis- Development of a general method for gas dispersion analyses on offshore platforms. *Parallel Computational Fluid Dynamics: Trends and Applications*, chapter 59, Elsevier Science B.V., Trondheim, Norway, 2000.
- Huser, A. Foyn, T. and Skottene, M. A CFD based approach to the correlation of maximum explosion overpressure to process plant parameters. *Journal of Loss Prevention in the Process Industries*, 22, p.324-331, 2009.
- Ivings, M.J., Gant, S.E., Saunders, C.J. and Pocock, D.J. Flammable gas cloud build up in a ventilated enclosure. *Journal of Hazardous Materials*, 184, p.170-176, 2010.
- Jaliliannosrati, H., Amin, N.A.S., Kiakalaieh, A.T. and Noshadi, I. Microwave assisted biodiesel production from *Jatropha curcas* L. seed by two-step in situ process: Optimization using response surface methodology. *Bioresource Technology*, 136, p.565-573, 2013.
- Johnson, D.M. The potential for vapour cloud explosions - Lessons from the Buncefield accident. *Journal of Loss Prevention in the Process Industries*, 23, p.291-297, 2010.
- Kermode, A.C. *Mechanics of Flight*. Pitman Publishing Limited, London, UK, 1972.
- Kjellén, U. Safety in the design of offshore platforms: Integrated safety versus safety as an add-on characteristic. *Safety Science*, 45, p.107-127, 2007.
- Kundu, P.K. and Cohen, I.M. *Fluid Mechanics*. 2nd edition, Academic Press, San Diego, USA, 2002.
- Lange, B., Larsen, S.E., Hojstrup, J. and Barthelmie, R. Importance of thermal effects and sea surface roughness for offshore wind resource assessment. *Journal of Wind Engineering and Industrial Aerodynamics*, 92, p.959-988, 2004.
- Lees, F.P. *Loss Prevention in the Process Industries - Hazard Identification, Assessment and Control*. 3rd edition, Butterworth-Heinemann, Oxford, UK, 2005.

- Maliska, C.R. *Transferência de Calor e Mecânica dos Fluidos Computacional*. 2nd edition, LTC Livros Técnicos e Científicos Editora S.A., Rio de Janeiro, Brasil, 2004.
- Mih, W.C. Equations for axisymmetric and two-dimensional turbulent jets. *Journal of Hydraulic Engineering*, 115, p.1715-1719, 1989.
- Minakshi, S., Rai, J.S.P. and Srivastava, D. Process modeling, optimization and analysis of esterification reaction of cashew nut shell liquid (CNSL)-derived epoxy resin using response surface methodology. *Journal of Hazardous Materials*, 185, p.1198-1204, 2011.
- Oyewole, S.A. and Cant, R.S. Statistical evaluation and analysis of safety intervention in the determination of an effective resource allocation strategy. *Journal of Loss Prevention in the Process Industries*, 23, p.585-593, 2010.
- Paté-Cornell, M.E. Learning from the Piper Alpha Accident: A postmortem analysis of technical and organizational factors. *Risk Analysis*, Vol. 13, No. 2, 1993.
- Pope, S.B. *Turbulent Flows*. 1 edition, Cambridge University Press; Morgantown, UK, 2000.
- Qiao, A. and Zhang, S. Advanced CFD modeling on vapor dispersion and vapor cloud explosion. *Journal of Loss Prevention in the Process Industries*, No.23, p. 843-848, 2010.
- Rastegar, S.O., Mousavia, S.M., Shojaosadatia, S.A and Sheibanib, S. Optimization of petroleum refinery effluent treatment in a UASB reactor using response surface methodology. *Journal of Hazardous Materials*, 197, p. 26–32, 2012.
- Rodrigues, M.I. and Iemma, A.F. *Planejamento de Experimentos e Otimização de Processos: Uma estratégia sequencial de planejamentos*. Casa do Pão; Campinas, BR, 2005.
- Vianna, S.S.V. and Cant, R.S. Explosion pressure prediction via polynomial mathematical correlation based on advanced CFD Modelling. *Journal of Loss Prevention in the Process Industries*, 25, p.81-89, 2012.
- Wakes, S.J., Holdo, A.E. and Meares, A.J. Experimental investigation of the effect orifice shape and fluid pressure has on high aspect ratio cross-sectional jet behaviour. *Journal of Hazardous Materials*, A89, p.1-27, 2002.
- Wakes, S.J. High aspect ratio orifice jet leaks within a production area of an offshore superstructure. *Third International Conference on CFD in the Minerals and Process Industries*, Melbourne, AUS, 2003.

Wilcox, D. C. *Turbulence Modeling for CFD*, Vol.1, 2nd edition, DCW Industries Inc, California, USA, 1994.

Wilkening, H., Baraldi, D. and Heitsch, M. CFD simulations of light gas release and mixing in the Battelle Model-Containment with CFX. *Nuclear Engineering and Design*, 238, p.618-626, 2008.

Zhang, J., Delichatsios, M.A. and Venetsanos, A.G. Numerical studies of dispersion and flammable volume of hydrogen in enclosures. *Hydrogen Energy*, 35, p.6431-6437, 2010.

Zhao, J., Jin, B. and Zhong, Z. Study of the separation efficiency of a demister vane with response surface methodology. *Journal of Hazardous Materials*, 147, p.263-269, 2007.

Appendix A

An Engineering Procedure for Gas Dispersion Analysis Using *ANSYS CFX 12.0*

Based on the CFD analysis conducted during this work, a simple engineering procedure was defined for gas dispersion study in an offshore module using the *ANSYS CFX 12.0* CFD software.

A.1 Building the geometry and mesh

When creating the geometry it is important to specify the different regions that will receive different boundary conditions in CFX - Pre Processor. The main regions that must be defined are: the leakage, the facilities and solid structures, the computational domain contour and the wind entrance.

Because gas dispersion phenomenon in an offshore module is an external flow problem, a computational domain must be created to cover all geometry and region under study. It is suggested that the computational domain dimensions are 2.4 times bigger than the offshore module dimensions so that its borders do not interfere in numerical solution and a reasonable number of control volumes are obtained.

A tetrahedral mesh can be used. According to the length scale of the geometry structures different mesh refinements are required. At the leakage region at least 10 control volumes is enough

to capture all effects. Control volumes 2.5 times smaller than the facilities size can be used at such regions.

A.2 CFX - Pre Processor

In CFX Pre Processor the mathematical model is implemented into CFD software. The properties of the fluid, the boundaries and initial conditions and the numerical scheme are specified.

The boundary conditions assigned to each region defined in the geometry are:

- Leakage - the "*Inlet*" condition is selected to indicate the entrance of a fluid flow into the computational domain. A value of mass flow or velocity can be set;
- Wind - the "*Inlet*" condition is also selected. A velocity value or field can be set. It is also possible to set an expression to define a wind speed profile.
- Facilities and Solid structures - the "*Wall*" condition is selected. The no slip and free slip conditions are available.
- Computational Domain Contour - the "*Opening*" condition is used to indicate that there is no pressure difference between the computational domain and the outer region.

The natural gas composition is defined by creating a new substance. The components of this substance are selected in a material list and their mass fraction can be specified.

A.3 CFX - Post Processor

In the post-processing phase the module region that is affected by the flammable cloud is verified. A plane is created above the platform deck and the natural gas molar fraction is analysed.

A volume is created based on the upper and lower flammable limits. An internal surface covers the volume where the natural gas concentration are higher than LFL while the outer surface comprises the volume where the atural gas concentration is higher than UFL.

The flammable cloud size could be calculated by using the function *volumeInt*. Such function integrates a specified variable over the volume location. The volume defined before is selected as location and the natural gas molar fraction is set as variable.

Appendix B

Additional CFD Results

Some dispersion scenarios described in Table 7.1 (Section 7.1) that given the largest flammable volumes are presented in Figures B.1 to B.12. A plane defined at 15 metres above platform deck is shown as example of the flammable region. The red zone represents the region of the gas cloud where the gas concentration exceed the UFL, while the light blue zone represents the cloud region where the gas concentration is near the LFL. So the flammable region comprises the colourful part between the red and the light blue zones.

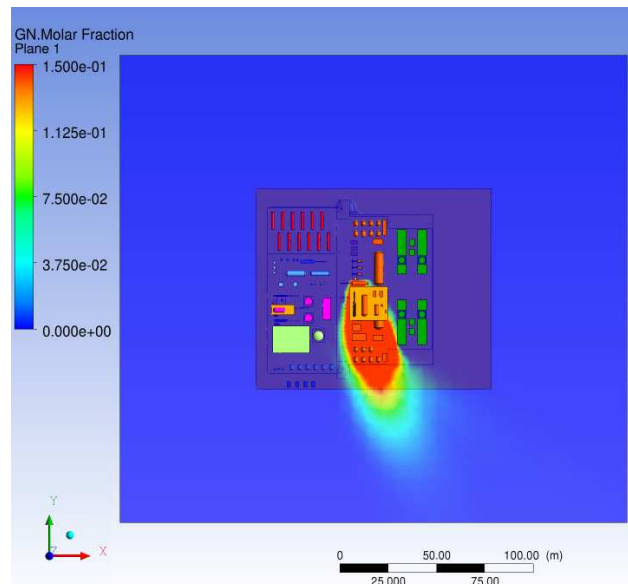


Figure B.1: Result of the CFD simulation considering the dispersion scenario 08 (see Table 7.1). The flammable region in a plane at 15 metres over platform deck is verified.

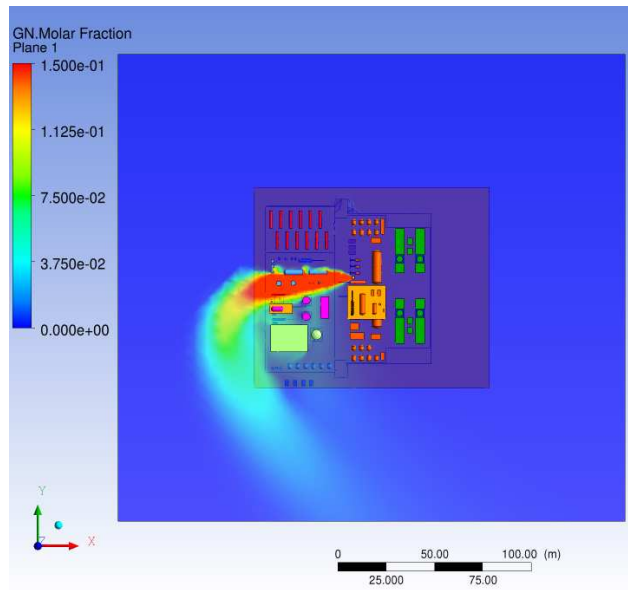


Figure B.2: Result of the CFD simulation considering the dispersion scenario 14 (see Table 7.1). The flammable region in a plane at 15 metres over platform deck is verified.

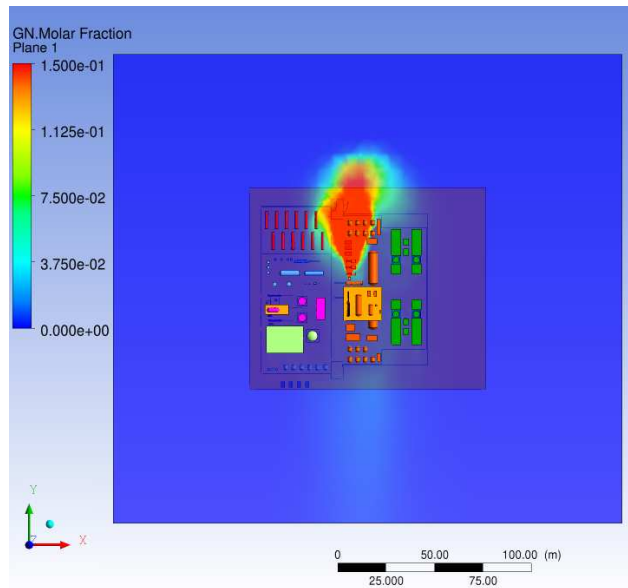


Figure B.3: Result of the CFD simulation considering the dispersion scenario 15 (see Table 7.1). The flammable region in a plane at 15 metres over platform deck is verified.

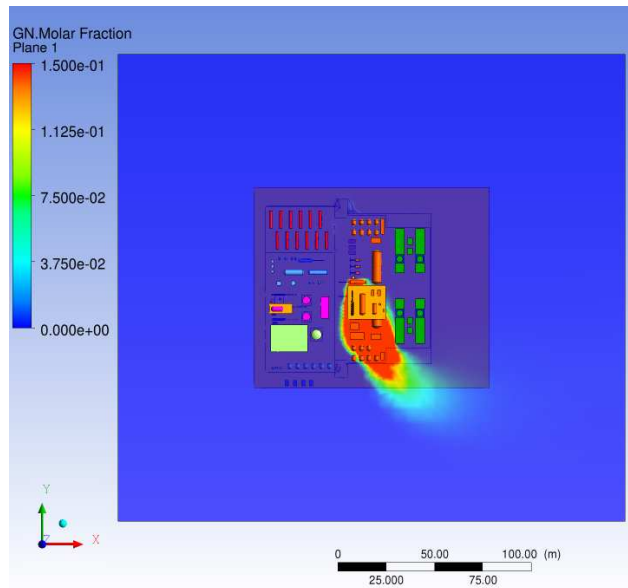


Figure B.4: Result of the CFD simulation considering the dispersion scenario 16 (see Table 7.1). The flammable region in a plane at 15 metres over platform deck is verified.

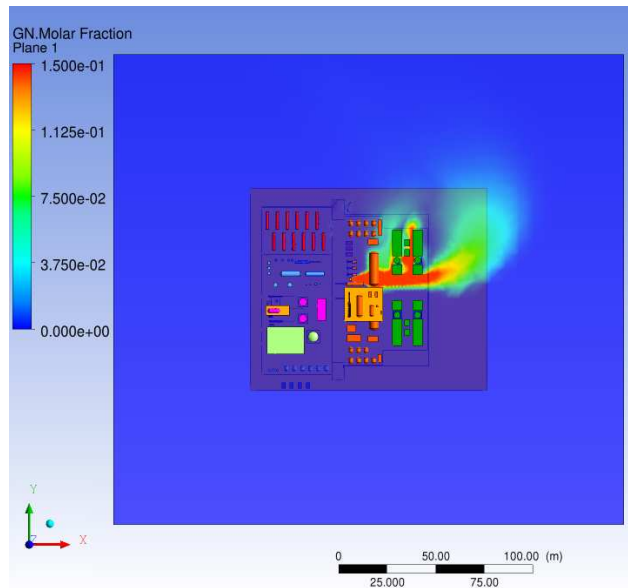


Figure B.5: Result of the CFD simulation considering the dispersion scenario 17 (see Table 7.1). The flammable region in a plane at 15 metres over platform deck is verified.

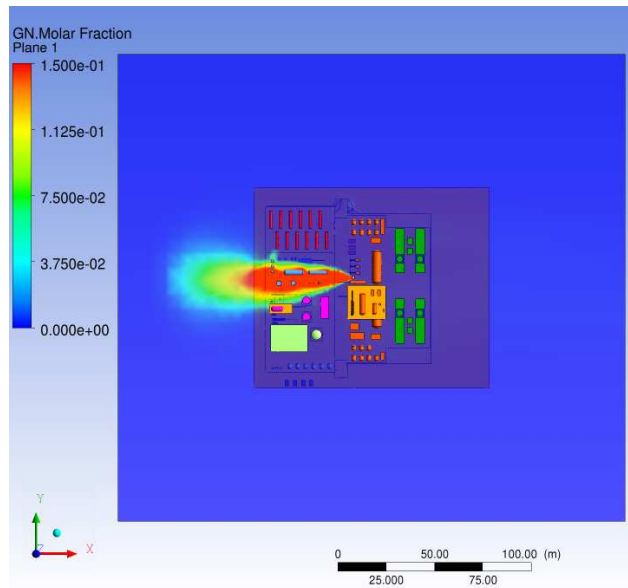


Figure B.6: Result of the CFD simulation considering the dispersion scenario 18 (see Table 7.1). The flammable region in a plane at 15 metres over platform deck is verified.

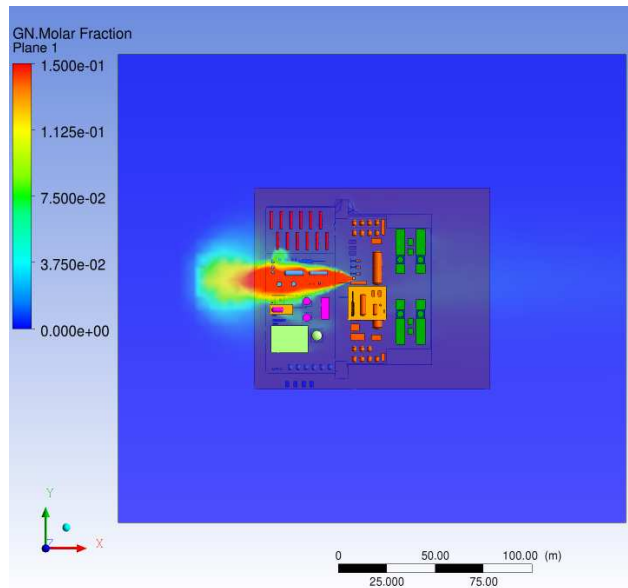


Figure B.7: Result of the CFD simulation considering the dispersion scenario 22 (see Table 7.1). The flammable region in a plane at 15 metres over platform deck is verified.

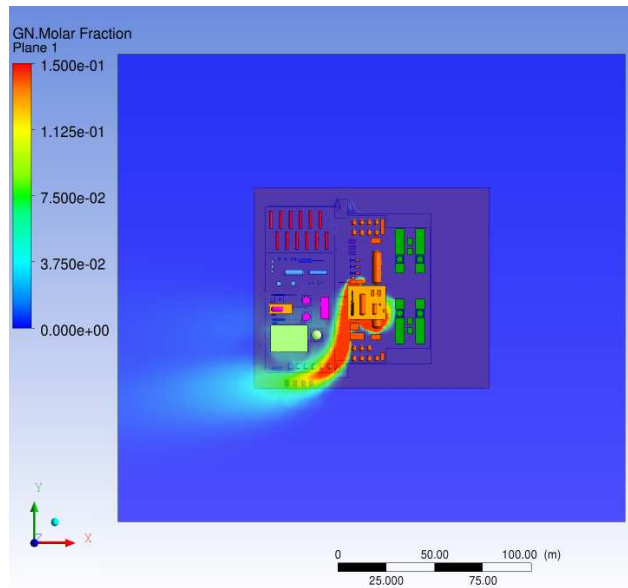


Figure B.8: Result of the CFD simulation considering the dispersion scenario 24 (see Table 7.1). The flammable region in a plane at 15 metres over platform deck is verified.

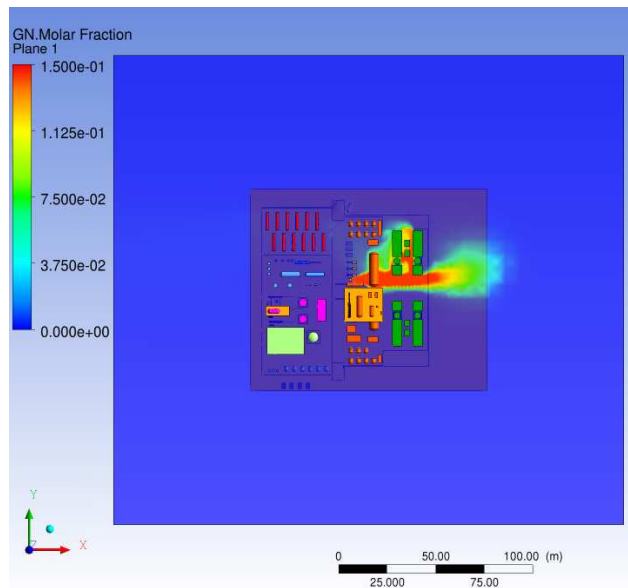


Figure B.9: Result of the CFD simulation considering the dispersion scenario 25 (see Table 7.1). The flammable region in a plane at 15 metres over platform deck is verified.

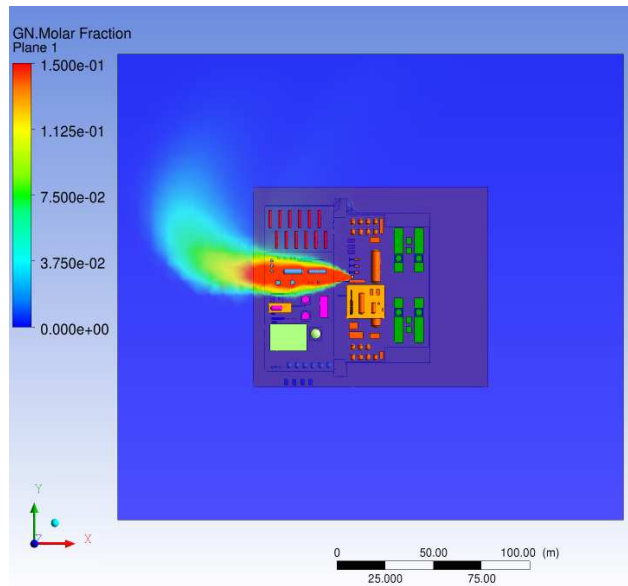


Figure B.10: Result of the CFD simulation considering the dispersion scenario 26 (see Table 7.1). The flammable region in a plane at 15 metres over platform deck is verified.

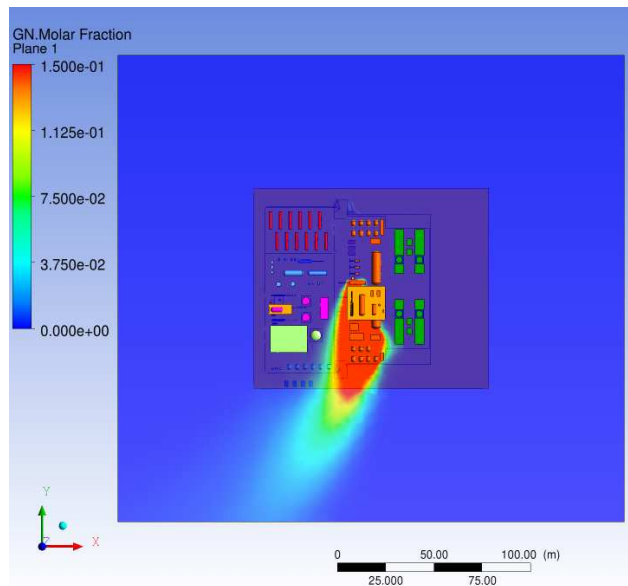


Figure B.11: Result of the CFD simulation considering the dispersion scenario 32 (see Table 7.1). The flammable region in a plane at 15 metres over platform deck is verified.

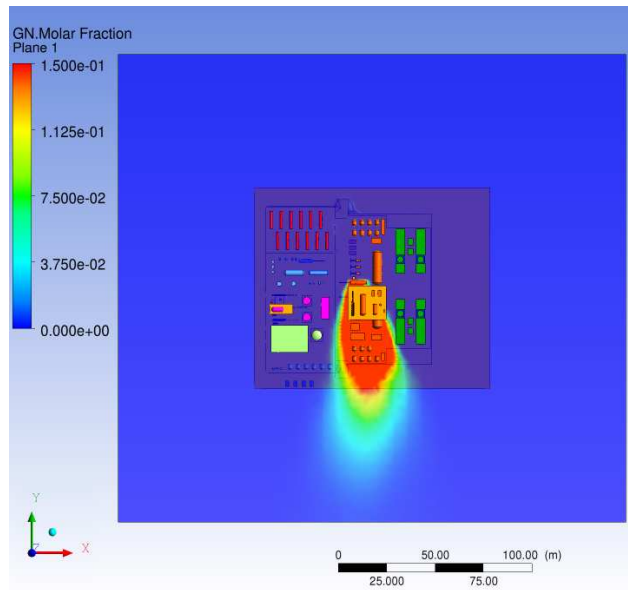


Figure B.12: Result of the CFD simulation considering the dispersion scenario 36 (see Table 7.1). The flammable region in a plane at 15 metres over platform deck is verified.